

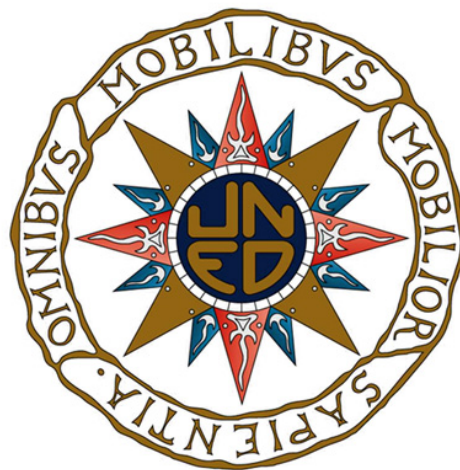
Doctoral Dissertation - Tesis Doctoral

Transformation methods for the integration of singular and near-singular functions in XFEM

Métodos de transformación para la integración de funciones
singulares y casi-singulares en XFEM

Alfredo Cano Cancela

2017



Doctoral advisor: Dr. Carlos A. Moreno González
Universidad Nacional de Educación a Distancia (UNED)
Faculty of Science
Department of Statistics, Operations Research and
Numerical Analysis

Author

Alfredo Cano Cancela. Máster E.E.E.S. en Matemáticas Avanzadas, UNED 2011.
Licenciado en Ciencias Físicas, UCM 1992.

Doctoral Advisor

Prof. Dr. D. Carlos Antonio Moreno González

Date of the graduation

July 2017

A Mari Carmen
A mis padres y hermanos

Agradecimientos

Quisiera expresar en estas breves líneas mi agradecimiento hacia la Universidad Nacional de Educación a Distancia (UNED), por su compromiso hacia la difusión del conocimiento en todos los ámbitos. Si la UNED no existiera, sería imposible que alumnos con perfiles diversos y heterogéneos, que quedan fuera de los conductos académicos convencionales, pudieran satisfacer sus inquietudes intelectuales.

Reiterar mi reconocimiento hacia todos los que fueron mis profesores durante el Máster de Matemáticas Avanzadas de la UNED.

Destacar asimismo, con especial gratitud, la dedicación de mi director de tesis doctoral, D. Carlos Moreno, por abrirme las puertas al apasionante mundo de la investigación científica y por su guía y estímulo durante el proceso de elaboración del presente trabajo.

No quisiera olvidarme de mis alumnos, de quienes aprendo cada día tanto como les enseño.

Por último, doy gracias al Maestro por regalarme la sed de aprender.

Contents

Abstract	1
1. Introduction	5
1.1. Overview	5
1.2. The (near-)singular integration problem in the XFEM framework	6
1.3. Transformation of quadrature rules	8
2. The isoparametric and pyramidal transformations	11
2.1. The isoparametric transformation	11
2.2. The pyramidal transformation, \mathcal{P}	12
2.2.1. The pyramidal transformation in 2D	13
2.2.2. Polar coordinates	15
2.2.3. The pyramidal transformation in 3D	16
2.2.4. The Jacobian of the pyramidal transformation in 3D	17
3. The singular integral in 2D	19
3.1. Overview	19
3.2. The regularizing transformation, \mathbf{R}	20
3.3. The radial kernel, $\mathbf{K}_1(\bar{\mathbf{u}})$	21
3.4. The angular kernel, $\mathbf{K}_2(\bar{\mathbf{v}})$	22
3.4.1. The complex poles of the algebraic kernel	25
3.4.2. The general form of the angular transformations	27
3.4.3. The cubic transformation	28
3.4.4. The sinh transformation	28
3.4.5. The sigmoidal transformation	29
3.5. A new class of transformations	30
3.5.1. Additional softening on the a posteriori transformation	32
3.5.2. An edge-singular kernel	33
3.6. Numerical results	34
4. The near-singular integral in 2D	41
4.1. Overview	41
4.2. The angular kernel $\mathbf{K}_2(\bar{\mathbf{v}})$	43
4.2.1. General form of the transformations	43
4.2.2. A posteriori transformations for $\mathbf{K}_2(\bar{\mathbf{v}})$	44
4.3. The radial kernel $\mathbf{K}_1(\bar{\mathbf{u}}, \bar{\mathbf{v}})$	45
4.3.1. A priori transformations for $\mathbf{K}_1(\bar{\mathbf{u}}, \bar{\mathbf{v}})$	46

4.3.2.	A posteriori transformations for $K_1(\bar{u}, \bar{v})$	47
4.3.3.	The singularities in G_β	48
4.4.	A new family of composite radial transformations	49
4.4.1.	The transformation G_1	49
4.4.2.	The transformation G_2	50
4.4.3.	The iterated sinh transformation	51
4.5.	A transformation for complete kernel regularization	51
4.6.	The integration of (near-)singular kernels over adjacent triangles	53
4.6.1.	The pyramidal transformation for adjacent triangles	54
4.6.2.	The near-singular kernel for adjacent triangles	55
4.6.3.	The regularizing transformation for the radial variable	56
4.7.	Numerical results	57
4.7.1.	Near-singularity strength, α	58
4.7.2.	Near-singularity perturbation, ε	58
4.7.3.	Integration domain, T	58
4.7.4.	The regular part of the integrand, $g(x, y)$	58
4.7.5.	Implemented methods	59
4.7.6.	Numerical results for adjacent triangles	60
5.	The singular integral in 3D	69
5.1.	Overview	69
5.2.	The radial kernel	70
5.3.	The angular kernel	71
5.3.1.	The behaviour of ϕ on the boundary of C_2	72
5.3.2.	The algebraic kernel	73
5.3.3.	Implementation of the methods proposed	74
5.4.	The Jacobian of the composite transformation	74
5.5.	Numerical results	74
5.5.1.	Simulations over pyramids	75
5.5.2.	Simulations over tetrahedra	77
6.	The optimal form of the cubic transformation	81
6.1.	Overview	81
6.2.	Part 1. Optimality of $\mathfrak{S}(t)$	82
6.2.1.	Left subinterval $0 \leq r \leq r_0$	84
6.2.2.	Right subinterval $r_0 < r \leq 1$	84
6.2.3.	The explicit value of r_0	85
6.3.	Part 2. Optimality of $\mathfrak{S}(v)$	86
6.3.1.	The affine transformation $t(v)$	86
6.3.2.	The explicit form of $\mathfrak{S}(v(r))$	89
6.3.3.	The case $0 < \bar{v}_p \leq \frac{1}{2}$ and $0 \leq r \leq r_0$	90
6.3.4.	The case $0 < \bar{v}_p \leq \frac{1}{2}$ and $r_0 < r \leq 1$	90
6.3.5.	The case $\bar{v}_p < 0$ and $0 \leq r \leq r_0$	92
6.3.6.	The case $\bar{v}_p < 0$ and $r_0 < r \leq 1$	98

6.3.7.	Lower bounds for $\mathfrak{S}(t(r_0))$ and $\mathfrak{S}(v(r_0))$	98
6.4.	Part 3. The optimal ellipse of analyticity \mathcal{E}_p	99
6.4.1.	The explicit form of $\mathfrak{R}(v(r))$	101
6.4.2.	The case $0 < \bar{v}_p \leq \frac{1}{2}$ and $0 \leq r \leq r_0$	101
6.4.3.	The case $0 < \bar{v}_p \leq \frac{1}{2}$ and $r_0 < r \leq 1$	112
6.4.4.	The case $\bar{v}_p < 0$ and $0 \leq r \leq r_0$	115
6.4.5.	The case $\bar{v}_p < 0$ and $r_0 < r \leq 1$	123
7.	Conclusions	125
7.1.	Overview	125
7.2.	Original contributions	126
7.3.	Future developments	127
A.	Inversion of the cubic equation	129
A.1.	The equation $Y = X(p^2 - X^2)$	129
A.2.	The equation $Y = X(p^2 + X^2)$	131
B.	Equivalent form of some transformations	133
B.1.	The PART Method	133
B.2.	The Exponential distance transformation	134
B.3.	The Exponential transformation	135
C.	Newton's method	137
D.	Truncation error under affine transformations	139
D.1.	The error term of the Gaussian quadrature	139
D.2.	Effect of an affine transformation	139
	Bibliography	141

Abstract

This doctoral thesis addresses the problem of numerical integration of singular and near-singular functions, in two and three dimensions, using variable transformation methods. It includes the analysis of transformations with a geometric purpose, i.e., they map the physical domain onto a parent, standard domain, and transformations of an algebraic nature, with the purpose of softening the (near-)singularities in the integrand.

Transformations used to map the physical element onto the parent domain are described in chapter 2. The most general case of a degenerate isoparametric map, such that it is homogeneous in one of its variables is presented, and its equivalence to the polar transformation is justified in the two-dimensional case. These maps induce a factorization of certain types of integral kernels into a radial and an angular part, allowing a separate, specific treatment of each factor.

The two-dimensional singular integration problem is examined in chapter 3. The radial kernel is completely regularized by means of a new scheme that removes its singularity. Regarding the angular kernel, it is shown to have the same form as the one-dimensional near-singular kernel, and thus the same set of transformations can be successfully applied to both kernels.

The two-dimensional near-singular kernel is the subject of chapter 4. Whilst the treatment of the angular kernel is exactly the same as in chapter 3, the radial kernel admits a whole new set of regularizing maps, taking advantage of the linear factor in the Jacobian of the degenerate isoparametric transformation. The generalization of the problem to adjacent triangles, in which the source point lies outside the integration domain is also considered.

The extension of the singular integration to three-dimensional domains is covered in chapter 5. The treatment of the radial kernel is very similar as in chapter 3, whereas the bivariate angular kernel, restricted to the boundary of the bidimensional angular domain, behaves very similarly to the near-singular one dimensional kernel, and yet the same set of softening transformations as in chapter 3 and chapter 4 can be suitable re-utilized in this situation.

Lastly, chapter 6 presents a proof of the optimal form of the well-known cubic transformation, employed as one of the most common alternatives to regularize the angular kernel in the three previous chapters.

All proposed methods have been extensively tested from the numerical point of view, showing that they are able to outperform the existing methods for a broad variety of situations.

Resumen

Esta tesis doctoral aborda el problema de la integración numérica de funciones singulares y casi-singulares, en dos y tres dimensiones, usando métodos de transformación de variables. Se incluye el análisis de transformaciones con un propósito geométrico, tales que transforman el dominio físico en un dominio maestro estandarizado, y transformaciones de naturaleza algebraica, con el propósito de suavizar las casi-singularidades del integrando.

Las transformaciones del elemento físico en el dominio maestro se describen en el Capítulo 2. Se presenta el caso más general de una transformación isoparamétrica degenerada que es homogénea en una de sus variables, y se justifica su equivalencia con la transformación polar en el caso bidimensional. Estas transformaciones inducen una factorización de ciertos tipos de núcleo singular en una parte radial y otra angular, permitiendo un tratamiento separado y específico de cada factor.

La integración singular en dos dimensiones se examina en el Capítulo 3. El núcleo radial se regulariza completamente por medio de un nuevo esquema que suprime su singularidad. Con respecto al núcleo angular, se muestra que tiene la misma forma que el núcleo casi-singular en una dimensión, de forma que el mismo conjunto de transformaciones se puede aplicar satisfactoriamente a ambos núcleos.

El núcleo casi-singular en dos dimensiones es el objeto del Capítulo 4. Aunque el tratamiento del núcleo angular es idéntico al del Capítulo anterior, el núcleo radial admite un nuevo conjunto de transformaciones de regularización, aprovechando un factor lineal presente en el jacobiano de la transformación isoparamétrica. Se considera también la generalización de este problema a triángulos adyacentes, en los cuales el punto fuente está situado fuera del dominio de integración.

La extensión de la integración singular a dominios tridimensionales se analiza en el Capítulo 5. El tratamiento del núcleo radial es muy similar al realizado en el Capítulo 3, mientras que en lo referido al núcleo angular en dos variables, su restricción a la frontera del dominio bidimensional se comporta de manera muy similar a la del núcleo casi-singular en una dimensión, por lo que el mismo conjunto de transformaciones de suavizado ya empleadas en los Capítulos 3 y 4 se puede reutilizar de forma satisfactoria en esta situación.

Finalmente, el Capítulo 6 presenta una prueba de la forma óptima de la conocida transformación cúbica, usada como una de las alternativas más habituales para la regularización del núcleo angular descrito en los tres Capítulos anteriores.

Todos los métodos propuestos se han sometido a ensayos numéricos exhaustivos, mostrando que son capaces de sobrepasar en rendimiento a los métodos existentes en una amplia variedad de situaciones.

1. Introduction

1.1. Overview

The growing importance of numerical methods for the solution of Partial Differential Equations, such as FEM, XFEM and BEM, acquired over the last decades, has revealed the necessity for efficient procedures of numerical quadrature, in both two and three dimensions, when the integrands are singular or near-singular functions of their arguments.

Several techniques have been developed to serve this purpose, including adaptive domain subdivision [21, 51], analytic or semi-analytic singularity subtraction [30, 23], quadrature rules adapted to specific integrands or domains [20, 41], composite quadratures [59], extrapolation techniques [44] and methods based upon variable transformations.

This work presents a systematic approach to the variable transformation methods, taking into account its two fundamental features, namely

- Geometric: since integrals are usually formulated over arbitrary elements in physical coordinates, changes of variables that express such integrals over a standard parent domain, typically a unit cube, are desirable. Moreover, these transformations may help improving the behaviour of singular integrands. A particular case of a degenerate isoparametric map, designated as pyramidal transformation, is shown to accomplish both objectives.
- Algebraic: even if the pyramidal transformation helps reducing the integrand sharpness, a further regularization may be needed to soften the remaining singularities. A thorough review of existing maps is performed, finding their optimal forms in some cases, and proposing new transformations otherwise. Since the regularizing maps are applied after composition with the pyramidal transformation, only normalized maps, such that the parent domain is kept unchanged, are considered.

All proposed methods have been subject to extensive numerical simulations, showing their improvement in performance over existing algorithms. A practical requirement has been the simplicity of code implementation for all methods, together with their efficiency in running time.

1.2. The (near-)singular integration problem in the XFEM framework

The first stage in the Finite Element Method (FEM), eXtended Finite Element Method (XFEM) and Boundary Element Method (BEM) is the meshing, by which the problem domain is partitioned into elements. Triangles and quadrilaterals are the most typical examples in two dimensions (2D), whereas in three dimensions (3D), tetrahedra, pyramids, prisms or 8-node hexahedra are common choices. Often, these elements have arbitrary shapes induced by complicated boundary conditions. The need to simplify the computation of the elementary matrices motivates a change of coordinates from a standard parent domain, usually the unit hypercube $C_n = [0, 1]^n$, onto the physical domain.

Affine transformations of triangles and tetrahedra, see e.g. [53, 36, 57, 69, 55, 47] together with isoparametric (multilinear) mappings of quadrilaterals, prisms and hexahedra, see e.g. [42, 40, 38, 66, 39, 18, 71, 41] are routinely utilized in regular FEM problems. Moreover, degenerate cases of the isoparametric map have been used since the 1960s in the XFEM context see e.g. [52, 58, 62, 42, 17], because the transformations and their Jacobians have certain homogeneity properties that facilitate the integration of the transformed kernels.

The degenerate transformation that will be used throughout this work maps squares onto triangles and cubes onto pyramids, and hence it will be designated as pyramidal transformation, \mathcal{P} . The most general n -dimensional form of \mathcal{P} , and conditions for its invertibility in 2D and 3D, are given in chapter 2.

As already mentioned, the other major problem that arises in XFEM and BEM is the numerical integration of (near-)singular functions. It is a well-known fact that standard quadrature rules usually produce inaccurate results for these integrands, see e.g. [24, 45, 60, 69, 55, 49], whose derivatives take very large, or even infinite values within the integration domain.

In order to articulate the preceding ideas in a more specific way, we recall that the truncation error of a one-dimensional quadrature rule is defined (see e.g. [62]) as

$$E(f) \equiv \int_a^b w(x)f(x)dx - \sum_{i=1}^k w_i f(x_i),$$

where f is the integrand, w the weighting function, $[a, b]$ the integration interval, k the order of the rule and $\{w_i, x_i\}$ the weights and nodes, respectively, of the quadrature rule. A bound for the truncation error is given below.

Theorem 1. *Let f be a function with continuous derivatives up to order $2k - 1$ in $[a, b]$, and piecewise continuous derivative of order $2k$. Then*

$$|E(f)| \leq e_{2k} \sup_{x \in [a, b]} |f^{(2k)}(x)|,$$

with

$$e_{2k} = \frac{1}{(2k)!} \int_a^b w(x) [P_k(x)]^2 dx,$$

in the case of a Gaussian rule, and P_k the monic polynomial whose zeros are the nodes of the quadrature formula.

Proof. Refer to [62], section 4.2. □

This implies that a further regularizing map, denoted \mathcal{R} throughout this work, is needed to attenuate, or soften, the remaining singularities in the integrand. In order to formulate a systematic approach, \mathcal{R} will always transform the standard parent domain onto itself.

Even though the regularization \mathcal{R} may appear completely independent from the pyramidal transformation \mathcal{P} , it will be justified in subsequent chapters that the Jacobian of \mathcal{P} actually helps building certain regularizing maps, that otherwise could not be implemented.

Another relevant aspect of \mathcal{R} is that, apart from softening the singularities in the integrand, it must be a smooth transformation itself, to avoid introducing new singularities in the process. This feature will introduce strong restrictions on the explicit form of the transformations proposed in the next chapters.

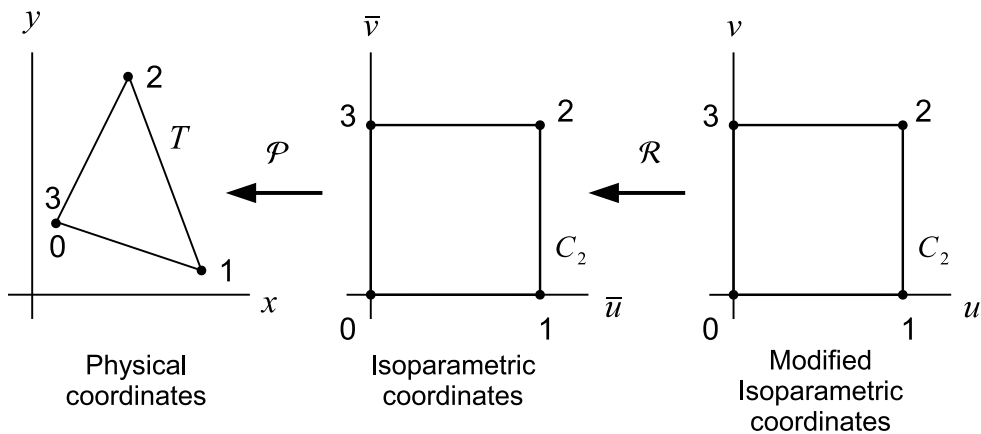


Figure 1.1.: Composition of Pyramidal and Regularizing maps in 2D

In order to illustrate the preceding paragraphs, Fig. 1.1 shows the composition of \mathcal{P} and \mathcal{R} in the two-dimensional case. As already mentioned, the integrands are (near-)singular functions of the physical (x, y) and isoparametric (\bar{u}, \bar{v}) coordinates, but are expected to be smooth functions when expressed in modified isoparametric coordinates (u, v) .

1.3. Transformation of quadrature rules

A quadrature rule Q over a standard closed domain D is defined by

$$Q(f) = \sum_{i=1}^{n_w} w_i f(\mathbf{u}_i), \quad (1.1)$$

where f is an integrable function over D , w_i and \mathbf{u}_i for $i = 1, \dots, n_w$ represent the weights and nodes associated to Q and n_w is the order of the rule.

A differentiable transformation $\mathcal{T} : D \subset \mathbb{R}^n \rightarrow T$ with positive Jacobian $J_{\mathcal{T}}$ from D onto a physical domain $T \subset \mathbb{R}^n$ allows to translate the rule Q from D to T . The quadrature rule is reformulated for an arbitrary integrand f over T as follows:

$$Q^*(f) = \sum_{i=1}^{n_w} w_i^* f(\mathbf{x}_i), \quad (1.2)$$

where the new weights and nodes are defined, for $i = 1, \dots, n_w$, by

$$w_i^* = J_{\mathcal{T}}(\mathbf{u}_i) w_i, \quad (1.3)$$

$$\mathbf{x}_i = \mathcal{T}(\mathbf{u}_i). \quad (1.4)$$

The scheme outlined above allows to perform integrations in the physical domain, by means of the weights and nodes of the modified quadrature rule (1.3)-(1.4), namely

$$\int_T f(\mathbf{x}) d\mathbf{x} \approx \sum_{i=1}^{n_w} w_i^* f(\mathbf{x}_i).$$

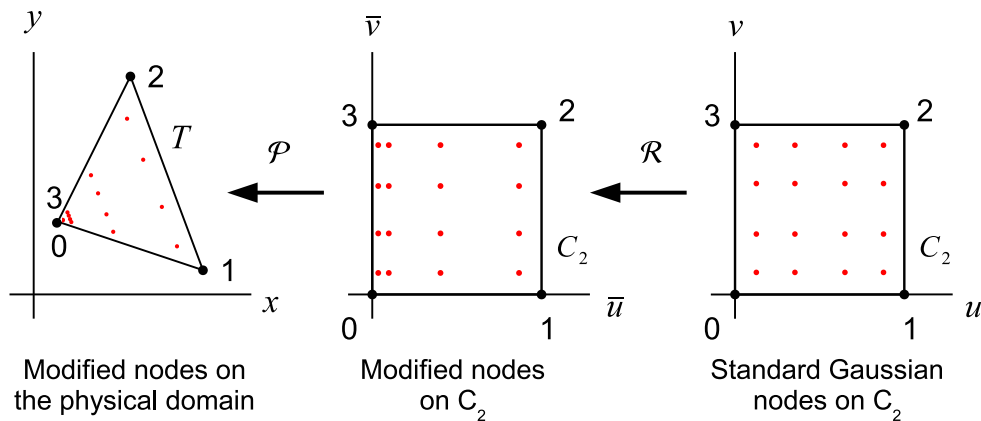


Figure 1.2.: Mapping of the quadrature rule nodes

Instead of changing variables in the physical integrand and computing (1.1) in the parent domain, it is much more efficient, from an implementation point of view, to

apply the transformations to a given set of standard weights and nodes and calculate the quadrature by means of (1.2), see e.g. [43, 57, 55, 3]. In our approach, the transformation \mathcal{T} is simply the result of composing the pyramidal and regularizing mappings, i.e.

$$\mathcal{T} = \mathcal{P} \circ \mathcal{R}.$$

All methods presented in this work make use of standard Gauss-Legendre rules exclusively, as illustrated in Fig. 1.2 for the two-dimensional case. The standard Gaussian nodes are mapped by the regularizing transformation \mathcal{R} onto the unit square $C_2 = [0, 1]^2$ in coordinates (\bar{u}, \bar{v}) . Furthermore, a pyramidal transformation \mathcal{P} maps the nodes onto the physical domain T , in coordinates (x, y) .

One feature shared by all (near-)singular methods, see e.g. [64, 31, 45, 60, 51, 34], is that the modified nodes, instead of being evenly distributed all over the physical domain, are clustered towards the singular point, namely vertex 0 of the triangle T in Fig. 1.2. This vertex corresponds to side 03 of the square in coordinates (\bar{u}, \bar{v}) , where the modified nodes have already gathered.

It should be pointed out, however, that too much clustering around the singular point does not necessarily improve the performance of a particular rule, since there should be enough points all through the rest of the element to compute the integral in an accurate way, see e.g. [32, 15].

2. The isoparametric and pyramidal transformations

2.1. The isoparametric transformation

The isoparametric transformation is a widely established technique in FEM problems (see e.g. [9, 18]). Its formulation in the n -dimensional case starts by considering the first-order shape functions in the unit interval, namely:

$$\begin{aligned} N_0(u) &= 1 - u, \\ N_1(u) &= u. \end{aligned}$$

By a tensor product method, it is easy to build the multilinear shape functions for the unit hypercube $C_n = [0, 1]^n$:

$$N_{\mathbf{i}}(\mathbf{u}) = \prod_{j=1}^n N_{i_j}(u^j), \quad (2.1)$$

where $\mathbf{i} = i_1 \cdots i_n$ is the multi-index with $i_j \in \{0, 1\}$ and $\mathbf{u} = (u^1, \dots, u^n)$ are the parent coordinates. The shape functions in (2.1) are the product of polynomials of degree one in each parent coordinate. As an example in 3D, with the usual notation $\mathbf{u} = (u, v, w)$, we have that $N_{010}(u, v, w) = (1 - u)v(1 - w)$.

The 2^n vertices of C_n can be mapped onto an arbitrary set $S = \{\mathbf{x}_{\mathbf{i}} \in \mathbb{R}^n : \mathbf{i} \in I_n\}$, with $I_n = \{0, 1\}^n$, of 2^n points in \mathbb{R}^n by the isoparametric transformation

$$\mathbf{x}(\mathbf{u}) = \sum_{\mathbf{i} \in I_n} N_{\mathbf{i}}(\mathbf{u}) \mathbf{x}_{\mathbf{i}}, \quad (2.2)$$

for all $\mathbf{u} \in C_n$.

The shape functions satisfy the interpolation property (see e.g. [18]): if $\mathbf{u}_{\mathbf{j}}$ is the \mathbf{j} -th vertex of C_n then $N_{\mathbf{i}}(\mathbf{u}_{\mathbf{j}}) = \delta_{\mathbf{i}\mathbf{j}}$, $\mathbf{i} \in I_n$, with $\delta_{\mathbf{i}\mathbf{j}}$ being the Kronecker tensor. It follows that (2.2) maps the vertices of C_n onto S : $\mathbf{x}(\mathbf{u}_{\mathbf{j}}) = \mathbf{x}_{\mathbf{j}}$. A consequence of this fact is the Partition of Unity (PU) property of the shape functions:

$$\sum_{\mathbf{i} \in I_n} N_{\mathbf{i}}(\mathbf{u}) = 1, \quad (2.3)$$

and since $N_{\mathbf{i}}(\mathbf{u}) \geq 0$ for $\mathbf{i} \in I_n$, we conclude that (2.2) expresses $\mathbf{x}(\mathbf{u})$ as a convex combination of the points $\mathbf{x}_{\mathbf{i}} \in S$. The image of C_n by this transformation is usually

called a multilinear element (see e.g. [19, 29, 66, 39, 18, 71, 13]). It is worth mentioning that the image of C_n through the isoparametric transformation may not fill the convex hull of the points \mathbf{x}_i , and thus a multilinear element need not be a convex set itself.

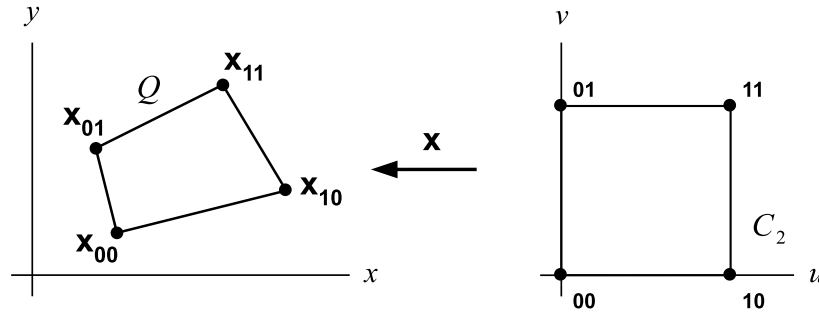


Figure 2.1.: Isoparametric transformation in 2D

In 2D, the element defined by (2.2) is the quadrilateral Q shown in Fig. 2.1, whereas in 3D the isoparametric element is the 8-node, curved-face hexahedron H displayed in Fig. 2.2.

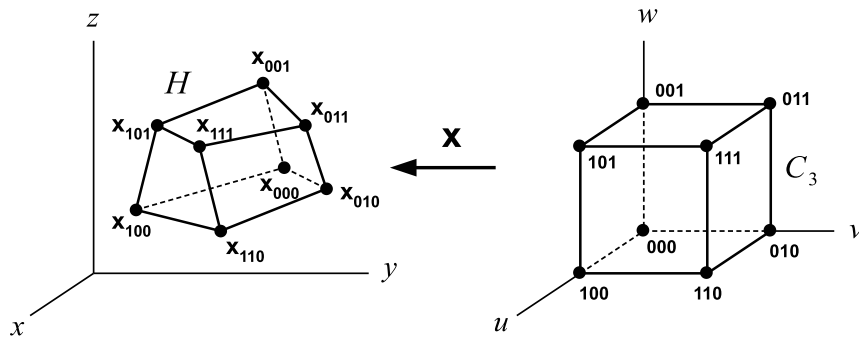


Figure 2.2.: Isoparametric transformation in 3D

2.2. The pyramidal transformation, \mathcal{P}

Apart from transforming a physical element onto the standard hypercube C_n , there are other algebraic properties of the coordinate change that may be desirable in certain situations, particularly when the integrand is singular.

For example, if the singular integrand is a homogeneous function, the use of a transformation that has, at least partially, separated variables may result in one or more variables factored out from the rest of the integral kernel, see e.g. [62]. Moreover, the Jacobian of the transformation may contribute to the total or partial cancellation of the singularity itself.

To this purpose, we focus now on isoparametric maps that are homogeneous in the first parent coordinate when \mathbf{x}_0 is taken as the origin, i.e.

$$\mathbf{x}(\mathbf{u}) - \mathbf{x}_0 = u\mathbf{r}(\mathbf{v}), \quad (2.4)$$

where $\mathbf{u} = (u, v^1, \dots, v^{n-1}) = (u, \mathbf{v})$ and $\mathbf{r}(\mathbf{v})$ is a linear combination of shape functions, that are polynomials of degree one in each of the variables v^1, \dots, v^{n-1} .

Since the general isoparametric transformation (2.2) is affine in each variable, it follows that

$$\mathbf{x}(\mathbf{u}) = (1 - u)\mathbf{x}(0, \mathbf{v}) + u\mathbf{x}(1, \mathbf{v}). \quad (2.5)$$

Hence, (2.5) takes the form (2.4) if and only if $\mathbf{x}(0, \mathbf{v}) = \mathbf{x}_0$ for $\mathbf{v} \in C_{n-1}$, or, by the PU property (2.3), when $\mathbf{x}_{0i_2 \dots i_n}$ collapse into \mathbf{x}_0 . It follows from (2.4) that

$$\mathbf{r}(\mathbf{v}) = \mathbf{x}(1, \mathbf{v}) - \mathbf{x}_0$$

and thus the base of the element, i.e. the points for which $u = 1$, corresponds to the $(n - 1)$ -dimensional face of a multilinear element. If we assume that $\mathbf{x}_{1i_2 \dots i_n} \neq \mathbf{x}_0$ it is then clear that $\mathbf{r}(\mathbf{v}) \neq \mathbf{0}$ for $\mathbf{v} \in C_{n-1}$. Indeed, the geometric interpretation of $\mathbf{r}(\mathbf{v})$ is the radius vector of the base points, $\mathbf{x}(1, \mathbf{v})$, measured from \mathbf{x}_0 .

The n -dimensional simplex has been considered in [58, 8] and an n -dimensional pyramid, with hyperplanar base, in [7]. However, the most general element for which a u -homogeneous degenerate map can be formulated is the curved-base pyramid obtained by collapsing all vertices of an $(n - 1)$ -dimensional face onto an apex \mathbf{x}_0 , as described above. This motivates the naming of (2.4) as pyramidal transformation, that will be denoted by \mathcal{P} throughout this work.

Particular cases of (2.4) in the lowest dimensions are commonly referred in the engineering literature as Duffy transformations [11, 49, 50, 47, 7], although the name ‘‘almost polar transformation’’ was introduced in [43] and the name ‘‘alpha-beta system’’ has been used in [56]. The term ‘‘Duffy-type’’ has also been used for other cases of non-homogeneous degenerate isoparametric mappings, formulated over non-pyramidal elements such as prisms, see e.g. [41], p. 188 for a three-dimensional example.

2.2.1. The pyramidal transformation in 2D

A number of (near-)singular methods in 2D make use of a degenerate isoparametric map that allows the representation of an arbitrary triangular element by means of the standard unit square $C_2 = [0, 1]^2$.

We start by denoting $\mathbf{x}_0 = \mathbf{x}_{00}, \mathbf{x}_1 = \mathbf{x}_{10}, \mathbf{x}_2 = \mathbf{x}_{11}, \mathbf{x}_3 = \mathbf{x}_{01}$ the vertices of Q in Fig. 2.1. Hence, the isoparametric transformation (2.2) takes the form

$$\mathbf{x}(u, v) = (1 - u)(1 - v)\mathbf{x}_0 + u(1 - v)\mathbf{x}_1 + uv\mathbf{x}_2 + (1 - u)v\mathbf{x}_3. \quad (2.6)$$

It is a well-known fact that the bilinear transformation (2.6) is invertible if and only if Q is convex, see e.g. [19, 40]. When the vertex \mathbf{x}_3 collapses onto \mathbf{x}_0 , the quadrilateral Q becomes a triangle T with vertices $\{\mathbf{x}_0, \mathbf{x}_1, \mathbf{x}_2\}$ (see Fig. 2.3), and the pyramidal transformation (2.4) can be written as

$$\mathbf{x}(u, v) = \mathbf{x}_0 + u\mathbf{r}(v), \quad (2.7)$$

with

$$\mathbf{r}(v) = (1 - v)(\mathbf{x}_1 - \mathbf{x}_0) + v(\mathbf{x}_2 - \mathbf{x}_0), \quad (2.8)$$

and Jacobian

$$J_{\mathcal{P}}(u, v) = 2|T|u, \quad (2.9)$$

where $|T|$ is the area of the triangle.

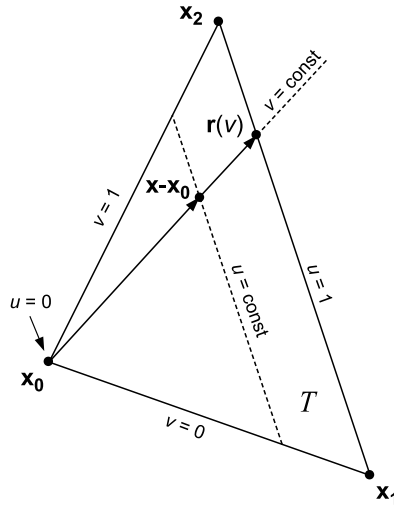


Figure 2.3.: Pyramidal element in 2D

For the standard triangle T_1 with vertices $\mathbf{x}_0 = (0, 0), \mathbf{x}_1 = (1, 0), \mathbf{x}_2 = (1, 1)$, the pyramidal transformation takes the usual form [11, 44, 49, 3]:

$$\mathbf{x}(u, v) = (u, uv), \quad (2.10)$$

$$J_{\mathcal{P}}(u, v) = u. \quad (2.11)$$

It should be pointed out that several authors, see e.g. [42, 36, 2, 34, 35] use the biunit square $[-1, 1]^2$ as the parent domain. Even though the unit and biunit squares are easily related by an affine transformation, the unit square enables the u -homogeneity property in (2.7) and (2.9), that no longer holds when expressing the transformations over $[-1, 1]^2$.

2.2.2. Polar coordinates

When integrating over triangles, some authors use polar coordinates to transform the physical domain, e.g. [24, 2, 33, 60], whereas others prefer a degenerate isoparametric map [11, 49, 56, 3]. A relationship between both schemes is now derived.

It has already been mentioned that $\mathbf{r}(v)$ in (2.8) is the radius vector of the points belonging to the edge $\mathbf{x}_1\mathbf{x}_2$, measured from \mathbf{x}_0 (Fig. 2.3). Let v_p denote the value of v corresponding to the triangle height, h_T (Fig. 2.4, left), noting that v_p need not belong to the interval $[0, 1]$. It is then clear (Fig. 2.4, right) that:

$$|\mathbf{r}(v)| = |\mathbf{x}_1 - \mathbf{x}_2| \left((v - v_p)^2 + \varepsilon_v^2 \right)^{1/2}, \quad (2.12)$$

where the parameter

$$\varepsilon_v = \frac{h_T}{|\mathbf{x}_1 - \mathbf{x}_2|} = \frac{2|T|}{|\mathbf{x}_1 - \mathbf{x}_2|^2}, \quad (2.13)$$

represents a triangle form factor that takes small values whenever the height of T is small compared to the length of the opposite site or, alternatively, when the area of T is small compared to that of the square of side $|\mathbf{x}_1 - \mathbf{x}_2|$.

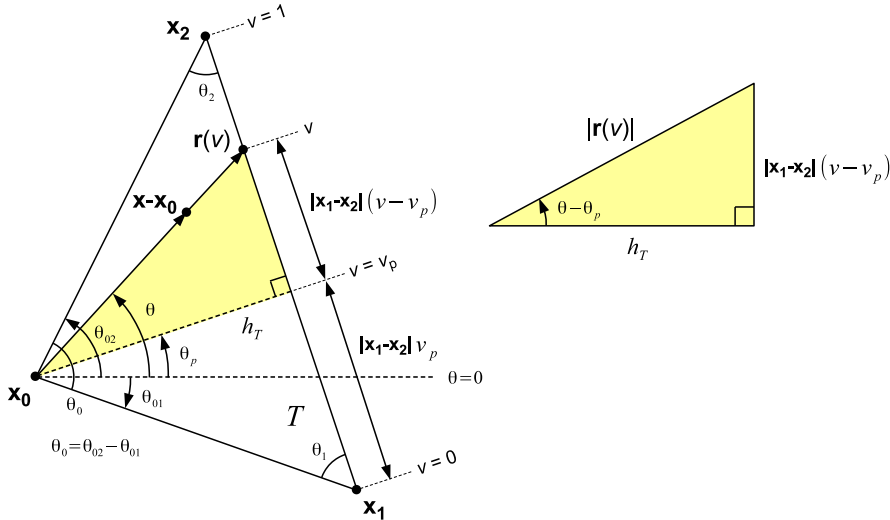


Figure 2.4.: Relationship between Pyramidal and Polar transformations

The conventional polar transformation is given by

$$\begin{aligned} x(\rho, \theta) &= x_0 + \rho \cos \theta, \\ y(\rho, \theta) &= y_0 + \rho \sin \theta, \\ J(\rho, \theta) &= \rho, \end{aligned}$$

with $\theta \in [\theta_{01}, \theta_{02}]$ and $\rho \in [0, R(\theta)]$ (Fig. 2.4), where we have defined

$$R(\theta) = |\mathbf{r}(v(\theta))|.$$

According to (2.7) it is immediate that

$$\rho = |\mathbf{x} - \mathbf{x}_0| = uR(\theta).$$

On the other hand, it is clear from Fig. 2.4, right, that

$$\tan(\theta - \theta_p) = \frac{|\mathbf{x}_1 - \mathbf{x}_2|}{h_T}(v - v_p),$$

where θ_p is the polar angle corresponding to the triangle height. Taking (2.13) into account we finally obtain

$$u(\rho, \theta) = \frac{\rho}{R(\theta)}, \quad (2.14)$$

$$v(\theta) = v_p + \varepsilon_v \tan(\theta - \theta_p). \quad (2.15)$$

This means that the polar (ρ, θ) and isoparametric (u, v) schemes are essentially interchangeable, and it motivates naming u as the radial variable and v as the angular one. However, the isoparametric system seems more straightforward due to the fact that the triangle is represented by a unit square, whereas in polar coordinates a curved domain is obtained. It is worth mentioning that a relationship between the polar and pyramidal transformation was derived in [47] for the particular case of the triangle T_1 (sec. 2.2.1), pointing out their similarities.

2.2.3. The pyramidal transformation in 3D

In 3D, the vertices \mathbf{x}_{001} , \mathbf{x}_{010} and \mathbf{x}_{011} of the 8-node hexahedron (Fig. 2.2) collapse onto \mathbf{x}_0 . A trilinear pyramid P is then obtained (Fig. 2.5) with 5 faces (4 of them triangles), 8 edges and 5 vertices. In general, the four vertices $\mathbf{x}_{1i_2i_3}$ are not coplanar, but rather belong to a doubly ruled surface (a hyperbolic paraboloid). The vertex $\mathbf{x}_0 = \mathbf{x}_{000}$ is usually called the pyramid apex.

With the usual notation $\mathbf{u} = (u, \mathbf{v}) = (u, v, w)$, the pyramidal transformation (2.4) takes the form

$$\mathbf{x}(\mathbf{u}) - \mathbf{x}_0 = u\mathbf{r}(v, w). \quad (2.16)$$

We remark that the most general 3D isoparametric element for which (2.16) exists is the curved-base pyramid in Fig. 2.5, and therefore other common elements in the FEM context, such as 6-node pentahedra, with triangular prisms as particular cases [38, 41] and 8-node non-degenerated hexahedra [70, 18] are excluded from a u -homogeneous transformation. These elements can always be partitioned into pyramids or tetrahedra, see e.g. [48].

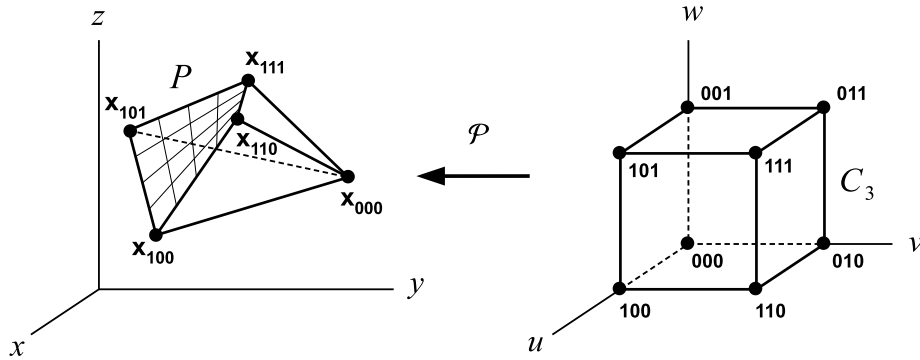


Figure 2.5.: Pyramidal transformation in 3D

For the standard pyramid P_1 [11, 49] with vertices $(0, 0, 0)$, $(1, 0, 0)$, $(1, 0, 1)$, $(1, 1, 0)$ and $(1, 1, 1)$ the pyramidal transformation (2.16) reduces to

$$\begin{aligned}\mathbf{x}(\mathbf{u}) &= (u, uv, uw), \\ J_{\mathcal{P}}(\mathbf{u}) &= u^2.\end{aligned}$$

Tetrahedra are obtained by collapsing two additional pyramid vertices, excluding the apex. If we make \mathbf{x}_{101} collapse with \mathbf{x}_{100} , (2.16) becomes

$$\begin{aligned}\mathbf{x}(\mathbf{u}) - \mathbf{x}_0 &= u(-\mathbf{x}_0 + (1-v)\mathbf{x}_{100} + v(1-w)\mathbf{x}_{110} + vw\mathbf{x}_{111}), \\ J_{\mathcal{P}}(\mathbf{u}) &= u^2vV_{10} = 6u^2vV_T,\end{aligned}\quad (2.17)$$

where V_T is the volume of the tetrahedron determined by \mathbf{x}_0 , \mathbf{x}_{100} , \mathbf{x}_{110} , \mathbf{x}_{111} . For the standard tetrahedron T_1 with vertices $(0, 0, 0)$, $(1, 0, 0)$, $(1, 1, 0)$ and $(1, 1, 1)$, considered e.g. in [58], the transformation (2.17) reduces to

$$\begin{aligned}\mathbf{x}(\mathbf{u}) &= (u, uv, uvw), \\ J_{\mathcal{P}}(\mathbf{u}) &= u^2v.\end{aligned}$$

Similar expressions exist for different examples of tetrahedra, see e.g. [57].

2.2.4. The Jacobian of the pyramidal transformation in 3D

Considerable effort has been dedicated to establishing the (local) invertibility of the isoparametric map for 8-node hexahedra, see e.g. [40, 70, 66, 39]. Sufficient conditions exist but, to our knowledge, no necessary and sufficient algebraic conditions for positive Jacobian have been derived yet.

The reasonable algebraic complexity of the pyramidal transformation (2.16) makes it possible to find a closed expression for its Jacobian, as well as a necessary and sufficient algebraic condition for its invertibility.

Theorem 2. *The Jacobian of the pyramidal transformation in 3D is*

$$J_{\mathcal{P}}(\mathbf{u}) = u^2 \sum_{\mathbf{i} \in I_2} N_{\mathbf{i}}(\mathbf{v}) V_{\mathbf{i}}, \quad (2.18)$$

for all $\mathbf{u} \in C_3$, where $V_{\mathbf{i}}$ is the (signed) volume of the parallelepiped determined by the edges $\mathbf{x}_{1i_1i_2} - \mathbf{x}_0$, $\mathbf{x}_{11i_2} - \mathbf{x}_{10i_2}$ and $\mathbf{x}_{1i_11} - \mathbf{x}_{1i_10}$ of the pyramid, namely

$$V_{\mathbf{i}} = \begin{vmatrix} \mathbf{x}_{1i_1i_2} - \mathbf{x}_0 & \mathbf{x}_{11i_2} - \mathbf{x}_{10i_2} & \mathbf{x}_{1i_11} - \mathbf{x}_{1i_10} \end{vmatrix}.$$

Proof. The Jacobian of the transformation (2.16) is given by the determinant:

$$\begin{aligned} J_{\mathcal{P}}(\mathbf{u}) &= \begin{vmatrix} \frac{\partial \mathbf{x}(\mathbf{u})}{\partial u} & \frac{\partial \mathbf{x}(\mathbf{u})}{\partial v} & \frac{\partial \mathbf{x}(\mathbf{u})}{\partial w} \end{vmatrix} \\ &= u^2 \begin{vmatrix} \mathbf{r}(\mathbf{v}) & \frac{\partial \mathbf{r}(\mathbf{v})}{\partial v} & \frac{\partial \mathbf{r}(\mathbf{v})}{\partial w} \end{vmatrix}. \end{aligned} \quad (2.19)$$

A direct application of the PU property (2.3) yields

$$\mathbf{r}(\mathbf{v}) = \sum_{\mathbf{i} \in I_2} N_{\mathbf{i}}(\mathbf{v})(\mathbf{x}_{1i_1i_2} - \mathbf{x}_0), \quad (2.20)$$

and recalling that $N_{\mathbf{i}}(\mathbf{v}) = N_{i_1}(v)N_{i_2}(w)$ it is immediate to show that the partial derivatives of $\mathbf{r}(\mathbf{v})$ are

$$\frac{\partial \mathbf{r}(\mathbf{v})}{\partial v} = \sum_{i_2 \in I_1} N_{i_2}(w) (\mathbf{x}_{11i_2} - \mathbf{x}_{10i_2}), \quad (2.21)$$

$$\frac{\partial \mathbf{r}(\mathbf{v})}{\partial w} = \sum_{i_1 \in I_1} N_{i_1}(v) (\mathbf{x}_{1i_11} - \mathbf{x}_{1i_10}). \quad (2.22)$$

It is then clear that $\frac{\partial^2 \mathbf{r}(\mathbf{v})}{\partial v^2} = \frac{\partial^2 \mathbf{r}(\mathbf{v})}{\partial w^2} = 0$, from where it follows that

$$\frac{\partial^2 J_{\mathcal{P}}(\mathbf{u})}{\partial v^2} = \frac{\partial^2 J_{\mathcal{P}}(\mathbf{u})}{\partial w^2} = 0,$$

and this means that the Jacobian of \mathcal{P} is a polynomial of degree one in each of the variables v , w . Taking (2.19)-(2.22) into account it is immediate to show that the value of $J_{\mathcal{P}}$ at the vertex $\mathbf{x}_{1i_1i_2}$ is $V_{\mathbf{i}}$, which finishes the proof. \square

Corollary 3. *The necessary and sufficient condition for $J_{\mathcal{P}}$ to be positive in the interior of C_3 is that all $V_{\mathbf{i}} \geq 0$, with at least one positive volume.*

3. The singular integral in 2D

3.1. Overview

This chapter analyzes the two-dimensional singular integral

$$I = \iint_T \frac{g(\mathbf{x})}{f(\mathbf{x} - \mathbf{x}_0)} d\mathbf{x}, \quad (3.1)$$

where T is an arbitrary triangle, g represents a non-singular integrable function and f is an α -positively homogeneous function, i.e., $f(t\mathbf{x}) = t^\alpha f(\mathbf{x})$ for $t > 0$. We assume that \mathbf{x}_0 is a vertex (apex) of T (Fig. 2.3). We also assume that f vanishes nowhere apart from the origin. A typical example in terms of the Euclidean distance would be $f(\mathbf{x}) = |\mathbf{x}|^\alpha$, where the real parameter α is the singularity strength, with $\alpha < 2$ for (3.1) to be finite.

From now on, we denote the parent (isoparametric) coordinates as $\bar{\mathbf{u}} = (\bar{u}, \bar{v})$, and hold the notation $\mathbf{u} = (u, v)$ for the modified isoparametric coordinates (recall Fig. 1.1), that will be introduced later on. Hence, the transformation (2.7), rewritten here for convenience, becomes:

$$\mathbf{x}(\bar{u}, \bar{v}) = \mathbf{x}_0 + \bar{u}\mathbf{r}(\bar{v}), \quad (3.2)$$

$$J_{\mathcal{P}} = 2|T|\bar{u}. \quad (3.3)$$

Applying this transformation to the integral (3.1) results in

$$I = 2|T| \iint_{C_2} g(\mathbf{x}(\bar{\mathbf{u}})) \bar{u}^{1-\alpha} \phi(\bar{v}) d\bar{\mathbf{u}}, \quad (3.4)$$

where $C_2 = [0, 1]^2$ and the scalar function ϕ is given by

$$\phi(\bar{v}) = \frac{1}{f(\mathbf{r}(\bar{v}))}. \quad (3.5)$$

Hence, the application of (3.2)-(3.3) to (3.1) conveys a double benefit. On the one hand, the integration domain is transformed onto a unit square, where standard quadrature rules can be readily used. On the other hand, the homogeneous integrand in physical variables becomes factorized into a radial part

$$K_1(\bar{u}) = \bar{u}^{1-\alpha}, \quad (3.6)$$

depending on \bar{u} , and an angular part

$$K_2(\bar{v}) = \phi(\bar{v}). \quad (3.7)$$

that is a function of \bar{v} . This enables a separate treatment of each factor in the kernel by means of further transformations able to attenuate the remaining singularities in each part of the integrand. Furthermore, these reasons account for the convenience of splitting physical quadrilaterals into triangles before performing the numerical integration.

An additional advantage of applying (3.2)-(3.3) is that the factor \bar{u} in the Jacobian helps attenuating the singularity in the radial part, since $\bar{u}^{1-\alpha}$ is a softer function than $\bar{u}^{-\alpha}$, unless $\alpha = 1$, in which case the singularity is completely cancelled, see e.g. [11, 53, 49]. This effect compensates the increase in the degree of $g(\mathbf{x}(\bar{\mathbf{u}}))$, in the polynomial case, as shown by numerical experiments.

As already mentioned, the transformation (3.2) may not suffice to completely remove the singularities in the integrand. For example, the radial kernel K_1 in (3.6) is regular for integer α , but for non-integer α the successive derivatives of $\bar{u}^{1-\alpha}$ may be singular at $\bar{u} = 0$. In fact, if $\alpha > 1$ the integrand itself is still singular at $\bar{u} = 0$, as pointed out e.g. in [49].

On the other hand, the angular kernel $\phi(\bar{v})$ is non-singular since, according to sec. 2.2, \mathbf{r} does not vanish and neither does $f(\mathbf{r})$. However, it will be shown that ϕ may have near-singularities, i.e., points where the function and/or its derivatives take very large, yet finite values. These near-singularities are in fact induced by an unfavourable geometry of the physical elements, i.e., highly distorted triangles. Even though the integral (3.4) is performed over a standard domain, the angular kernel (3.7) still depends on the parameters \bar{v}_p and ε_v . Thus, transformations that incorporate information on the geometry of the element will be shown to perform better, in numerical simulations, than other alternatives that do not.

3.2. The regularizing transformation, \mathcal{R}

Numerical experiments show that the direct application of Gaussian quadrature rules to the integral (3.4) does not produce accurate results in the general case, see e.g. [24, 45, 60, 69, 55, 49]. It is then clear that a further transformation is needed in order to regularize the integral kernel, attenuating its remaining singularities.

More specifically, we consider an arbitrary differentiable transformation \mathcal{R} , that maps C_2 onto itself. The reason for maintaining a standard integration domain is that only the integrand singularities must be dealt with, therefore no additional singularities appear due to the transformed domain being distorted itself, as pointed out in e.g. [60, 3].

From now on we focus, for simplicity, on transformations with separated variables, whose parametric equations are

$$\bar{u} = \bar{u}(u), \tag{3.8}$$

$$\bar{v} = \bar{v}(v), \tag{3.9}$$

3.3 The radial kernel, $K_1(\bar{u})$

subject to the boundary conditions

$$\begin{aligned}\bar{u}(0) &= \bar{v}(0) = 0, \\ \bar{u}(1) &= \bar{v}(1) = 1,\end{aligned}$$

i.e., \bar{u} and \bar{v} transform the unit interval $[0, 1]$ onto itself. The transformations (3.8) and (3.9) will be referred as regularizing or softening transformations throughout this work.

Several strategies have been proposed to find the optimal forms of \bar{u} and \bar{v} . In general, all these transformations can be split into two categories:

1. Smooth transformations (a couple of typical examples are the sinh and cubic transformations) with the objective of obtaining a transformed kernel that is softer, to some degree, than the original one. We remark that the transformed kernel might still be a (near-)singular function, even though its sharpness has been reduced. These transformations will be designated “a priori” for the rest of this work.
2. Transformations obtained after imposing a certain regularization condition over the kernel, in order to turn it smooth. These transformations, also known as reciprocal methods [72], might be (near-)singular themselves, justifying the need for additional softening in the independent variables. These ones will be designated “a posteriori” transformations from now on.

A brief description of some of the schemes developed in the literature for radial and angular transformations is given in the next two sections.

3.3. The radial kernel, $K_1(\bar{u})$

The most obvious idea for attenuating the singular behaviour of K_1 might seem to augment the value of the exponent of \bar{u} , so the successive derivatives are softer functions. This can be accomplished by applying a power transformation, i.e., a smooth regularizing transformation given by

$$\bar{u}(u) = u^{\beta_1},$$

for some integer value of the exponent β_1 . This idea was first considered in [2] for the case $\beta_1 = 2$ and then developed in a more systematic way in [49] for the case where the regular integrand $g(\mathbf{x})$ is a polynomial basis function. The value of β_1 in [49] is taken as the lowest integer for which both $g(\mathbf{x}(\bar{\mathbf{u}}))$ and the radial kernel

$$\bar{u}^{-2\beta_1-1-\alpha\beta_1},$$

keep being polynomials in (\bar{u}, \bar{v}) . However, this can be done in an easy way only when α has a particular form, such as an integer or the quotient of small integers. In these

cases, as pointed out by the authors, the numerical results clearly demonstrate the superior accuracy and efficiency of the generalized transformation over the standard transformation with $\beta_1 = 1$.

On the other hand, if α has a more arbitrary form, there might not be any small integer β_1 such that the quantity $\alpha\beta_1$ is another integer, and in this case the performance of the method is seriously affected. These situations happen frequently in the XFEM literature, and need to be taken into account. For instance, the singularity near the tip of a sharp angular notch is of the type $\frac{1}{r^\alpha}$, where α depends on the notch angle.

Numerical experiments show that the optimal value of β_1 grows quickly with α , in case α is not the quotient of small integers. In consequence, the global performance of the method deteriorates for strong singularities with $\alpha > 1$, $\alpha \neq \frac{3}{2}$, due to the increased polynomial degrees. A new radial transformation that overcomes this problem will be described in sec. 3.5.

It is worth mentioning that a power transformation was already proposed in [58], such that its composition with the isoparametric mapping yields constant Jacobian. This transformation was applied to a multidimensional case involving non-singular integrands.

3.4. The angular kernel, $K_2(\bar{v})$

Depending on the actual form of f in (3.1), different transformations may be suitable or not. The most common example in practice, known as the algebraic kernel, occurs for $f(\mathbf{x}) = |\mathbf{x}|^\alpha$. In this case, recalling (2.12) and Fig. 2.4, the angular kernel in (3.5) can be expressed as

$$K_2(\bar{v}) = \phi(\bar{v}) = \frac{\phi_N(\bar{v})}{|\mathbf{x}_1 - \mathbf{x}_2|^\alpha},$$

where ϕ_N is the near-singular kernel in one dimension, given by

$$\phi_N(\bar{v}) = \left((\bar{v} - \bar{v}_p)^2 + \varepsilon_v^2 \right)^{-\alpha/2}, \quad (3.10)$$

with \bar{v}_p and ε_v as defined in sec. 2.2.2. We remark that ϕ_N is a dimensionless function, i.e. it does not depend on the absolute dimensions of the physical triangle, but rather on its shape, or form factor.

The near-singular algebraic kernel ϕ_N has received considerable attention over the last 30 years [24, 64, 65, 45, 46, 32, 15, 69, 22, 23]. The next paragraphs provide a geometric, descriptive motivation on where the difficulties to the numerical integration of ϕ_N arise. A more rigorous justification of the facts suggested here is developed in sec. 3.4.1.

It is commonly admitted that as the near-singularity perturbation ε_v in (3.10) becomes smaller, the integration of ϕ_N is more difficult when compared to triangles with large ε_v . Some recent works have considered extreme cases for which ε_v reaches

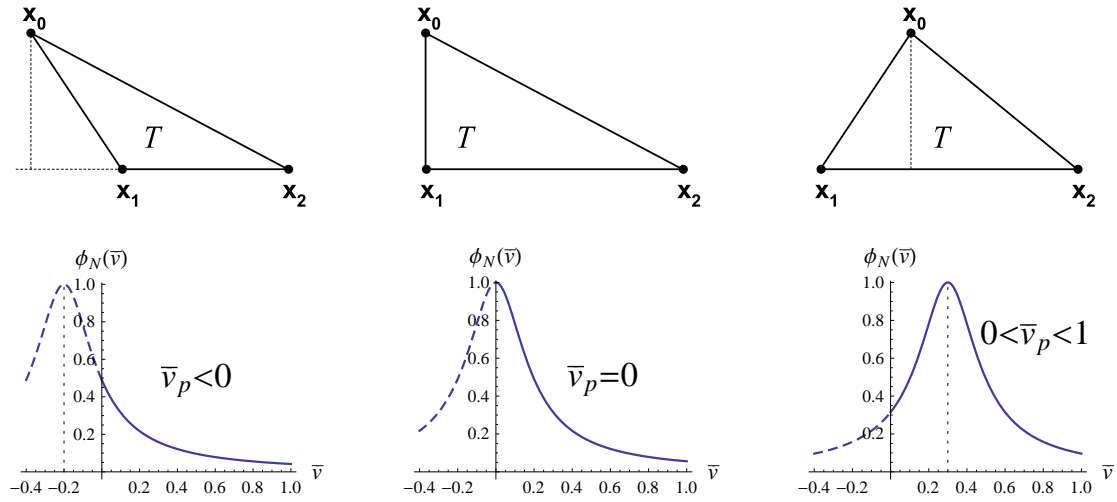


Figure 3.1.: Position of the peak point \bar{v}_p

10^{-10} or even less [22, 73, 23]. However, since this near-singularity is induced by the distortion of the triangular element, it is expected that ε_v will not be too small if a proper meshing has been performed.

On the other hand, it is clear from (3.10) that ϕ_N has a relative maximum at the peak point \bar{v}_p . Thus, it is expected that the integration of ϕ_N is more difficult whenever \bar{v}_p lies inside the integration interval, a circumstance that is also recognized by a number of authors, see e.g. [24, 6, 1, 46, 32, 33, 22, 23].

Three different examples of triangles are depicted in Fig. 3.1, for which the peak point lies outside, on the boundary or inside the interval $\bar{v} \in [0, 1]$ (the cases with $\bar{v}_p = 1$ and $\bar{v}_p > 1$ are easily obtained by symmetry). The situations in which \bar{v}_p is very close, or belongs to the interval $[0, 1]$ are expected to be the most difficult to deal with, specially if the perturbation ε_v is small, implying a narrow peak. The reader may refer to sec. 3.4.1 for a more rigorous justification on these heuristic arguments regarding ε_v and \bar{v}_p .

We remark that when both unfavourable conditions concur, i.e. $\varepsilon_v \ll 1$ and $\bar{v}_p \in (0, 1)$, an obtuse apex angle θ_0 is obtained (recall Fig. 2.4), which is commonly acknowledged as a difficult element to integrate on, see e.g. [24, 6, 1, 53, 46, 32, 33, 50, 22, 23]. Some authors perform interval splitting at \bar{v}_p [6, 1, 46, 32], whereas others recommend triangle bisection whenever $\theta_0 > \frac{2\pi}{3}$, see e.g. [60, 56, 34]. However, it will be justified in sec. 3.4.1 that there exist triangles with acute angle θ_0 , where the integration is as difficult as in the obtuse case.

A situation with large apex angle θ_0 may not be avoided in practice even if an adequate meshing is in place. A typical example would be the crack-growth problem considered in some XFEM applications. Since the mesh remains fixed and the position of the crack-tip varies with time, it may happen that the crack-tip is situated at an extremely close position to the triangle edges. If the physical triangle is split into subtriangles at the crack-tip, as it is usually the case, one or more of the

subtriangles may have very obtuse angles, and the transformation methods proposed in this chapter will likely fail to produce accurate results.

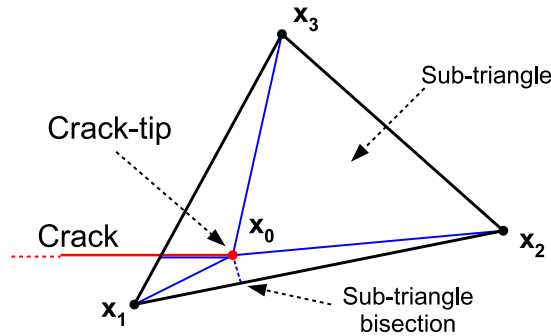


Figure 3.2.: Crack-tip and obtuse subtriangles

The obvious solution to this shortcoming would be to perform further splitting on the subtriangles in order to avoid very obtuse angles at the crack-tip, as illustrated in Fig. 3.2. Notice that this problem also affects the triangles that are adjacent to the crack-tip, that would need further splitting too. More details on how to implement softening transformations over adjacent triangles are given in sec. 4.6.

With respect to the existing integration methods in 2D, they usually focus on the cancellation of the radial singularity, whereas the angular variable may have possibly received less attention. For instance, [44] assumes that the angular kernel $\phi(\bar{v})$ is an innocuous function since it is regular for all \bar{v} . While this is true for standard integration domains, numerical experiments show that the truncation error is mainly contributed by the angular kernel if a seriously distorted triangle is employed.

A remarkable exception which does take the angular kernel into consideration is the method described in [2], that proposes a transformation on the polar angle of the form

$$t = \frac{1}{2} \log \left(\frac{1 + \sin(\theta - \theta_p)}{1 - \sin(\theta - \theta_p)} \right), \quad (3.11)$$

where θ takes values between θ_{01} and θ_{02} as in Fig. 2.4. Hence, (3.11) incorporates information on the geometry of the triangle, recall sec. 3.1. This map was first considered in [24] for near-singular integrals, and can be shown to be equivalent to a sinh transformation on the isoparametric variable \bar{v} , see Appendix B for details. The sinh transformation is analyzed in sec. 3.4.4 below.

Another transformation that is worth mentioning is the trigonometric mapping introduced in [53], that can be seen as the composition of a degenerate isoparametric

map and a regularizing transformation over the angular variable, given by

$$\begin{aligned}\bar{u}(u) &= u, \\ \bar{v}(v) &= \sin^2\left(\frac{\pi}{2}v\right).\end{aligned}$$

Unfortunately, neither this transformation nor its generalization to other exponents different from 2, incorporate any information on the geometric parameters \bar{v}_p and ε_v . Numerical experiments show that the performance of this trigonometric map is similar to the plain pyramidal transformation.

We next give some justification on how the appropriate softening transformations can be chosen for the angular algebraic kernel.

3.4.1. The complex poles of the algebraic kernel

There exist classical, well-known results that establish a relationship between the truncation error of Gaussian quadrature rules and the integrand complex poles, see e.g. [62, 10]. The key result for our purposes, following the exposition in [10], page 312, can be enunciated as follows.

Theorem 4. *The integration of a function f over the interval $[-1, 1]$ by means of a Gaussian quadrature rule has a truncation error that is bounded by*

$$|E_{G_k}(f)| \leq \frac{\pi(\rho + \rho^{-1})}{\rho^{2k+1}} \max_{z \in \mathcal{E}_\rho} |f(z)|, \quad (3.12)$$

with G being the Gaussian rule, k its order and \mathcal{E}_ρ an ellipse of semi-axis sum ρ , with foci at the endpoints of the integration interval, such that $f(z)$ is analytic in its interior.

Proof. Refer to [10], section 4.6. □

This result guarantees that the error bound in (3.12) decreases as the semi-axis sum ρ increases. However, the bound on $|f(z)|$ should also be taken into consideration, as it might grow for larger ellipses \mathcal{E}_ρ . Numerical experiments suggest that the error bound actually decreases for the kind of integrands considered in this work, and hence this question will not be further investigated.

Even though (3.12) applies to the symmetric interval $[-1, 1]$, this result can be immediately extended to the unit interval $[0, 1]$ through an affine transformation, with no effect on the truncation error, see Appendix D.

It is immediate to show that the equation of an ellipse with foci at points $(0, 0)$ and $(1, 0)$ is

$$\frac{\left(X - \frac{1}{2}\right)^2}{b^2 + \frac{1}{4}} + \frac{Y^2}{b^2} = 1,$$

from where it is clear that the semi-axis sum is a monotonically increasing function of the semi-minor axis b , namely

$$\rho(b) = b + \sqrt{b^2 + \frac{1}{4}}.$$

Therefore, the truncation error bound in the quadrature rule decreases as b increases. Since the uniparametric family of all non-intersecting confocal ellipses with foci at $(0, 0)$ and $(1, 0)$ fills the plane, the largest ellipse such that $f(z)$ is analytic in its interior will be referred as the ellipse of analiticity, see Fig. 3.3.

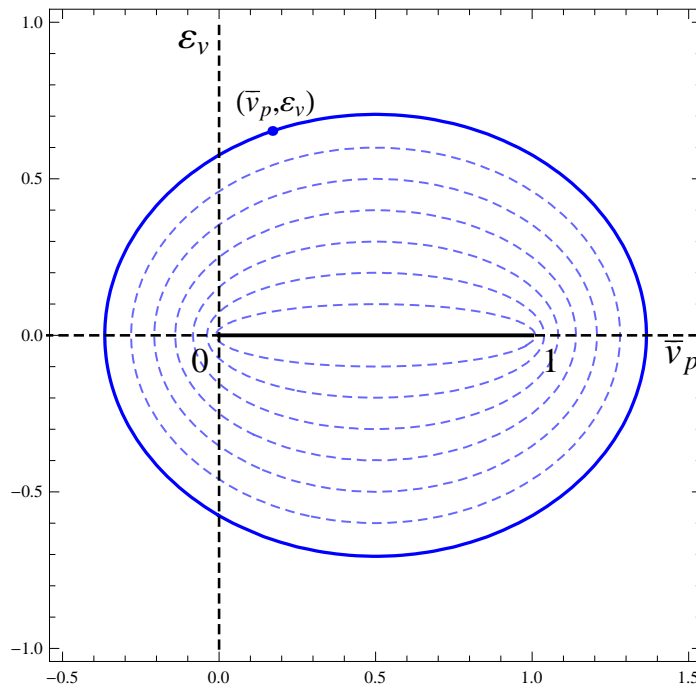


Figure 3.3.: Confocal ellipses and the ellipse of analiticity

This way, the semi-minor axis of this ellipse can be regarded as a measure of the distance from the kernel poles to the integration interval. In other words, a point (\bar{v}_p, ϵ_v) is said to be further away than another one from the integration interval $[0, 1]$ if its ellipse of analiticity has a larger semi-minor axis b , an idea that has been developed e.g. in [14].

In order to reduce the truncation error in the numerical quadratures, we will look for softening transformations capable of taking the complex poles of the integrand further away from the integration interval. More precisely, the near-singular kernel (3.10) has its poles originally located at

$$\bar{v} = \bar{v}_p \pm i\epsilon_v. \quad (3.13)$$

It is clear from the preceding discussion that both conjugate poles determine the same ellipse of analiticity, whose semi-minor axis b satisfies the equation

$$\frac{\left(\bar{v}_p - \frac{1}{2}\right)^2}{b^2 + \frac{1}{4}} + \frac{\varepsilon_v^2}{b^2} = 1.$$

Thus, the truncation error is expected to be large whenever (3.13) determine a small ellipse of analiticity, i.e., one with small values of b and $\rho(b)$. Fig. 3.4 shows several relative positions of the complex poles (3.13) in such a small ellipse.

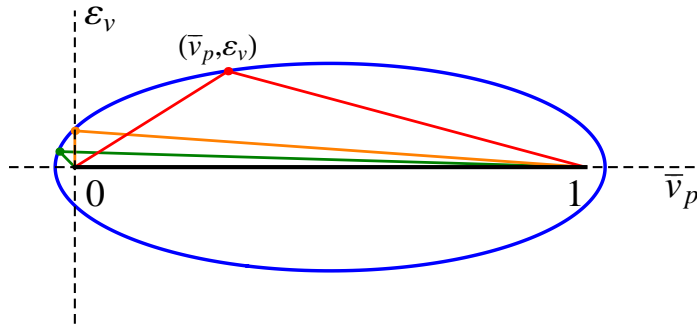


Figure 3.4.: Complex poles on a small ellipse of analiticity

An interesting outcome of this analysis is that physical triangles in coordinates (x, y) , recall sec. 2.2.2, are similar to the corresponding triangles displayed in Fig. 3.4, whose base is the interval $[0, 1]$ and its opposite vertex lies on the ellipse. This provides a more solid justification on the shape of unfavourable physical triangles. Triangles with very obtuse apex angles (coloured in red in Fig. 3.4) are not the only ones where integration is difficult, there also exist triangles with acute apex angles (in orange and green in Fig. 3.4) where the numerical quadrature is subject to the same error bound given in (3.12).

We conclude that, when (3.13) determine a small ellipse, softening transformations are necessary, with the purpose of producing a modified kernel with poles displaced to a new position in which a larger ellipse of analiticity can be drawn. The next subsections describe the general form of these transformations, together with a brief account on the most common examples.

3.4.2. The general form of the angular transformations

We are now concerned with softening transformations of the form

$$\bar{v}(v) = \bar{v}_p + h(t(v)), \quad (3.14)$$

where $h(t)$ is a non-linear, bijective function that maps $[0, 1]$ onto itself independently of \bar{v}_p , and $t(v)$ is an affine map of the form

$$t(v) = t_0 + (t_1 - t_0)v, \quad (3.15)$$

whose goal is to ensure that $\bar{v}(v)$ also maps $[0, 1]$ onto itself, i.e.

$$t_j = h^{-1}(j - \bar{v}_p), \quad j = 0, 1. \quad (3.16)$$

We remark that $j - \bar{v}_p$ need not belong to the interval $[0, 1]$, and hence the hypothesis of h being bijective in \mathbb{R} is necessary. The reason for this is that h transforms $t \in [t_0, t_1]$ onto $\bar{v} \in [-\bar{v}_p, 1 - \bar{v}_p]$, and this last interval can be placed anywhere on the real line. In case $\bar{v}_p = 0$, it is immediate from the definitions above that $t(v)$ becomes the identity.

We next consider a number of non-linear mappings, commonly employed in the near-singular integration context, that comply with the conditions specified above, and serve the purpose of moving the kernel poles further away from the integration interval, hence reducing the truncation errors.

3.4.3. The cubic transformation

The cubic transformation, introduced in [64], was one of the first attempts aimed at flattening the near-singular kernel ϕ_N . It is a transformation of the form

$$h(t, r) = rt + (1 - r)t^3, \quad (3.17)$$

where $r \in [0, 1]$ is a parameter to be established.

The cubic transformation is commonly acknowledged to have limited effectiveness due to the difficulty of finding the optimal value of r in (3.17). An approximate expression for optimal r was derived in [64] and extended in [33], but it has been established [61] that a deviation of 1% in the optimal value results in a severe loss of accuracy when computing the integrals involved.

A detailed analysis on the effect of the cubic transformation over the complex poles of ϕ_N allows to determine that the value of r for which those poles are moved furthest away from the integration interval (recall sec. 3.4.1) is

$$r_0(\varepsilon_v) = \frac{3}{2}\varepsilon_v^{2/3} \left[\left(\sqrt{1 + \varepsilon_v^2} + 1 \right)^{1/3} - \left(\sqrt{1 + \varepsilon_v^2} - 1 \right)^{1/3} \right], \quad (3.18)$$

$$= 3\varepsilon_v \sinh \left[\frac{1}{3} \sinh^{-1} \left(\frac{1}{\varepsilon_v} \right) \right]. \quad (3.19)$$

See chapter 6 for a proof of this statement.

3.4.4. The sinh transformation

The sinh transformation was first introduced, following an ‘‘a priori’’ reasoning, in [32], although equivalent maps had been proposed previously (see e.g. [24, 45]). It has found wide acceptance in the near-singular integration context ever since, see e.g. [60, 69, 3, 68, 73, 22, 23]. It is worth mentioning that [3] develops a systematic ‘‘a posteriori’’ approach to the sinh and other related transformations.

The explicit form of the transformation is

$$h(t) = \varepsilon_v \sinh(\mu t), \quad \mu(\varepsilon_v) = \sinh^{-1} \frac{1}{\varepsilon_v}. \quad (3.20)$$

Unlike the cubic transformation, the sinh transformation has no free parameter that needs to be optimized. The application of (3.20) to the near-singular kernel in (3.10) results in

$$\phi_N(\bar{v}(v)) = \frac{1}{\varepsilon_v^\alpha \cosh^\alpha(\mu t(v))},$$

with $t(v)$ as in (3.15)-(3.16). Thus, the new kernel poles coincide with the zeros of the cosh function. Since the closest of these zeros is at a distance $\frac{\pi}{2}$ from the real axis, it is straightforward to show that the transformed poles are located at

$$v = -\frac{t_0}{t_1 - t_0} + i \frac{\pi}{2\mu(t_1 - t_0)}.$$

A detailed analysis to establish that these transformed poles are in fact further away from the integration interval than the original poles is carried out in [14].

As already mentioned, other transformations proposed in the literature can be shown to be equivalent to sinh, refer to Appendix B for details.

3.4.5. The sigmoidal transformation

Yet another common alternative for the regularization of the angular kernel is the sigmoidal transformation. Nevertheless, it will be shown in this subsection that its softening effect is less clear than in the case of the cubic and sinh transformations, according to the behaviour of the transformed kernel poles.

There exist various maps that satisfy the requirements of a sigmoidal transformation, see e.g. [31]. One of the most common choices is

$$h(v) = \frac{v^\omega}{v^\omega + (1 - v)^\omega}, \quad (3.21)$$

with ω being an integer exponent of moderate value, usually $\omega = 2$. The sigmoidal transformation is applied over the polar angle θ , see e.g. [34]:

$$\theta(v) = \theta_{01} + (\theta_{02} - \theta_{01})h(v).$$

Therefore, the transformation for the isoparametric variable \bar{v} , taking (2.15) into account, becomes:

$$\bar{v}(v) = \bar{v}_p + \varepsilon_v \tan(\theta(v) - \theta_p). \quad (3.22)$$

In case of $\omega = 1$, it follows that $h(v) = v$ and (3.22) is equivalent to the angular part of the polar transformation (2.15).

The application of (3.22) to the near-singular kernel $\phi_N(\bar{v})$ in (3.10) produces a transformed kernel

$$\phi_N(\bar{v}(v)) = \frac{1}{\varepsilon_v^\alpha} \cos^\alpha(\theta(v) - \theta_p).$$

Thus, the poles of this kernel coincide with those of $h(v)$, that can be obtained by equating the denominator of (3.21) to zero:

$$v^\omega + (1 - v)^\omega = 0.$$

This equation is easily solved to

$$\begin{aligned} v &= \frac{1}{2} + \frac{i}{2} \frac{\sin \varphi_k}{1 + \cos \varphi_k} \\ &= \frac{1}{2} + \frac{i}{2} \tan \frac{\varphi_k}{2}, \end{aligned}$$

with $\varphi_k = \frac{\pi}{\omega}(1 + 2k)$, $k = 0, \dots, \omega - 1$. The real part of this poles takes the worst possible value, at the midpoint of the integration interval. On the other hand, the imaginary part of the closest pole to the real axis occurs for $k = 0$ and $k = \omega - 1$, and takes a value of $\pm \frac{1}{2} \tan \frac{\pi}{2\omega}$. Thus, the complex poles are moved closer to the real axis as ω grows, resulting in a smaller ellipse of analyticity, recall sec. 3.4.1.

A consequence of these facts is that the sigmoidal transformation is likely to have a limited efficiency, as confirmed by numerical experiments.

3.5. A new class of transformations

The previous section has revealed the remarkable fact that the singular integral in 2D, at least in the case of algebraic kernel, is closely related to the near-singular integration in 1D when the singular vertex, or apex, is close to the opposite edge. In consequence, well established near-singular techniques can be readily implemented on the angular variable of a truly singular integral in 2D. This fact, together with the exponent increase described in sec. 3.3, allows for the softening of both variables in the factorized kernel of (3.4).

Nevertheless, it is possible to find an a posteriori approach for the regularizing transformation, in both the radial and angular variables, that makes no assumption on the particular form of the angular kernel. The question is how to choose the most appropriate transformation, even assuming that none of them would suit all types of singularity.

In order for the integration rule to be efficient, the integrand should take the most adequate form. Since g remains arbitrary, we can only impose a condition over the singular part of the integrand, together with the Jacobian of the regularizing transformation \mathcal{R} . The simplest option occurs for the kernel becoming a constant. If \mathcal{R} has separated variables, as in (3.8)-(3.9), this condition reduces to

$$\bar{u}^{1-\alpha} \phi(\bar{v}) \frac{d\bar{u}}{du} \frac{d\bar{v}}{dv} = c_0, \quad (3.23)$$

where c_0 is a constant that depends on the singularity strength α and the physical triangle T (through the angular kernel ϕ), but not on the variables (u, v) .

We notice from (3.23) that the factor $\bar{u}^{1-\alpha} \frac{d\bar{u}}{du}$ depending on u must be a constant, because otherwise, when fixing the variable v and varying u , the product would not be a constant. The same holds for the variable v and hence (3.23) can be split into two first-order ordinary differential equations (ODE):

$$\bar{u}^{1-\alpha} \frac{d\bar{u}}{du} = c_1, \quad (3.24)$$

$$\phi(\bar{v}) \frac{d\bar{v}}{dv} = c_2, \quad (3.25)$$

subject to the boundary conditions

$$\begin{aligned} \bar{u}(0) &= \bar{v}(0) = 0, \\ \bar{u}(1) &= \bar{v}(1) = 1, \end{aligned}$$

with $c_1 c_2 = c_0$.

Since (3.24)-(3.25) are first-order equations, only one boundary condition can be imposed per equation, say $\bar{u}(0) = \bar{v}(0) = 0$. However, the constants c_1 and c_2 have not been fixed yet (they remain arbitrary), and this gives an additional degree of freedom that makes it possible to impose the second boundary condition $\bar{u}(1) = \bar{v}(1) = 1$. This way, the solution of (3.24) can be obtained in closed form:

$$\bar{u}(u) = u^{\frac{1}{2-\alpha}}, \quad (3.26)$$

$$c_1 = \frac{1}{2-\alpha}. \quad (3.27)$$

With respect to (3.25), it is clear that it might not be solvable in closed form, unless the angular kernel takes a very simple form. However, it can be solved numerically, as described next. We start by integrating both sides of (3.25) between 0 and $\bar{v}(v)$ to yield

$$F(\bar{v}) = c_2 v, \quad (3.28)$$

where F is the function defined by

$$F(\bar{v}) = \int_0^{\bar{v}} \phi(s) ds,$$

from where it follows

$$\begin{aligned} c_2 &= F(1), \\ \bar{v}(v) &= F^{-1}(c_2 v). \end{aligned}$$

Thus, \bar{v} is defined implicitly by (3.28). We remark that the invertibility of (3.28) is guaranteed by the Implicit Function Theorem, since $\frac{dF(\bar{v})}{d\bar{v}} = \phi(\bar{v})$, and according to (3.5), ϕ cannot vanish as long as f is well-defined in T .

The need to solve a differential equation that depends on the specific geometry of the element could, at first sight, compromise the efficiency of the method. However, it is a fundamental fact that this processing is necessary only at the nodes of the Gaussian quadrature rule. In other words, it suffices solving (3.28) over a discrete set of points. Newton's method provides a straightforward way to perform the inversion of the function F , as numerical experiments have made evident.

The increased cost of calculating the transformation at these points is justified by the considerable benefit of having a quadrature rule that achieves a high degree of precision with a lower number of integration nodes, and suitable for any regular function g . Details on how to implement Newton's method on (3.28) can be found in Appendix C.

3.5.1. Additional softening on the a posteriori transformation

The procedure outlined above allows to determine an a posteriori transformation, i.e., one whose equations are not chosen "up-front", but rather emerge as solutions of two ODEs. This approach has the obvious advantages that it can be applied to any singular integrand, and that it produces a constant kernel.

However, a significant shortcoming of this strategy comes from the fact that the functions \bar{u} , \bar{v} are not guaranteed to be smooth transformations themselves. In the case of the radial transformation, it is evident from (3.26) that the successive derivatives of \bar{u} can be singular at the origin, even for positive values of α , due to the fact that the exponent of u may not be an integer. Regarding the angular solution \bar{v} , it has already been mentioned in sec. 3.4 that the angular kernel may exhibit a near-singular behaviour for distorted triangles of the type shown in Fig. 3.4. These singularities are carried back to the regular part of the integrand through the composition $g(\mathbf{x}(\bar{\mathbf{u}}(\mathbf{u})))$, compromising the global efficiency of the algorithm.

The most obvious idea to help overcome this drawback is to relax the condition (3.23) by letting its right hand side be a polynomial, rather than forcing it to be a constant. Thus, the following modification to (3.24) is considered:

$$\bar{u}^{1-\alpha} \frac{d\bar{u}}{du} = c_1(n_1 + 1)u^{n_1}, \quad (3.29)$$

with n_1 being a positive integer that can be determined empirically. For example, if monomials up to degree two are used as the regular part of the integrand, i.e., $g(x, y) = x^i y^j$, $i + j \leq 2$ over the standard triangle T_1 (sec. 2.2.1), the optimal values of n_1 , for which the numerical quadrature converges faster, can be picked from Tab. 3.1.

The solution obtained in this case is

$$\bar{u}(u) = u^{\frac{n_1+1}{2-\alpha}}, \quad (3.30)$$

where the term $(n_1 + 1)u^{n_1}$ in (3.29) can be seen as the derivative of a softening polynomial $\sigma(u) = u^{n_1+1}$, that transforms $[0, 1]$ onto itself and produces a softer solution \bar{u} in (3.30). The value of c_1 in (3.29) is the same as in (3.27).

Table 3.1.: Optimal exponent n_1 for $\bar{u}(u) = u^{\frac{n_1+1}{2-\alpha}}$

α	< 0.5	< 0.9	< 1.2	< 1.5	< 1.7	< 1.9	< 2
n_1	6	5	4	3	2	1	0

We recall that the idea of increasing the exponent to soften \bar{u} has been used in [49], for α being an integer or the ratio of two small integers. The proposed transformation (3.30) can be readily used for any value of $\alpha < 2$, in other words, the exponent $\frac{n_1+1}{2-\alpha}$ need not be an integer for the quadrature rule to perform efficiently. Particularly, fast convergence rates are achieved for strong singularities with $\alpha > 1.5$.

Regarding the angular kernel, numerical experiments show that \bar{v} may be near-singular at one or both endpoints of the integration interval $[0, 1]$, depending on the singularity strength α and the geometry of the triangle T . This fact suggests the convenience of relaxing the condition in (3.25) by allowing its right-hand side to also have a polynomial form, namely

$$\phi(\bar{v}) \frac{d\bar{v}}{dv} = c_2 \frac{d\tau}{dv}, \quad (3.31)$$

where $\tau(v)$ is a polynomial that transforms $v \in [0, 1]$ onto itself. Unfortunately, there seems to be no straightforward procedure, apart from trial and error, to find such polynomials, due to the high sensitivity of the near-singularities in $\bar{v}(v)$ to the problem constraints α and $T(\bar{v}_p, \varepsilon_v)$.

Nevertheless, by moderately increasing the exponent of u in (3.30), the solution becomes smooth enough at the origin, and this makes the numerical feasible by means of a standard Gaussian rule, even though the degree of the rule needs to be slightly increased.

To summarize, the transformation that satisfies (3.30) and (3.28) is

$$\mathcal{R} : \begin{cases} \bar{u}(u) & = u^{\frac{n_1+1}{2-\alpha}}, \\ \bar{v}(v) & = F^{-1}(c_2 v), \\ J_{\mathcal{R}}(u, v) & = c_1 c_2 (n_1 + 1) u^{\frac{n_1-1+\alpha}{2-\alpha}} \frac{1}{\phi(\bar{v}(v))}, \end{cases} \quad (3.32)$$

and the composition with the pyramidal transformation \mathcal{P} is

$$\mathcal{P} \circ \mathcal{R} : \begin{cases} \mathbf{x}(u, v) & = \mathbf{x}_0 + u^{\frac{n_1+1}{2-\alpha}} \mathbf{r}(\bar{v}(v)), \\ J_{\mathcal{P} \circ \mathcal{R}}(u, v) & = 2|T| c_1 c_2 (n_1 + 1) u^{\frac{2n_1+\alpha}{2-\alpha}} \frac{1}{\phi(\bar{v}(v))}, \end{cases}$$

with \mathbf{x} in the physical triangle T .

3.5.2. An edge-singular kernel

The flexibility in equations (3.24)-(3.25), that make no previous assumption on the integrand form, allows us to consider different types of kernels, as long as they keep

being homogeneous functions of their coordinates. We develop in this subsection, for illustrative purposes, a very simple example of an edge-singular kernel.

We consider the function

$$f(\mathbf{x}) = (x - y)^\alpha,$$

over the triangle T_1 with vertices $(0, 0)$, $(1, 0)$ and $(1, 1)$. It should be pointed out that in this case, it is necessary that $\alpha < 1$ for the integral (3.1) to converge. Applying the pyramidal transformation (2.10)-(2.11) it follows

$$\begin{aligned} \mathbf{r}(\bar{v}) &= (1, \bar{v}), \\ \phi(\bar{v}) &= \frac{1}{(1 - \bar{v})^\alpha}, \end{aligned}$$

and the differential equation (3.25) takes the form

$$\frac{1}{(1 - \bar{v})^\alpha} \frac{d\bar{v}}{d\bar{v}} = c_2,$$

satisfying the boundary conditions $\bar{v}(0) = 0$ and $\bar{v}(1) = 1$. Hence, the solution can be obtained in closed form as

$$\bar{v}(v) = 1 - (1 - v)^{\frac{1}{1-\alpha}}.$$

In this case, both solutions \bar{u} and \bar{v} depend on non-integer powers, and thus additional softening is needed. More specifically, we introduce softening polynomials, namely integer powers u^{n_1+1} and $(1 - v)^{n_2+1}$, in the corresponding equations (3.24)-(3.25) to prevent the singular behaviour in the solutions. This way, the composite transformation $\mathcal{P} \circ \mathcal{R}$ becomes

$$\mathcal{P} \circ \mathcal{R} : \begin{cases} x &= u^{\frac{n_1+1}{2-\alpha}}, \\ y &= u^{\frac{n_1+1}{2-\alpha}} \left(1 - (1 - v)^{\frac{n_2+1}{1-\alpha}} \right), \\ J &= \frac{n_1+1}{2-\alpha} \frac{n_2+1}{1-\alpha} (x - y)^\alpha u^{n_1} (1 - v)^{n_2}. \end{cases} \quad (3.33)$$

The optimal exponents n_1 and n_2 in (3.33) can be chosen empirically depending on the values of $g(\mathbf{x})$ and α .

3.6. Numerical results

The algorithms described in the previous sections are now tested in a variety of situations, including the combination of different methods for the radial and angular variables. The underlying idea is to take advantage of the factorized kernel in (3.4) and apply independent transformations in \bar{u} and \bar{v} to produce a scheme that, by incorporating softening in both variables, is able to outperform other algorithms that focus in just one variable.

As already justified in sec. 1.3, integrations are always performed on the physical domain by means of modified nodes and weights, obtained from

$$\begin{aligned}\mathbf{x}_j &= \mathbf{x}(\bar{\mathbf{u}}(\mathbf{u}_j)), \\ w_j^* &= J_{\mathcal{P} \circ \mathcal{R}}(\mathbf{u}_j) w_j,\end{aligned}$$

for $j = 1, \dots, n_w$, where \mathbf{u}_j and w_j are the standard Gaussian nodes and weights, respectively, for the quadrature rule of order n_w .

The singular part of the physical integrand is the algebraic vertex-singular kernel given by $\frac{1}{|\mathbf{x}-\mathbf{x}_0|^\alpha}$. Regarding the regular part of the integrand, the following functions are considered:

$$g(x, y) = (x - x_0)^i (y - y_0)^j f_\ell(\theta),$$

with $i + j \leq d_m$, d_m is the total degree of monomials, $\theta = \tan^{-1} \frac{y-y_0}{x-x_0}$ and $f_\ell(\theta)$ is the angular part of the crack-tip, or branch functions [48, 2, 55, 63], given by:

$$\begin{aligned}f_1(\theta) &= \sin \frac{\theta}{2}, \\ f_2(\theta) &= \cos \frac{\theta}{2}, \\ f_3(\theta) &= \sin \frac{\theta}{2} \sin \theta, \\ f_4(\theta) &= \cos \frac{\theta}{2} \sin \theta.\end{aligned}$$

If no crack-tip function is being used, it suffices taking $f_0(\theta) = 1$.

The seven methods implemented for comparison purposes are:

- \mathcal{P} : Pyramidal transformation in 2D, as described in sec. 2.2.1. There is no regularization in any of the variables (\bar{u}, \bar{v}) .
- Trig: Trigonometric transformation [53] described in sec. 3.4. Like the case of the pyramidal transformation, this method implements no regularization in the parent coordinates (\bar{u}, \bar{v}) .
- Pow: Composition of \mathcal{P} with the power transformation [49] described in sec. 3.3. This method implements regularization in the radial variable only.
- PS (Power-Sinh): The method in [2], but expressed over C_2 , see sec. 3.3 and sec. 3.4. It is the composition of \mathcal{P} with a power transformation $\bar{u}(u) = u^2$ in the radial variable, and a sinh transformation (3.20) in the angular variable. Thus, softening in both variables is incorporated in this method, though the radial softening is only adequate for integer and half-integer values of α .
- Cub: It is built as a combination of methods. It consists of a pyramidal transformation \mathcal{P} , followed by a posteriori radial regularization (as described in sec. 3.5.1), together with a priori angular regularization by means of the cubic transformation (as outlined in sec. 3.4.3).

- Sinh: The same as Cub, but the angular regularization is accomplished by means of the sinh transformation described in sec. 3.4.4.
- ODE: Composition of \mathcal{P} with the entire a posteriori regularization described in sec. 3.5. Additional softening in the radial variable (3.30) has been applied, with exponents n_1 picked from Tab. 3.1. As already mentioned, no additional softening is applied in the angular variable, due to the high sensitivity of the solution to the algebraic and geometric problem constraints.

Numerical experiments The exact value of the integral

$$I = \iint_T \frac{(x - x_0)^i (y - y_0)^j f_\ell(\theta)}{|\mathbf{x} - \mathbf{x}_0|^\alpha} d\mathbf{x},$$

is evaluated by means of a high-degree rule. Each graphic displays the parameters d_m (monomial degree), f_ℓ (crack-tip function being used), α (singularity strength), β_1 (exponent in the power transformation), n_1 (exponent in the radial softening) and r_0 (optimal value of the cubic transformation).

Standard triangle T_1 All methods are initially tested on the standard triangle T_1 (sec. 2.2.1), with no crack-tip function, for the values

$$\alpha = -0.34, 0.23, 0.5, 0.79, 1, 1.22, 1.5, 1.83. \quad (3.34)$$

The corresponding results are shown in Fig. 3.5.

It is evident that methods with no regularization perform more poorly, even for integer or half-integer values of α , although the pyramidal transformation coincides with the power method for $\alpha = 1$. The trigonometric transformation behaves very similarly to \mathcal{P} for almost all values of α . The power transformation deteriorates for increasing values of α , unless $\alpha = 1.5$, whereas the Power-Sinh method is only competitive for integer and half-integer values of α . The three procedures that do implement true regularization in both variables (Cub, Sinh and ODE) perform consistently well.

Moderately distorted triangle A moderately distorted triangle, with vertices at $\mathbf{x}_0 = (0, 0)$, $\mathbf{x}_1 = (1, -2)$, $\mathbf{x}_2 = (1, 3)$ is also considered, for the same values of α as in (3.34). The corresponding results are shown in Fig. 3.6.

It is clear that all methods deteriorate when applied over an obtuse triangle, although the Cubic and Sinh transformations keep performing consistently well, with a slight advantage for the Sinh transformation. The ODE method shows a high sensitivity to the singularity strength, although it is able to outperform all methods for a certain range of intermediate α values.

Strongly distorted triangle Finally, a more demanding scenario on a strongly distorted triangle, including monomials of greater degree and a crack-tip function, is considered. More specifically, a triangle with vertices $\mathbf{x}_0 = (0, 0)$, $\mathbf{x}_1 = (1, -3)$, $\mathbf{x}_2 = (1, 7)$ is tested, with monomials of degree $d_m = 3$ and a crack-tip function $f_1(\theta)$. The results are shown in Fig. 3.7.

All methods show a similar behaviour as in the case of the moderately distorted triangle, although they all deteriorate to a greater extent, due to the more peaked integrand in both variables.

Conclusions Methods that regularize both parent coordinates are clearly superior to algorithms with softening in one or no variable. Furthermore, the proposed methods are able to perform consistently well for a variety of situations, including different integration domains, singularity strengths and integrand types. In the case where α is an integer or semi-integer, small values of the exponent β_1 for the power transformation described in sec. 3.3 suffice to attain a fast convergence. However, for more arbitrary values of α , the scheme introduced in sec. 3.5.1 shows a better performance.

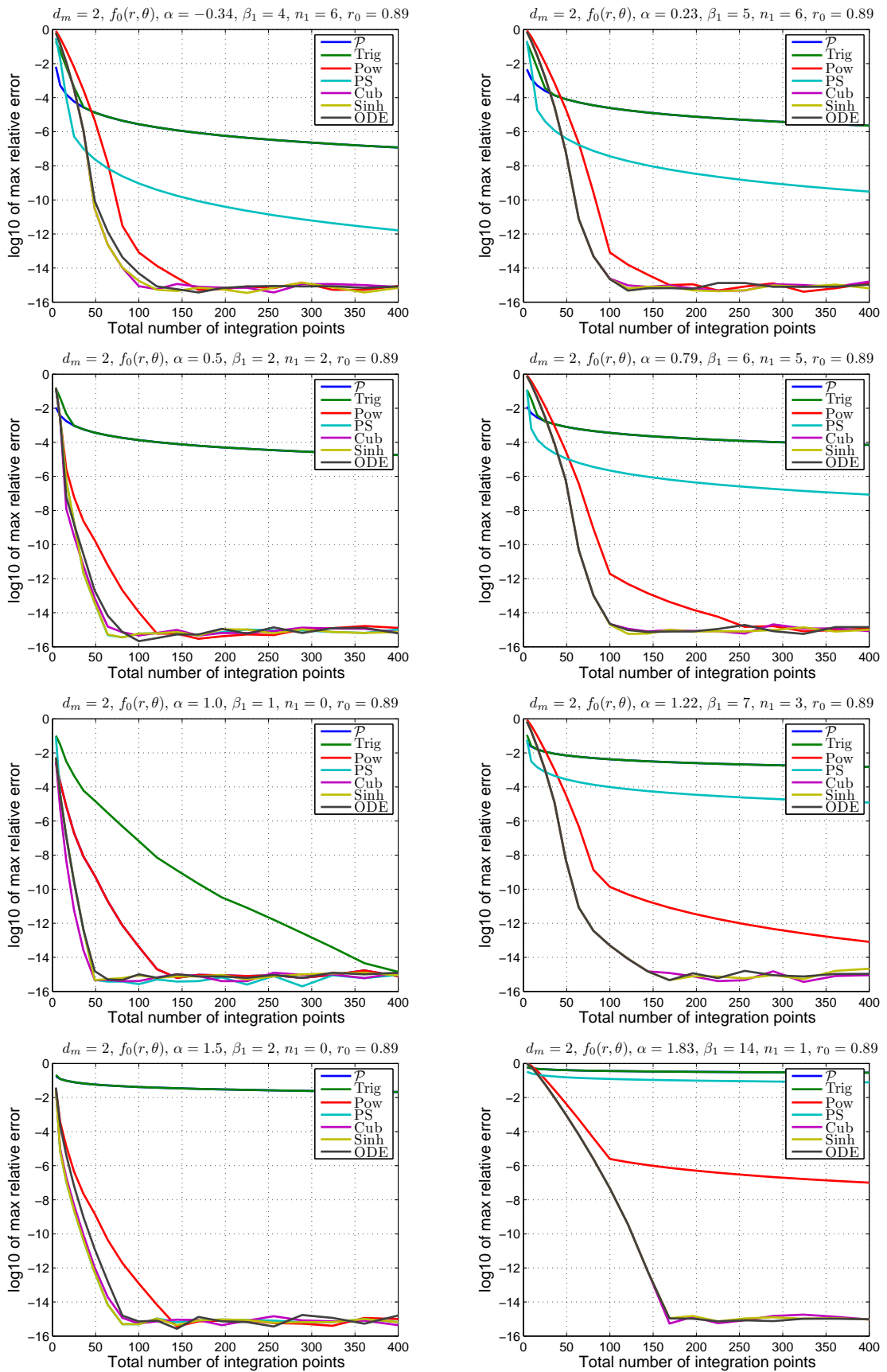


Figure 3.5.: Standard triangle T_1

3.6 Numerical results

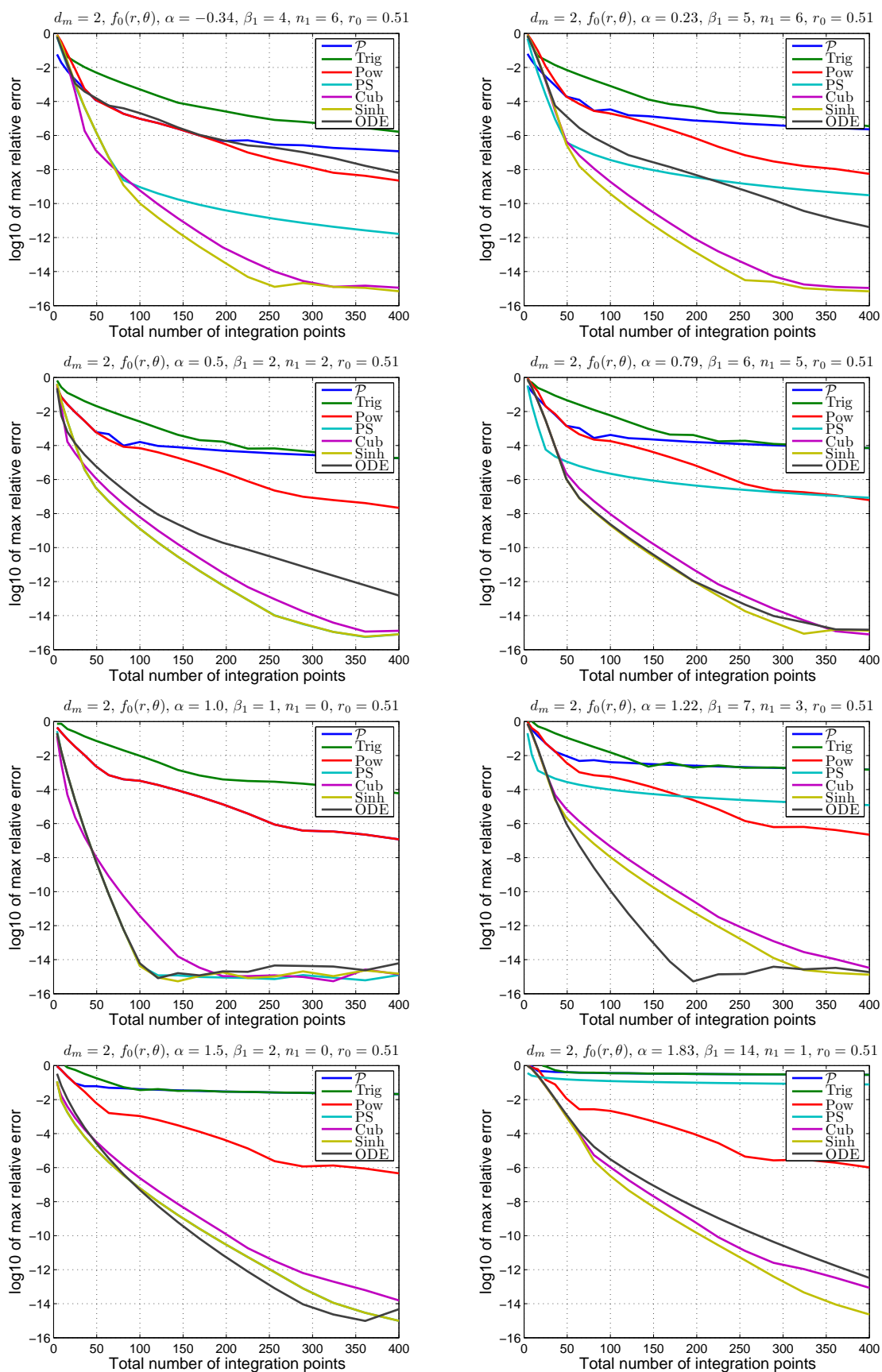


Figure 3.6.: Moderately distorted triangle

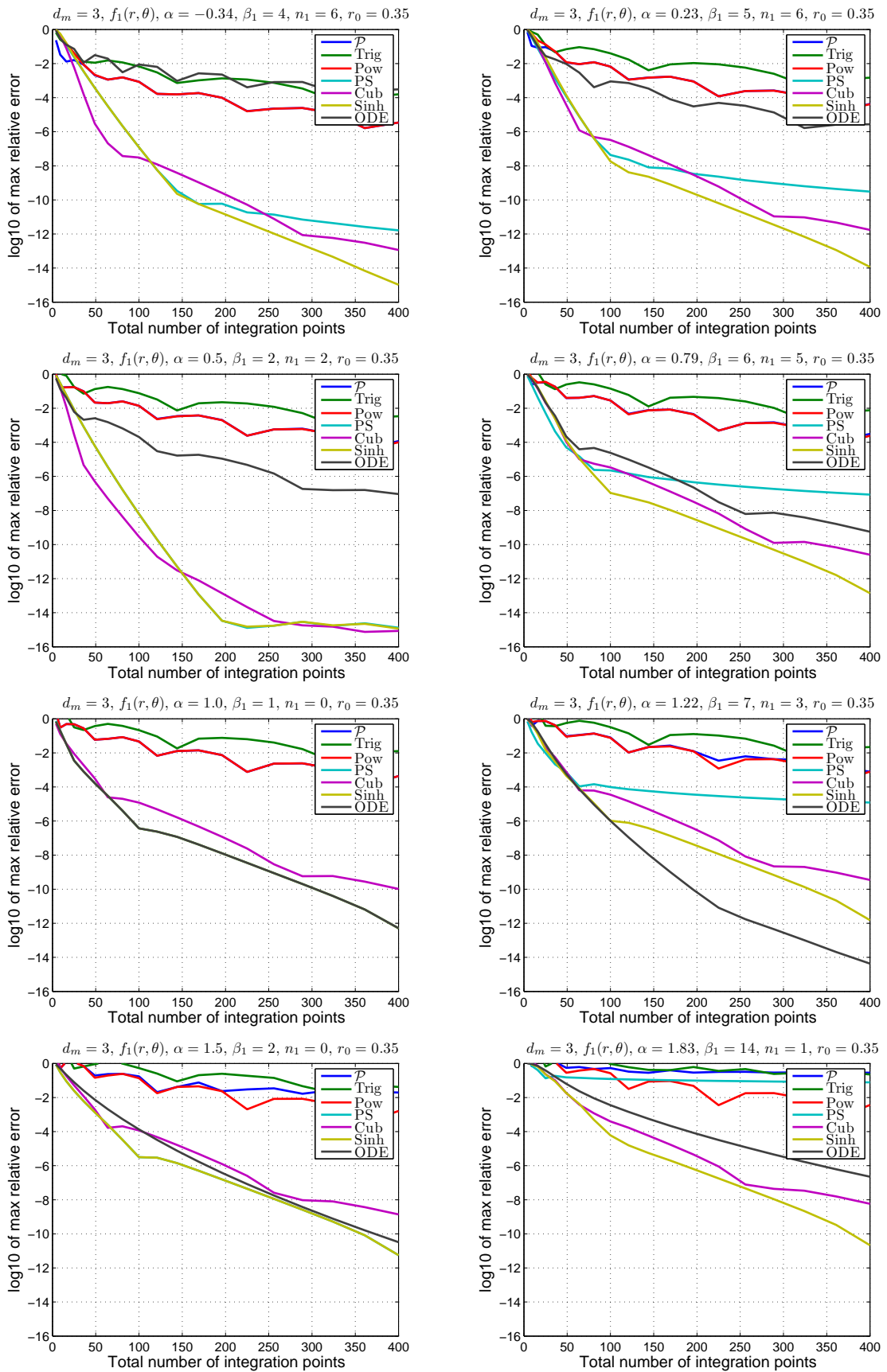


Figure 3.7.: Strongly distorted triangle

4. The near-singular integral in 2D

4.1. Overview

This chapter focuses on the near-singular integral with algebraic kernel

$$I = \iint_T \frac{g(\mathbf{x})}{(|\mathbf{x} - \mathbf{x}_0|^2 + \varepsilon^2)^{\alpha/2}} d\mathbf{x}, \quad (4.1)$$

where g is a non-singular integrable function, $\alpha \in \mathbb{R}$ is the singularity strength and T is an arbitrary triangle with vertices $\{\mathbf{x}_0, \mathbf{x}_1, \mathbf{x}_2\}$, as in chapter 3. The parameter ε is the algebraic near-singularity, that measures the distance between the point \mathbf{x}_s in Fig. 4.1 and its projection on the plane that contains the triangle T , that is assumed to be the triangle apex \mathbf{x}_0 .

In the BEM context, the point \mathbf{x}_s is commonly called source point, see e.g. [25, 46, 33, 22] and, in some contexts, observation point [37, 60]. The point \mathbf{x} is usually denominated field point, see e.g. [53, 45, 69]. It should be mentioned that in XFEM applications, the singular point lies in the same plane as the physical triangle, originating a different kind of near-singular integrals over adjacent elements. This situation will be briefly discussed in sec. 4.6.

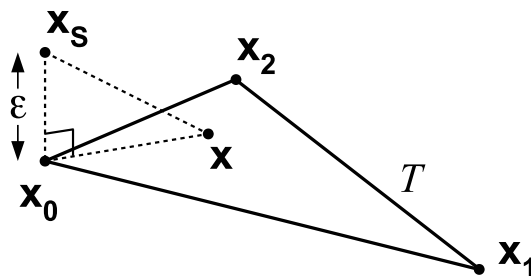


Figure 4.1.: The algebraic near-singularity ε

Even though integral (4.1) is motivated by the three-dimensional interpretation of Fig. 4.1, typical of BEM applications, the integration is performed over a planar triangle. Therefore, this chapter focuses on a two-dimensional bivariate integrand that admits, to some extent, a similar treatment as the singular integral in 2D developed in chapter 3.

We remark that the integral I in (4.1) can be evaluated for any real value of α . Some authors [25, 61, 72, 15, 34, 35, 23] distinguish between weakly near-singular

integrals, with $\alpha < 2$, for which I would take a finite value if $\varepsilon = 0$, and strongly near-singular integrals, with $\alpha \geq 2$, for which I would not be finite if $\varepsilon = 0$.

It will be a conclusion of this chapter that the determination of the suitable methods for evaluating (4.1) depends strongly on whether the singularity strength is above or below the critical value $\alpha = 2$.

Proceeding as in chapter 3 we denote the parent coordinates as $\bar{\mathbf{u}} = (\bar{u}, \bar{v})$. The application of the pyramidal transformation (2.7) to (4.1) produces

$$I = 2|T| \iint_{C_2} \frac{g(\mathbf{x}(\bar{u}, \bar{v}))\bar{u}}{(\bar{u}^2 |\mathbf{r}(\bar{v})|^2 + \varepsilon^2)^{\alpha/2}} d\bar{u}d\bar{v}. \quad (4.2)$$

We define the dimensionless function

$$b(\bar{v}) = \frac{\varepsilon}{|\mathbf{r}(\bar{v})|}, \quad (4.3)$$

and recall equation (2.12) to deduce

$$|\mathbf{r}(\bar{v})|^\alpha = \frac{|\mathbf{x}_1 - \mathbf{x}_2|^\alpha}{\phi_N(\bar{v})}, \quad (4.4)$$

with ϕ_N defined in (3.10) and rewritten here for convenience

$$\phi_N(\bar{v}) = \frac{1}{((\bar{v} - \bar{v}_p)^2 + \varepsilon_v^2)^{\alpha/2}}. \quad (4.5)$$

This lets us express the integral (4.2) as

$$I = \frac{2|T|}{|\mathbf{x}_1 - \mathbf{x}_2|^\alpha} \iint_{C_2} g(\mathbf{x}(\bar{u}, \bar{v}))K(\bar{u}, \bar{v})d\bar{u}d\bar{v}, \quad (4.6)$$

where the function defined by

$$K(\bar{u}, \bar{v}) = \phi_N(\bar{v}) \frac{\bar{u}}{(\bar{u}^2 + b(\bar{v})^2)^{\alpha/2}}, \quad (4.7)$$

is the kernel of the near-singular integral. This kernel is factorized into an angular part

$$K_2(\bar{v}) = \phi_N(\bar{v}) = \frac{1}{((\bar{v} - \bar{v}_p)^2 + \varepsilon_v^2)^{\alpha/2}}, \quad (4.8)$$

and a radial part

$$K_1(\bar{u}, \bar{v}) = \frac{\bar{u}}{(\bar{u}^2 + b(\bar{v})^2)^{\alpha/2}}. \quad (4.9)$$

The angular kernel K_2 does not depend on the algebraic near-singularity ε , but rather on the parameters \bar{v}_p and ε_v that are determined, as we know, by the geometry of the triangular element T . Hence, the angular kernel is exactly the same as in the

two-dimensional singular integral in (3.7), and will receive a very similar treatment in this chapter.

On the other hand, the radial kernel K_1 depends on the algebraic near-singularity ε and, to a lesser extent, on the geometry of the element through the term $b(\bar{v})$. Instead of a constant, there is a linear factor \bar{u} in the numerator of (4.9) and the variable \bar{u} is not displaced from its origin, as it happens with K_2 .

Apart from these differences, both kernels are formally the same, and this will help us simplify the further treatment of the transformations proposed. The similarities between both kernels have already been pointed out in e.g. [3], though non-standard domains were used for that purpose.

As noticed previously by other authors [25, 60, 3, 34], the integral kernel in (4.7) does not have its variables completely separated, since the radial kernel also depends on the angular variable. Unlike the singular integral in 2D, any transformation applied over the angular kernel will affect the radial kernel too.

A great amount of effort has been devoted to the treatment of (4.8) and (4.9) over the last decades. In the next two sections we provide a brief survey on the main transformations that have been proposed for each separate part of the kernel.

Since the angular kernel K_2 depends only on \bar{v} , it suffices finding a univariate map $\bar{v} = \bar{v}(v)$ from $[0, 1]$ onto itself for its regularization. However, the radial kernel also depends on \bar{v} , so it will be necessary to determine a bivariate transformation $\bar{u} = \bar{u}(u, v)$ from C_2 onto $[0, 1]$, that depends on v through $\bar{v}(v)$. For this reason, the angular kernel will be analyzed firstly.

4.2. The angular kernel $K_2(\bar{v})$

We recall that the geometric near-singularity ε_v only depends on the geometry of the triangle T . In consequence, this near-singularity should not be very severe if a proper meshing has been performed.

4.2.1. General form of the transformations

As stated in sec. 3.4.1 and sec. 3.4.2 we look for non-linear regularizing maps that are able to move the complex poles of K_2 further away from the integration interval. The general form of these transformations is rewritten here for convenience:

$$\bar{v}(v) = \bar{v}_p + h(t(v)), \quad (4.10)$$

$$t(v) = t_0 + (t_1 - t_0)v, \quad (4.11)$$

$$t_j = h^{-1}(j - \bar{v}_p), \quad j = 0, 1, \quad (4.12)$$

with h transforming $[0, 1]$ onto itself independently of \bar{v}_p , as already justified in sec. 3.4.2.

A number of a priori mappings were already considered in sec. 3.4, of which the cubic and sinh transformations are the most relevant ones, recall sec. 3.4.3 and

sec.3.4.4. These schemes can be reutilized in exactly the same manner with the angular kernel K_2 in (4.8).

However, the fact that the kernel K in (4.7) does not have completely separated variables, induces a slightly different treatment on the a posteriori mappings that are appropriate for this kernel, as described in the next subsection.

4.2.2. A posteriori transformations for $K_2(\bar{v})$

As already introduced in sec.3.5, a posteriori transformations are obtained after applying a certain regularization condition over the kernel K_2 , namely

$$\frac{1}{((\bar{v} - \bar{v}_p)^2 + \varepsilon_v^2)^{\beta/2}} \frac{d\bar{v}}{d\bar{v}} = \bar{c}_2, \quad (4.13)$$

where the exponent β may or may not coincide with the singularity strength α . Applying the chain rule to (4.10)-(4.11) yields

$$\frac{d\bar{v}}{d\bar{v}} = \frac{dh}{dt} \frac{dt}{d\bar{v}} = \frac{dh}{dt} (t_1 - t_0),$$

from where it follows

$$\frac{1}{(h(t)^2 + \varepsilon_v^2)^{\beta/2}} \frac{dh}{dt} = c_2, \quad (4.14)$$

with $c_2 = \frac{\bar{c}_2}{t_1 - t_0}$. We note that c_2 depends on β and the geometry of the problem, but not on the variable \bar{v} . Since h maps $[0, 1]$ onto itself, c_2 is evaluated to

$$c_2 = \int_0^1 \frac{1}{(s^2 + \varepsilon_v^2)^{\beta/2}} ds,$$

that can be easily related to the well-known integral representation of the Gaussian Hypergeometric Function (see e.g. [54]) to yield

$$c_2 = \frac{1}{\varepsilon_v^\beta} {}_2F_1 \left(\frac{\beta}{2}, \frac{1}{2}; \frac{3}{2}; -\frac{1}{\varepsilon_v^2} \right).$$

A large number of authors [24, 46, 37, 60, 72, 56, 3] have considered the solution to (4.14) in case β is an integer, namely $\beta = 1, 2, 3$. These transformations will be denoted F_β throughout the rest of this paper, even when applied to the radial kernel. We summarize the explicit form of such solutions in Tab.4.1.

Table 4.1.: Transformations F_β

β	c_2	$h(t)$
1	$\sinh^{-1}\left(\frac{1}{\varepsilon_v}\right)$	$\varepsilon_v \sinh(c_2 t)$
2	$\frac{1}{\varepsilon_v} \tan^{-1}\left(\frac{1}{\varepsilon_v}\right)$	$\varepsilon_v \tan(\varepsilon_v c_2 t)$
3	$\frac{1}{\varepsilon_v^2 \sqrt{1 + \varepsilon_v^2}}$	$\frac{\varepsilon_v^3 c_2 t}{\sqrt{1 - \varepsilon_v^4 c_2^2 t^2}} = \frac{\varepsilon_v t}{\sqrt{1 + \varepsilon_v^2 - t^2}}$

We notice that F_1 is the sinh transformation described in sec. 3.4.4 applying an a priori reasoning. Furthermore, F_2 is the tangent function, that coincides, after rescaling, with the angular part of the polar transformation (2.14)-(2.15). A consequence of this fact is that the polar transformation is equivalent to a pyramidal map composed with an F_2 transformation in the angular variable (followed by affine rescaling to integrate over the unit square).

Once the transformation $h(t)$ has been determined, the parameters t_j in (4.11) can be calculated by means of (4.12), allowing the construction of the composite transformation (4.10).

In the case $\beta = \alpha$, for non-integer α , numerical integration of (4.14) would be necessary, following the same procedure explained in sec. 3.5. However, turning K_2 into a constant does not produce a constant kernel K , because its variables are not completely separated. For this reason, it is more convenient to propose a modified scheme for complete kernel regularization, that will be described further in this chapter, in sec. 4.5.

4.3. The radial kernel $K_1(\bar{u}, \bar{v})$

Due to the formal similarities between the angular and radial kernels in (4.8)-(4.9), all transformations (a priori and a posteriori) proposed for K_2 can be readily reformulated for K_1 , with the difference that the radial variable \bar{u} is always centered at the origin, rather than displaced from it, as it happens with \bar{v} . Moreover, the radial transformation \bar{u} depends on both independent variables (u, v) .

The most relevant transformations, that will be used in numerical simulations, are listed below. The explicit dependences $\bar{u} = \bar{u}(u, v)$, $b = b(\bar{v})$, $c_1 = c_1(\bar{v})$, $r_0 = r_0(\bar{v})$ and $\bar{v} = \bar{v}(v)$ have been omitted for brevity:

- F_1 (sinh): $\bar{u} = b \sinh(c_1 u)$, $c_1 = \sinh^{-1}\left(\frac{1}{b}\right)$
- F_2 (tan): $\bar{u} = b \tan(bc_1 u)$, $c_1 = \frac{1}{b} \tan^{-1}\left(\frac{1}{b}\right)$
- Cubic: $\bar{u} = r_0 u + (1 - r_0)u^3$, $r_0 = 3b \sinh\left(\frac{1}{3} \sinh^{-1}\left(\frac{1}{b}\right)\right)$, as in (3.19)

Unlike the angular kernel, the algebraic near-singularity $b(\bar{v})$ in K_1 can be very severe. Taking (4.3) into account, it is clear that b depends not only on the geometry of the triangle T , but also on the parameter ε , that can be arbitrarily small. Some recent works on crack growth or thin layer elements have considered values $\varepsilon = 10^{-10}$ and smaller, see e.g. [22, 73, 23].

As a consequence, many of the transformations already described for the angular kernel happen to be incapable of attenuating a very severe radial near-singularity. Numerical experiments show that the softening effect of these transformations (most notably the cubic, the sinh and the rest of F_β) does not suffice to produce accurate numerical results.

New, different methods have been proposed over the years, aimed at producing a stronger softening effect over K_1 , sometimes at the cost of using transformations that are not completely smooth themselves. We give a brief description of the most relevant techniques in the next subsections.

4.3.1. A priori transformations for $K_1(\bar{u}, \bar{v})$

The PART method The PART method was introduced in [24, 25, 26]. It consists of a polar transformation composed with a number of regularization maps in the radial variable. Their equivalent form in (\bar{u}, \bar{v}) coordinates is provided in Tab.4.2. The explicit dependences $\bar{u} = \bar{u}(u, v)$, $b = b(\bar{v})$, $\bar{v} = \bar{v}(v)$, $t = t(u, v)$, $t_j = t_j(v)$ have been omitted for brevity.

Table 4.2.: Radial transformations in the PART method

Name	Equation	t_0	t_1
L_2	$\bar{u} = \sqrt{t^2 - b^2}$	b	$\sqrt{b^2 + 1}$
Log- L_2	$\bar{u} = \sqrt{e^{2t} - b^2}$	$\log b$	$\frac{1}{2} \log(b^2 + 1)$
Log- L_1	$\bar{u} = e^t - b$	$\log b$	$\log(b + 1)$
$L^{-1/5}$	$\bar{u} = -t^{-5} - b$	$-b^{-1/5}$	$-(b + 1)^{-1/5}$

The purpose of the transformation t is very similar to that in the angular case: it consists of a bivariate function of (u, v) , affine in its first argument, ensuring that \bar{u} maps C_2 onto $[0, 1]$. Its general form is

$$t(u, v) = t_0(v) + (t_1(v) - t_0(v))u, \quad (4.15)$$

where the explicit form of t_j for each transformation is given in Tab.4.2.

Apart from these radial transformations, it should be mentioned that the PART method proposes a transformation in the polar angle of the form

$$t = \frac{h_T}{2} \log \left(\frac{1 + \sin(\theta - \theta_p)}{1 - \sin(\theta - \theta_p)} \right), \quad (4.16)$$

4.3 The radial kernel $K_1(\bar{u}, \bar{v})$

that can be shown to be equivalent to a sinh transformation in the isoparametric variable \bar{v} , see Appendix B for details. We recall from sec. 3.4 that a very similar form of the transformation (4.16) was later presented in [2].

The exponential distance transformation An exponential distance transformation was proposed in [45] and later considered in [56]. It can be expressed (omitting explicit dependences) as

$$\bar{u} = \frac{1}{2}(e^t - b^2 e^{-t}),$$

with $t_0 = \log b$, $t_1 = \log(1 + \sqrt{1 + b^2})$ and $t(u, v)$ as in (4.15).

It is possible to show that this transformation is equivalent to F_1 (sinh) in the radial variable, see Appendix B for details.

The exponential transformation Another exponential transformation, proposed in [72] and later considered in [68], can be expressed as

$$\bar{u} = b(e^t - 1),$$

with $t_0 = 0$, $t_1 = \log(1 + \frac{1}{b})$ and $t(u, v)$ as in (4.15).

As with the previous case, a simple renormalization shows that this transformation is equivalent to Log- L_1 in the PART method, refer to Appendix B for details.

4.3.2. A posteriori transformations for $K_1(\bar{u}, \bar{v})$

The presence of the linear factor \bar{u} in (4.9) makes it possible to build a new set of a posteriori transformations, that have no direct equivalent in the angular kernel, i.e., they are exclusive of the near-singular radial kernel.

The idea is to apply a regularizing condition to K_1 , similar to that in (4.14):

$$\frac{\bar{u}}{(\bar{u}^2 + b(\bar{v})^2)^{\beta/2}} \frac{\partial \bar{u}}{\partial u} = c_1(\bar{v}), \quad (4.17)$$

subject to the boundary conditions $\bar{u}(0, v) = 0$, $\bar{u}(1, v) = 1$. Notice that c_1 in (4.17) needs to be a function of \bar{v} , since the radial kernel depends on \bar{v} through $b(\bar{v})$. Its value can be obtained integrating both sides of (4.17) in the interval $[0, 1]$:

$$c_1(\bar{v}) = \begin{cases} \frac{(1+b(\bar{v})^2)^{1-\frac{\beta}{2}} - b(\bar{v})^{2-\beta}}{2-\beta}, & \text{if } \beta \neq 2, \\ \frac{1}{2} \log\left(1 + \frac{1}{b(\bar{v})^2}\right), & \text{if } \beta = 2, \end{cases} \quad (4.18)$$

Once c_1 is known, the solution of (4.17) can be easily obtained, by explicit integration and inversion, to be $\bar{u}(u, v) = G_\beta(u, \bar{v}(v))$, with

$$G_\beta(u, \bar{v}) = \begin{cases} b(\bar{v}) \sqrt{\left(\left[\left(1 + \frac{1}{b(\bar{v})^2} \right)^{1-\frac{\beta}{2}} - 1 \right] u + 1 \right)^{\frac{2}{2-\beta}} - 1}, & \text{if } \beta \neq 2, \\ b(\bar{v}) \sqrt{e^{\log\left(1+\frac{1}{b(\bar{v})^2}\right)u} - 1}, & \text{if } \beta = 2. \end{cases} \quad (4.19)$$

The transformations G_β with integer β have been considered by a number of authors, see e.g. [24, 46, 37, 60, 56, 3], some of them applying an a priori reasoning. We notice that G_1 is equivalent to the L_2 transformation in the PART method, and G_2 is equivalent to the Log- L_2 transformation in the PART method. The case $\beta = \alpha$ has been considered in [25], where a number of disadvantages of G_α are enumerated, to eventually suggest G_2 as a simpler and more robust alternative.

It should be mentioned that the transformations F_β (resp. G_β) are referred as R-Linear (resp. R-Constant) in [3], where they are systematically analyzed for $\beta = 1, 2, 3$.

4.3.3. The singularities in G_β

It is easy to verify that $\bar{u}(u, v) = G_\beta(u, \bar{v}(v))$ has singular derivative at $u = 0$:

$$\lim_{u \rightarrow 0} \frac{\partial \bar{u}}{\partial u} = \infty,$$

and this severely limits the efficiency of the procedure, unless the regular part of the integrand in (4.1) is a constant, i.e. $g(\mathbf{x}) = 1$. This problem can be partially solved by applying additional regularization on the independent variable u , by means of a softening function $\sigma(u)$, usually a low-degree polynomial, that maps $[0, 1]$ onto itself. This way, (4.17) becomes

$$\frac{\bar{u}}{(\bar{u}^2 + b(\bar{v})^2)^{\beta/2}} \frac{\partial \bar{u}}{\partial u} = c_1(\bar{v}) \frac{d\sigma}{du}, \quad (4.20)$$

whose solution is given by $\bar{u}(u, v) = G_\beta(\sigma(u), \bar{v}(v))$.

The case $\sigma(u) = u^q$ with integer q has been considered in [60] for integer values of β . It is possible to show that in case $\sigma(u) = u^2$, then

$$\lim_{u \rightarrow 0} \frac{\partial \bar{u}}{\partial u} < \infty,$$

resulting in a much better numerical convergence of the algorithm, at least for the cases $\beta = 1, 2$. The transformation G_3 has singularities at $u = 1$, as well as $u = 0$, as pointed out in [60], resulting in a very poor performance of the quadrature rule. Therefore, G_3 will not be further considered in numerical simulations.

4.4. A new family of composite radial transformations

This section describes a procedure to formulate an iterative scheme of composite transformations of the form

$$G_1^k X,$$

i.e. a composition of k consecutive transformations G_1 , with $k = 1, 2, 3, \dots$, with a last transformation X of any of the types described in the previous section, including G_1 itself. Numerical experiments show that some of these transformations are able to outperform the classical methods for a wide range of values of the singularity strength α .

A brief analysis on the transformation G_2 , together with a description of the iterated sinh transformation, completes this section.

4.4.1. The transformation G_1

Taking $\beta = 1$, $\sigma(u) = u^2$ in (4.18) and (4.19) yields

$$c_1(\bar{v}) = \sqrt{1 + b(\bar{v})^2} - b(\bar{v}), \quad (4.21)$$

$$G_1(u, \bar{v}) = \sqrt{c_1(\bar{v})^2 u^2 + 2c_1(\bar{v})b(\bar{v})u}. \quad (4.22)$$

Recalling that $\bar{u}(u, v) = G_1(u^2, \bar{v}(v))$ it follows

$$\frac{\partial \bar{u}}{\partial u} = 2c_1(\bar{v}) \frac{c_1(\bar{v})u^3 + b(\bar{v})u}{\bar{u}}. \quad (4.23)$$

The key point here is to substitute the solution \bar{u} and its derivative, not into the kernel K_1 with $\beta = 1$, but into the kernel K_1 with arbitrary α . Performing this substitution yields

$$\frac{\bar{u}}{(\bar{u}^2 + b(\bar{v})^2)^{\alpha/2}} \frac{\partial \bar{u}}{\partial u} = 2c_1(\bar{v})^{2-\alpha} \frac{u}{(u^2 + b_2(\bar{v})^2)^{\alpha-1}}, \quad (4.24)$$

with $b_2(\bar{v}) = \sqrt{\frac{b(\bar{v})}{c_1(\bar{v})}}$. Since $b(\bar{v}) \ll 1$ in a near-singular problem, it follows from (4.21) that $c_1(\bar{v}) \approx 1$ and $b_2(\bar{v}) \approx \sqrt{b(\bar{v})}$.

The interpretation of (4.24) is that by applying G_1 to the kernel with arbitrary α , a new kernel is obtained with the same form as the original one, but with the near-singularity perturbation attenuated, and a different value of the near-singularity strength: $\frac{\alpha}{2} \rightarrow \alpha - 1$. The immediate consequence is that a new regularizing condition of the type (4.20) can be applied over the right hand side of (4.24).

If we take again $\beta = 1$ for the new regularization, i.e., if we apply G_1 over the modified kernel, yet another kernel of the same type as in (4.24) is obtained, with a near-singularity parameter that equals, approximately, $\sqrt[4]{b(\bar{v})}$. It is then clear that this procedure can be iterated, producing a sequence of kernels that are respectively

easier to integrate, until a last transformation X is applied. The composite map eventually obtained is denoted $G_1^k X$ for short.

Writing $G_1^k X = G_1 \circ (G_1^{k-1} X)$, the term $G_1^{k-1} X$ can be regarded as the additional softening applied over the transformation G_1 . This way, the additional softening emerges from solving a sequence of differential equations of the type (4.17), rather than being introduced by an empirical trial-and-error procedure. Furthermore, the additional softener $G_1^{k-1} X$ incorporates automatically the dependence on v , that was not present, e.g., in the case $\sigma(u) = u^2$.

However, as stated in previous sections, softening the radial kernel K_1 does not suffice to obtain good convergence rates, it is also required that the transformations used for that purpose are smooth themselves. Numerical simulations show that there exist compositions $G_1^k X$, with $X = F_\beta$ or G_β , smooth enough to outperform the existing methods for a wide range of values of α , namely $\alpha < 2.5$ and $\alpha > 6$. In the interval $\alpha \in [2.5, 6]$ there exist other solutions that show a better performance, as described below.

4.4.2. The transformation G_2

The transformation G_2 has been considered by a number of authors [24, 46, 60, 56, 3]. As it happens with G_1 , it is easy to show that $\bar{u}(u, v) = G_2(u, \bar{v}(v))$ has singular derivative at $u = 0$, but this drawback is solved by taking an additional softener $\sigma(u) = u^2$, i.e. $\bar{u}(u, v) = G_2(u^2, \bar{v}(v))$, as proposed e.g. in [60].

The derivative of \bar{u} can be readily computed

$$\frac{\partial \bar{u}}{\partial u} = b(\bar{v})^2 c_1(\bar{v}) \frac{e^{2c_1(\bar{v})\sigma(u)} d\sigma}{\bar{u} du}.$$

As in the previous subsection, the key point here is to substitute \bar{u} and $\frac{\partial \bar{u}}{\partial u}$ not in the kernel K_1 with $\beta = 2$, but in the kernel K_1 with arbitrary α , given in (4.9). Performing the substitution produces

$$\frac{\bar{u}}{(\bar{u}^2 + b(\bar{v})^2)^{\alpha/2}} \frac{\partial \bar{u}}{\partial u} = b(\bar{v})^{2-\alpha} c_1(\bar{v}) e^{(2-\alpha)c_1(\bar{v})\sigma(u)} \frac{d\sigma}{du}. \quad (4.25)$$

We notice that the transformed kernel is a decreasing exponential in u for $\alpha > 2$, and as a consequence of this fact, G_2 can be successfully applied in all situations with $\alpha \geq 2$. In particular, the numerical results of G_2 in the case $\alpha = 3$ are much better than those obtained by F_3 or G_3 . Moreover, the transformation G_2 is able to outperform the other methods in the range $\alpha \in [2.5, 3.5]$.

Unfortunately, there seems to be no easy way to find a composition $G_2 X$ that further improves the performance of the composite transformation. The reason for this is that, after removing the singularity of $\bar{u}(u, v) = G_2(u^2, \bar{v}(v))$ at $u = 0$, there remains a near-singularity at $u = 1$, whereas the transformed kernel (4.25) is near-singular itself at $u = 0$. Hence, a transformation that simultaneously attenuates both near-singularities, at $u = 0$ and $u = 1$, does not seem feasible.

4.4.3. The iterated sinh transformation

The idea of iterating transformations to strengthen the global softening effect has already been considered in [15, 35]. An iterated sinh transformation (i-sinh or F_1^2) is formulated on the biunit square $[-1, 1]^2$, without previously applying a polar or isoparametric transformation. We provide here, for implementation purposes, its equivalent form when applied to the radial kernel over the unit square C_2 .

A first sinh transformation is applied on \bar{u} , whose explicit expression, omitting dependences, is

$$\bar{u} = b \sinh(c_1 \tilde{u}), \quad c_1 = \sinh^{-1} \left(\frac{1}{b} \right),$$

with \tilde{u} being an intermediate variable. In this case, the near-singular perturbation, b , coincides with the distance of the kernel complex poles to the real axis.

Next, a second sinh transformation is applied on \tilde{u} , but taking a different value for the near-singular perturbation, namely

$$b_2 = \frac{\pi}{2c_1}.$$

It is shown in [35] that b_2 is the new distance of the transformed kernel poles to the real axis. Hence, the second sinh transformation takes the form

$$\tilde{u} = b_2 \sinh(d_1 u), \quad d_1 = \sinh^{-1} \left(\frac{1}{b_2} \right).$$

The i-sinh transformation (i.e. the composition between \bar{u} and \tilde{u}) shows an excellent convergence rate, for large values of the strength parameter α , in agreement with the numerical experiments performed in [35]. More specifically, it is able to outperform the other methods in the range $\alpha \in [3.5, 6]$.

We remark that the i-sinh transformation can also be applied to the angular kernel, although the benefits there seem less clear than in the radial case.

4.5. A transformation for complete kernel regularization

The transformations proposed in the previous sections try to force separately each factor of the kernel, K_1 and K_2 , to be as simple as possible. Since $c_1(\bar{v})$ is not a constant, neither is the whole transformed kernel, more specifically, the product of (4.13) and (4.17) gives

$$K(\bar{u}, \bar{v}) \frac{d\bar{v}}{d\bar{v}} \frac{\partial \bar{u}}{\partial u} = c_1(\bar{v}) \bar{c}_2 \neq \text{const.}$$

Extending the ideas introduced in sec. 3.5, a condition over the whole kernel is now imposed, namely

$$K_1(\bar{u}, \bar{v}) \frac{\partial \bar{u}}{\partial u} K_2(\bar{v}) \frac{d\bar{v}}{d\bar{v}} = c_0, \quad (4.26)$$

where c_0 depends on the problem parameters α , ε and the triangle T , but not on the variables (\bar{u}, \bar{v}) . The condition over K_1 is the same as in (4.17) rewritten here for convenience

$$K_1(\bar{u}, \bar{v}) \frac{\partial \bar{u}}{\partial u} = c_1(\bar{v}), \quad (4.27)$$

with c_1 as in 4.18 for the case $\beta = \alpha$. Substituting (4.27) into (4.26) we obtain the condition for K_2 , namely

$$c_1(\bar{v}) K_2(\bar{v}) \frac{d\bar{v}}{dv} = c_0. \quad (4.28)$$

It should be pointed out that (4.28) is a slight modification of (4.13), that ensures the whole transformed kernel becomes regularized. The value of c_0 can be evaluated numerically by means of

$$c_0 = \int_0^1 c_1(\bar{v}) K_2(\bar{v}) d\bar{v}.$$

Once c_0 is known, the solution $\bar{v}(v)$ is computed first, by solving (4.28) numerically. More specifically, the Newton-Rahpson method can be applied at the Gaussian nodes $\{v_i\}_{i=1}^{n_w}$, see Appendix C for details. After $\bar{v}(v)$ is known, the radial solution $\bar{u}(u, v)$ is obtained by means of (4.19) for the case $\beta = \alpha$.

As already indicated in previous sections, the regularization of the whole kernel does not suffice to obtain a smooth integrand in (4.1), unless $g(\mathbf{x})$ is a constant. The solutions $\bar{v}(v)$ and $\bar{u}(u, v)$ may be singular themselves, and these singularities are carried back to the integrand through the composition $g(\mathbf{x}(\bar{u}, \bar{v}))$. One way to overcome this difficulty is to apply additional softening by performing a substitution on the independent variables, namely

$$\begin{aligned} u &\rightarrow \sigma(u), \\ v &\rightarrow \tau(v), \end{aligned}$$

where σ and τ are non-linear functions, usually polynomials of low degree, that map the interval $[0, 1]$ onto itself. This means that new, weaker conditions are imposed over the angular and radial kernels:

$$c_1(\bar{v}) K_2(\bar{v}) \frac{d\bar{v}}{dv} = c_0 \frac{d\tau}{dv}, \quad (4.29)$$

$$K_1(\bar{u}, \bar{v}) \frac{\partial \bar{u}}{\partial u} = c_1(\bar{v}) \frac{d\sigma}{du} \quad (4.30)$$

Unfortunately, there seems to be no direct way to determine σ and τ , apart from the choice $\sigma(u) = u^2$ considered in previous sections. Empirical evidence shows a strong dependence of σ and τ on the problem parameters α , ε and T .

4.6. The integration of (near-)singular kernels over adjacent triangles

So far, we have focused on the integration of singular (chapter 3) and near-singular (chapter 4) kernels over source triangles, such that the (projection of the) source point \mathbf{x}_s coincides with one of the triangle vertices, say \mathbf{x}_0 , as shown in Fig. 4.2. The source triangle T may possibly be the result of subdividing a physical triangle at the singular point, recall Fig. 3.2 in sec. 3.4.

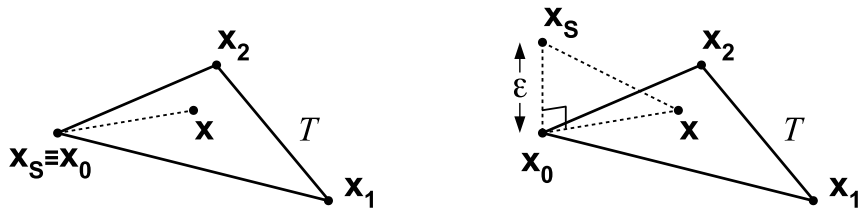


Figure 4.2.: Source triangle. Singular (left) and near-singular (right) integrals

This section focuses on adjacent triangles T' , contiguous to a source triangle T , but such that the (projection of the) source point lies outside the triangle T' itself. The situation with the source point on the same plane as the triangle usually occurs in XFEM, whereas the source point outside that plane is typical of BEM. In this last case, the projection of the source point over the triangle plane is denoted \mathbf{x}_p , as illustrated in Fig. 4.3.

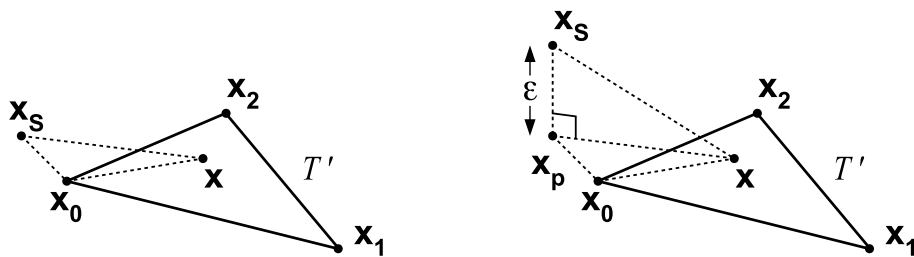


Figure 4.3.: Adjacent triangle in XFEM (left) and BEM (right)

Hence, the integral under consideration in this section will be

$$I = \iint_{T'} \frac{g(\mathbf{x})}{|\mathbf{x} - \mathbf{x}_s|^\alpha} d\mathbf{x}. \quad (4.31)$$

It is clear that this integral reduces to (3.1) if $\mathbf{x}_s = \mathbf{x}_0$ (i.e. $\varepsilon = 0$) and to (4.1) if $\mathbf{x}_p = \mathbf{x}_0$ with $\varepsilon > 0$. Furthermore, the integral (4.31) keeps being near-singular whenever the distance between \mathbf{x}_s and the triangle edges is small, for both cases $\varepsilon = 0$ and $\varepsilon > 0$, and further treatment of the integral kernel is required. A similar reasoning as with the integrals over source triangles is followed:

- A pyramidal transformation \mathcal{P} expresses the integral (4.31) over the standard domain $C_2 = [0, 1]^2$.
- A regularizing transformation \mathcal{R} softens the remaining singularities in the integrand.

Details on how to implement both transformations are provided in the subsections below.

4.6.1. The pyramidal transformation for adjacent triangles

We start from the pyramidal transformation in 2D described in sec. 2.2.1

$$\begin{aligned}\mathbf{x}(\bar{u}, \bar{v}) - \mathbf{x}_0 &= \bar{u}\mathbf{r}(\bar{v}), \\ J_{\mathcal{P}}(\bar{u}, \bar{v}) &= 2|T'|\bar{u},\end{aligned}$$

that maps the unit square C_2 onto the adjacent triangle T' . Before applying this transformation to (4.31), we write

$$\mathbf{x}(\bar{u}, \bar{v}) - \mathbf{x}_s = (\mathbf{x}(\bar{u}, \bar{v}) - \mathbf{x}_0) - (\mathbf{x}_s - \mathbf{x}_0),$$

from where it follows, by direct substitution

$$I = \iint_{C_2} \frac{g(\mathbf{x}(\bar{\mathbf{u}}))2|T'|\bar{u}}{|\bar{u}\mathbf{r}(\bar{v}) - (\mathbf{x}_s - \mathbf{x}_0)|^\alpha} d\mathbf{x}. \quad (4.32)$$

Denoting by $\mathbf{x} \cdot \mathbf{y}$ the scalar product of the vectors \mathbf{x} and \mathbf{y} , the denominator of (4.32) can be manipulated as follows

$$\begin{aligned}|\bar{u}\mathbf{r}(\bar{v}) - (\mathbf{x}_s - \mathbf{x}_0)|^2 &= [\bar{u}\mathbf{r}(\bar{v}) - (\mathbf{x}_s - \mathbf{x}_0)] \cdot [\bar{u}\mathbf{r}(\bar{v}) - (\mathbf{x}_s - \mathbf{x}_0)] \\ &= \bar{u}^2|\mathbf{r}(\bar{v})|^2 - 2\bar{u}\mathbf{r}(\bar{v}) \cdot (\mathbf{x}_s - \mathbf{x}_0) + |\mathbf{x}_s - \mathbf{x}_0|^2.\end{aligned}$$

Notice that in a source triangle T it holds

$$\mathbf{r}(\bar{v}) \cdot (\mathbf{x}_s - \mathbf{x}_0) = 0,$$

since both vectors are perpendicular, and

$$|\mathbf{x}_s - \mathbf{x}_0| = \varepsilon, \quad \varepsilon \geq 0.$$

Next, the following dimensionless functions are defined

$$\bar{u}_p(\bar{v}) = \frac{\mathbf{r}(\bar{v}) \cdot (\mathbf{x}_s - \mathbf{x}_0)}{|\mathbf{r}(\bar{v})|^2}, \quad (4.33)$$

$$b(\bar{v}) = \frac{1}{|\mathbf{r}(\bar{v})|^2} \sqrt{|\mathbf{r}(\bar{v})|^2 |\mathbf{x}_s - \mathbf{x}_0|^2 - (\mathbf{r}(\bar{v}) \cdot (\mathbf{x}_s - \mathbf{x}_0))^2}, \quad (4.34)$$

where $b(\bar{v})$ is well-defined as a consequence of the Cauchy-Schwarz inequality. For a source triangle, it is clear that (4.33) and (4.34) reduce to

$$\begin{aligned} \bar{u}_p(\bar{v}) &= 0, \\ b(\bar{v}) &= \frac{\varepsilon}{|\mathbf{r}(\bar{v})|}, \end{aligned}$$

in agreement with equation (4.3), prior in this chapter.

Taking (4.4)-(4.5) into account, the integral (4.32) can be written as

$$I = \frac{2|T'|}{|\mathbf{x}_1 - \mathbf{x}_2|^\alpha} \iint_{C_2} g(\mathbf{x}(\bar{\mathbf{u}})) \phi_N(\bar{v}) \frac{\bar{u}}{((\bar{u} - \bar{u}_p(\bar{v}))^2 + b(\bar{v})^2)^{\alpha/2}} d\bar{\mathbf{u}}. \quad (4.35)$$

We next analyze the near-singularities of this kernel, pointing out its similarities with the kernel in (4.6)-(4.7).

4.6.2. The near-singular kernel for adjacent triangles

As in the case of source triangles, the integral kernel of (4.35) is composed of two parts. The angular kernel is given by

$$K_2(\bar{v}) = \phi_N(\bar{v}) = \frac{1}{((\bar{v} - \bar{v}_p)^2 + \varepsilon_v^2)^{\alpha/2}}, \quad (4.36)$$

and is exactly the same as in the source triangle, though this time the geometric parameters \bar{v}_p and ε_v are obviously referred to the adjacent triangle T' . This means that the same treatment as in chapter 3 and sec. 4.2 is adequate for this type of triangles.

On the other hand, the radial kernel is

$$K_1(\bar{u}, \bar{v}) = \frac{\bar{u}}{((\bar{u} - \bar{u}_p(\bar{v}))^2 + b(\bar{v})^2)^{\alpha/2}}. \quad (4.37)$$

that does not have the same form as in sec. 4.3, since the radial variable \bar{u} is now displaced from its origin by a quantity $\bar{u}_p(\bar{v})$, according to (4.33). The following transformation is then necessary over \bar{u} :

$$\bar{u}(u, v) - \bar{u}_p(\bar{v}(v)) = h(z(u, \bar{v}(v))), \quad (4.38)$$

where h is a non-linear injective transformation that maps $[0, 1]$ onto itself and z is an affine transformation in u that ensures that the transformation maps C_2 onto

$\bar{u} \in [0, 1]$. Thus, the role of z is completely similar to that of $t(v)$ in chapter 3. Its explicit form is

$$z(u, \bar{v}) = z_0(\bar{v}) + (z_1(\bar{v}) - z_0(\bar{v}))u, \quad (4.39)$$

with $z_j(\bar{v})$ given by

$$z_j(\bar{v}) = h^{-1}(j - \bar{u}_p(\bar{v})), \quad j = 0, 1. \quad (4.40)$$

4.6.3. The regularizing transformation for the radial variable

The affine renormalization (4.39)-(4.40) imposes a very significant restriction over the transformations that can be used to regularize the radial variable, since the non-linear part of the transformation, h , must be an invertible function. In particular, this excludes the transformations of the type G_β (sec. 4.3.2), that are based on square roots.

This means that there is no advantage in this case coming from the factor \bar{u} in the numerator of (4.37), and thus the situation is similar to that in the angular kernel, that lacks the indicated factor. As a consequence of this fact, the suitable methods need to deal with triangles where the minimum distance between \mathbf{x}_p and the triangle edges is not too small, typically of the same order of magnitude as ε_v , but not as small as ε , that can take extreme values of 10^{-10} relative to the triangle height.

With respect to the procedures for complete kernel regularization, as described in sec. 4.5, they might not be the most appropriate for this case, since the analogous to differential equation (4.27) would be

$$\frac{\bar{u}}{((\bar{u} - \bar{u}_p(\bar{v}))^2 + b(\bar{v})^2)^{\alpha/2}} \frac{\partial \bar{u}}{\partial u} = c_1(\bar{v}), \quad (4.41)$$

that can be analytically solved but not inverted. Moreover, the numerical solution of (4.41) would involve the calculation of a bivariate function $\bar{u}(u, v)$, likely to incur a high computational cost.

By this elimination process we conclude that the only suitable methods to handle adjacent triangles are injective functions, among which the most relevant examples are the cubic, sinh and i-sinh transformations. The explicit expressions of each of the transformations are briefly indicated below.

The cubic transformation It is a transformation of the type (4.38) in which

$$h(z) = r_0 z + (1 - r_0) z^3,$$

where the optimal function r_0 has the same formal expression as in (3.19):

$$r_0(\bar{v}) = 3b(\bar{v}) \sinh \left(\frac{1}{3} \sinh^{-1} \left(\frac{1}{b(\bar{v})} \right) \right),$$

and $z_j(\bar{v})$ are the roots of

$$j - \bar{u}_p(\bar{v}) = r_0 z_j(\bar{v}) + (1 - r_0) z_j(\bar{v})^3,$$

whose explicit expression, according to (A.8), is

$$z_j(\bar{v}) = 2\sqrt{\frac{r_0(\bar{v})}{3(1-r_0(\bar{v}))}} \sinh \left[\frac{1}{3} \sinh^{-1} \left(\frac{3}{2r_0(\bar{v})} \sqrt{\frac{3(1-r_0(\bar{v}))}{r_0(\bar{v})}} (j - \bar{u}_p(\bar{v})) \right) \right].$$

The sinh transformation This transformation is formally analogous to (3.20) with

$$h(z) = b \sinh(\mu z), \quad \mu(\bar{v}) = \sinh^{-1} \left(\frac{1}{b(\bar{v})} \right),$$

and $z_j(\bar{v})$ given by

$$z_j(\bar{v}) = \frac{\sinh^{-1} \left(\frac{j - \bar{u}_p(\bar{v})}{b(\bar{v})} \right)}{\sinh^{-1} \left(\frac{1}{b(\bar{v})} \right)}, \quad j = 0, 1.$$

The i-sinh transformation A first sinh transformation is applied to the kernel in (4.37), namely

$$\bar{u} - \bar{u}_p(\bar{v}) = b(\bar{v}) \sinh(\mu(\bar{v})(z_0(\bar{v}) + (z_1(\bar{v}) - z_0(\bar{v}))\tilde{u})),$$

where \tilde{u} is an intermediate variable. This produces a transformed kernel with a factor

$$\cosh(\mu(\bar{v})(z_0(\bar{v}) + (z_1(\bar{v}) - z_0(\bar{v}))\tilde{u})),$$

whose closest complex poles to the real axis have imaginary parts given by

$$b_2(\bar{v}) = \frac{\pi}{2\mu(\bar{v})(z_1(\bar{v}) - z_0(\bar{v}))}.$$

According to [15], a second sinh transformation is applied, of the form

$$\tilde{u}(u, v) = b_2(\bar{v}(v)) \sinh(\mu_2(\bar{v})u), \quad \mu_2(\bar{v}) = \sinh^{-1} \left(\frac{1}{b_2(\bar{v})} \right).$$

4.7. Numerical results

Some of the procedures described in the previous sections are now tested. Even though the integral in (4.1) depends on α , ε , T and g , numerical experiments will show that it is possible to choose the optimal method attending exclusively to the parameter α . In other words, the optimal method selected in each case is robust enough to withstand changes in ε , T and/or g .

The parameters related to the integral (4.1) are now briefly described.

4.7.1. Near-singularity strength, α

It is the main parameter in simulations, and the one that determines the optimal transformation in each case. Arbitrary values in the continuous range $\alpha \in [-2, 10]$ are tested. However, since there are transformations that perform specially well for particular values of α (integers or half-integers), those specific situations have been considered as well.

4.7.2. Near-singularity perturbation, ε

To be precise, the near-singularity perturbation is given by the dimensionless function $b(\bar{v})$ in (4.3). However, since we can test, without loss of generality, triangles of height one, it follows that ε and $b(\bar{v})$ have the same order of magnitude. According to recent works [22, 73, 23], all methods have been tested for values of ε between 10^{-1} and 10^{-12} , although the typical value that will be displayed in simulations is $\varepsilon = 10^{-7}$. As already mentioned, the optimal transformation chosen in each case shows low sensitivity upon changes in the value of ε .

4.7.3. Integration domain, T

Recalling sec. 3.4.1, numerical quadrature becomes a more difficult task for physical triangles similar to those displayed in Fig. 3.4. Since all methods perform successfully over the standard triangle T_1 (sec. 2.2.1), a quite elongated triangle with vertices $\mathbf{x}_0 = (0, 0)$, $\mathbf{x}_1 = (1, -2)$, $\mathbf{x}_2 = (1, 3)$ will be used throughout simulations. This triangle has an apex angle $\theta_0 = \frac{3\pi}{4}$ that induces a significant distortion in $K_2(\bar{v})$ and in consequence softening in the angular variable becomes relevant.

For more distorted triangles, all methods degrade significantly, and differences among them vanish. This fact may appear surprising at first sight, because the near-singularity in $K_1(\bar{u}, \bar{v})$ can be several orders of magnitude stronger than in $K_2(\bar{v})$. However, it should be taken into account that different, much more powerful methods based on G_β are employed to regularize the algebraic near-singularity in K_1 . In case the apex angle θ_0 is extremely obtuse, interval splitting at \bar{v}_p or triangle bisection seem the most reasonable options, see e.g. [6, 1, 46, 32, 60, 56, 34].

4.7.4. The regular part of the integrand, $g(\mathbf{x}, \mathbf{y})$

We consider the same regular integrands as in the previous chapter, namely

$$g(x, y) = (x - x_0)^i (y - y_0)^j f_\ell(\theta),$$

with $i + j \leq d_m$, d_m being the monomial degree, and $f_\ell(\theta)$ a crack-tip function, whose explicit form was given in sec. 3.6. The monomial degree is set to $d_m = 2$ throughout simulations, and no crack-tip function is used by default, i.e. $f_0(\theta) = 1$. However, it has been checked that the optimal methods are robust (in other words, they do not degrade significantly) when the monomial degree is augmented up to $d_m = 4$, and/or a crack-tip function is used.

4.7.5. Implemented methods

The iterative scheme described in sec. 4.4 makes it possible to construct a large number of composite methods. Among them, numerical experiments allow to pick those ones that are optimal for a certain range of values of α , i.e. methods that are able to outperform the other ones for a given range of the parameters.

Except for the method introduced in sec. 4.5, the angular map is independent of the radial one, i.e., a single method may consist of any combination of radial and angular transformations. However, all methods displayed in simulations incorporate the same kind of transformation in both variables. In particular, all methods $G_1^k X$ implement a sinh transformation in the angular variable. Since moderate angular distortion is assumed, no noticeable change in performance is due to a replacement in the angular transformation of a particular method.

Some of the methods described in previous sections show a limited performance and will not be displayed, most notably F_3 , G_3 , Log- L_1 (exponential) and $L_1^{-1/5}$. The sinh-sigmoidal method, introduced in [34], consists of a sinh transformation in the radial variable and a sigmoidal transformation (sec. 3.4.5) in the polar, or angular, variable. Its convergence proves to be slightly slower than a pure F_1 (sinh) transformation in both variables, and it will not be displayed, either.

As the behaviour of the kernel is quite different for values of α above or below the critical value $\alpha = 2$, the methods considered in each situation differ. The best options selected for each case are enumerated below.

The case $\alpha \leq 2$ The methods displayed on simulations are:

- Pyramidal transformation \mathcal{P} (sec. 2.2.1).
- F_1 (sec. 4.3). It is a sinh transformation in both variables \bar{u} and \bar{v} .
- G_1 (sec. 4.4.1). This method is equivalent to PART L_2 , see sec. 4.3.2.
- Cubic (sec. 3.4.3 and sec. 4.3). It is a cubic transformation in both variables \bar{u} and \bar{v} .
- ODE (sec. 4.5).
- Composite methods G_1^2 , G_1^3 , G_1^4 , $G_1\text{Cub}$, G_1F_1 (sec. 4.4.1).

The results are shown in Fig. 4.4 and Fig. 4.5. For negative even values of α the integral kernel becomes polynomial and thus a simple pyramidal transformation suffices to reach machine-precision with very few integration points.

These numerical experiments indicate that for arbitrary values of $\alpha \leq 2$ there exist at least one composite method that is able to outperform the classical methods, most notably the PART and the sinh transformations. Nevertheless, the performance of the methods show a strong dependence on the value of α , and the optimal method should be carefully selected among all available options.

The case $\alpha > 2$ The methods displayed in this case are:

- F_2 (sec. 4.3). It is a tangent transformation in both variables \bar{u} and \bar{v} .
- G_2 (sec. 4.4.2). This method is equivalent to PART Log- L_2 (see sec. 4.3.2) but implementing an F_2 (tan) transformation in the variable \bar{v} . We recall that the PART method implements a transformation in the polar angle that can be shown to be equivalent to sinh, see Appendix B.
- Iterated sinh or F_1^2 (sec. 4.4.3). It is an i-sinh transformation in both variables \bar{u} and \bar{v} .
- Composite methods $G_1^3, G_1^4, G_1^5, G_1\text{Cub}, G_1F_1, G_1F_2, G_1^3F_2$ (sec. 4.4.1).

The numerical results are shown in Fig. 4.6 and Fig. 4.7.

It is worth noting that G_2 is the best method for values of $\alpha \in (2.5, 3.5)$. It is in fact much superior to the method G_3 obtained by taking $\beta = 3$ in (4.17), that has been considered in [25, 60, 3]. Moreover, G_3 performs very poorly for all values of α and it is therefore not displayed.

The i-sinh method is the best performer for $\alpha \in (3.5, 6)$, when applied over the transformed kernel $K(\bar{u}, \bar{v})$. It should be pointed out that the authors in [35] apply the method directly to the integrand defined on a biunit square, without previously transforming a physical triangular domain. Thus, there is no factor \bar{u} coming from the Jacobian of the polar or pyramidal transformations in [35].

In case α is a large integer, the method F_2 largely outperforms the other methods, although this behaviour is not robust, in the sense that it does not hold in case α is not an integer, or if the degree of the monomials, d_m , is augmented. The reason for this is that the radial kernel K_1 has a factor $\cos^{\alpha-3}(c_1u)$ after the transformation has been applied, but the solution itself depends on $\tan(c_1u)$. It is clear that only for integer α and moderate values of d_m the kernel is a smooth function (cosine) that is easy to integrate. Nevertheless, it is a significant fact that a simple F_2 transformation obtains almost perfect results, if $d_m \leq 2$, for such an important case in practice as the flux integral with $\alpha = 5$, see e.g. [26, 33].

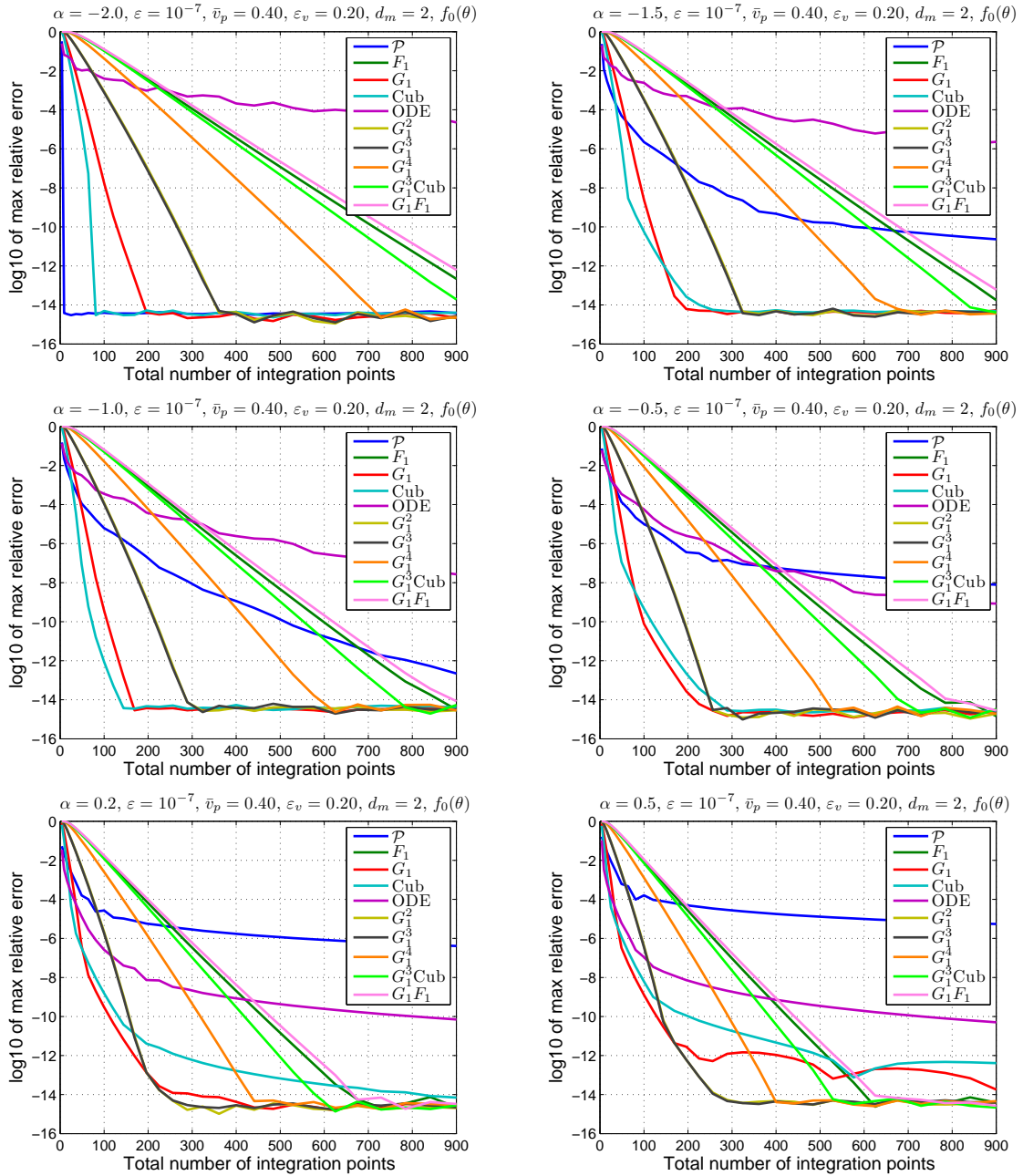
Finally, for arbitrary values of $\alpha > 6$, the methods $G_1^k F_2$ are able to outperform i-sinh and the rest of the methods.

4.7.6. Numerical results for adjacent triangles

The methods described in sec. 4.6 are also tested for a variety of situations, with both $\varepsilon = 0$ and $\varepsilon > 0$. The adjacent triangle has vertices at $\mathbf{x}_0 = (0, 0)$, $\mathbf{x}_1 = (1, -1)$ and $\mathbf{x}_2 = (1, 2)$. The (projection of the) source point is located at $\mathbf{x}_p = (0, 0.1)$. The regular part of the integrand is a monomial of degree $d_m = 2$, and the values of α lie within the interval $(0, 4)$.

The case $\varepsilon = 0$ The results are displayed in Fig. 4.8. As expected, the i-sinh method is only able to outperform cubic and sinh for large values of α .

The case $\varepsilon > 0$ It is identical to the case $\varepsilon = 0$, unless the value of ε is large enough to be comparable to the minimum distance between \mathbf{x}_p and the triangle edges. For instance, in case that $\varepsilon = 0.1$, all methods show an improvement in performance, since the effect of ε is to move the source point further away from the triangle vertices, producing a softer near-singularity. The corresponding results are shown in Fig. 4.9.

Figure 4.4.: Near-singular integral for $\alpha \leq 2$, part 1

4.7 Numerical results

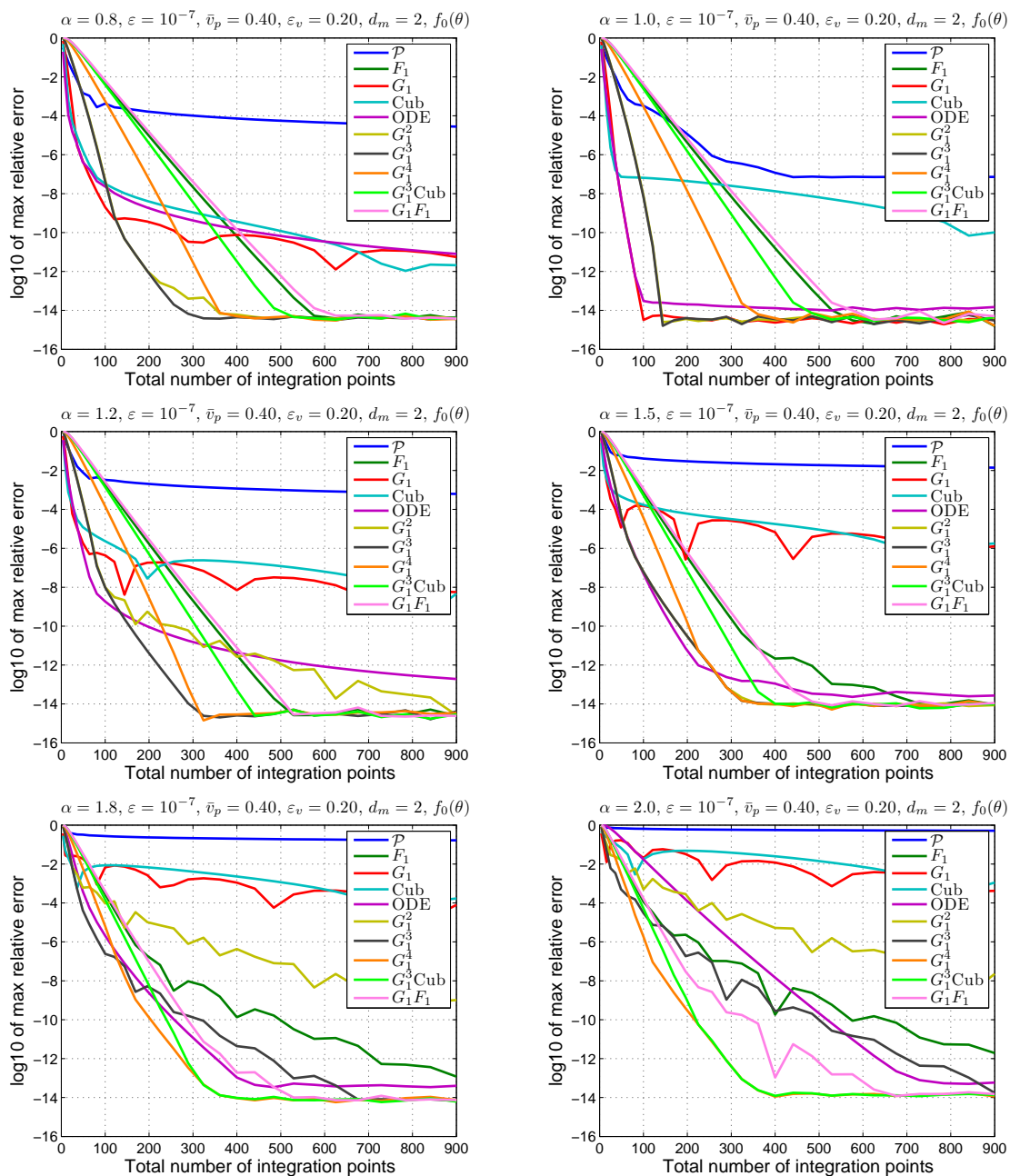
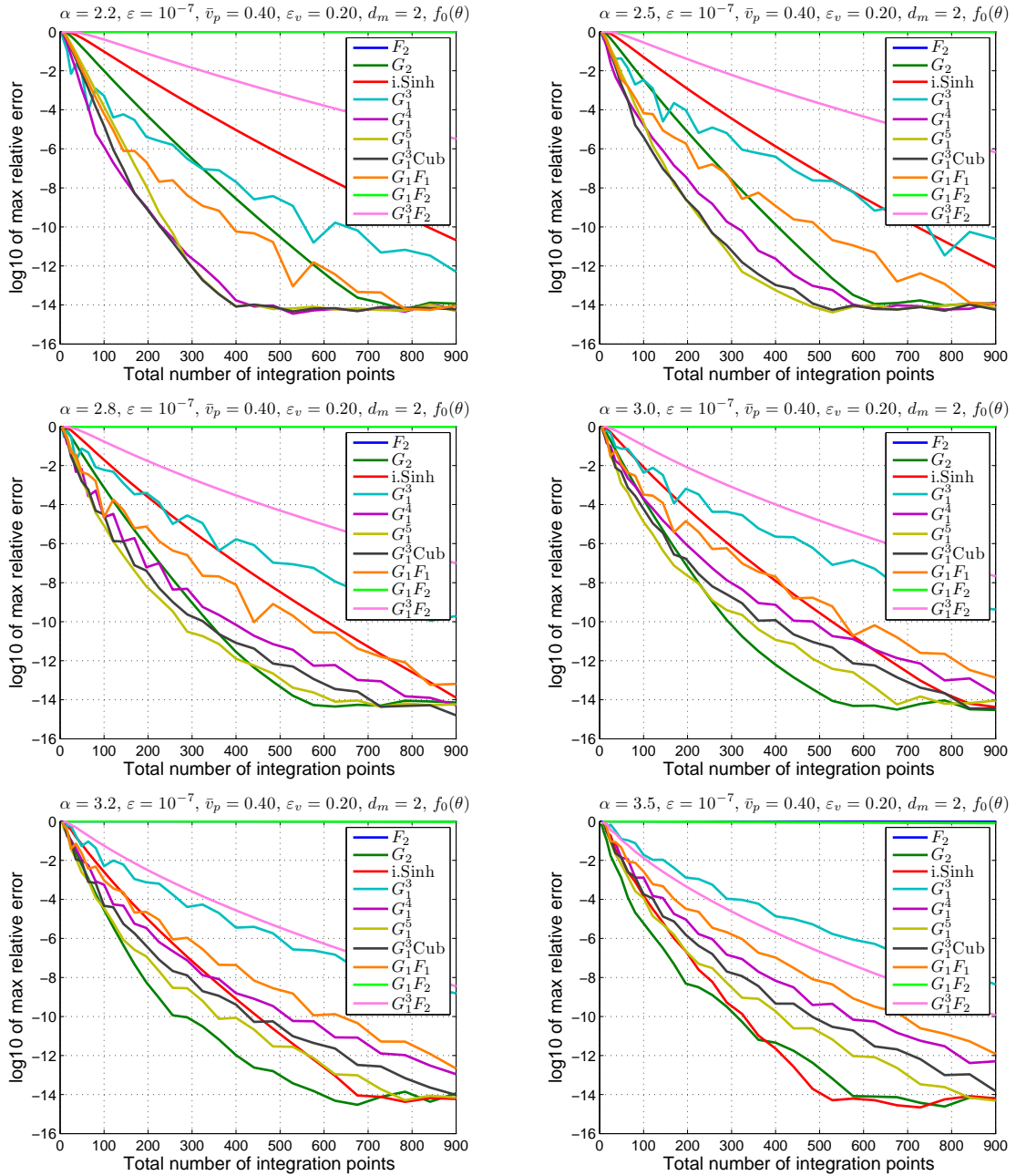


Figure 4.5.: Near-singular integral for $\alpha \leq 2$, part 2

Figure 4.6.: Near-singular integral for $\alpha > 2$, part 1

4.7 Numerical results

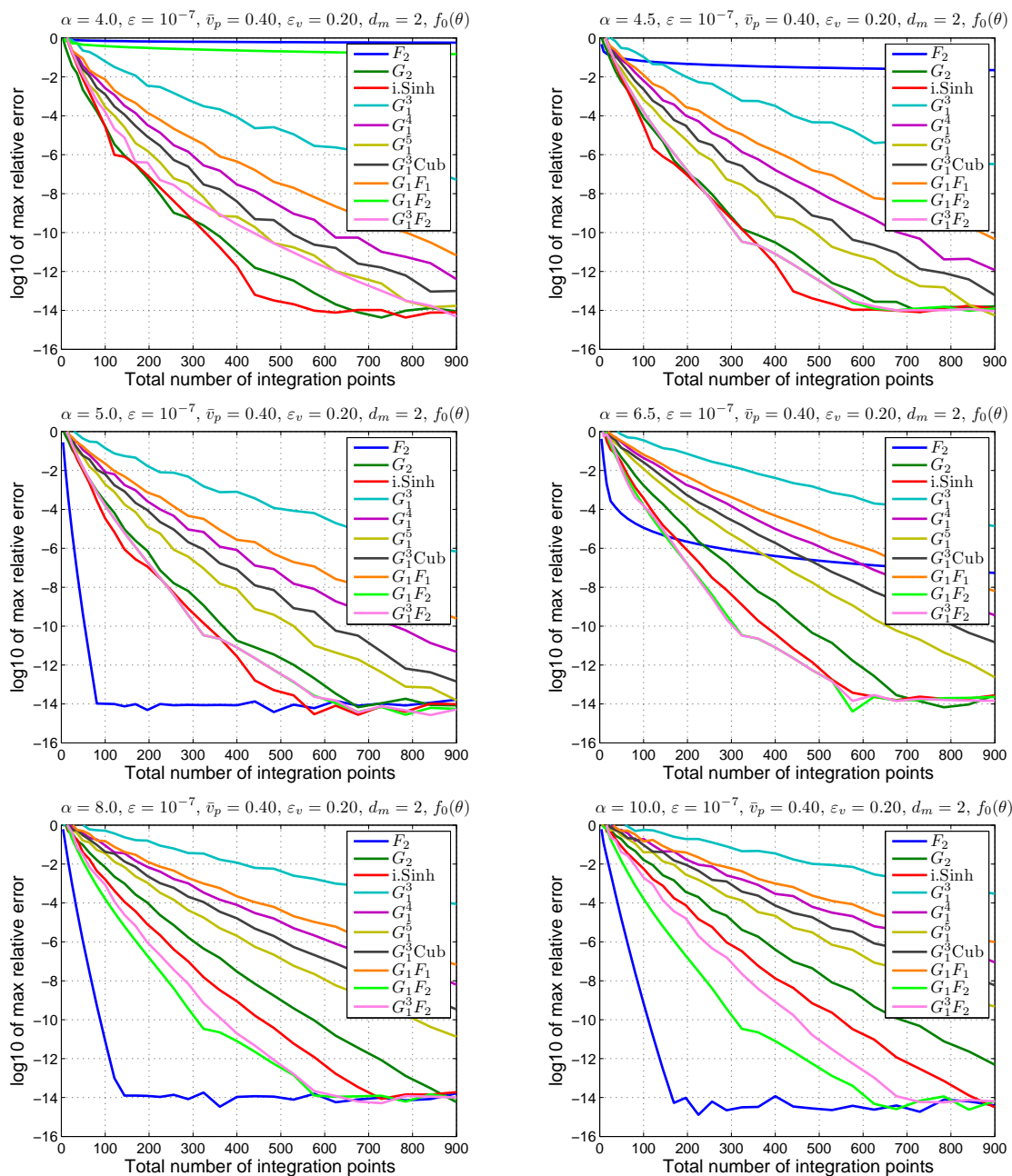
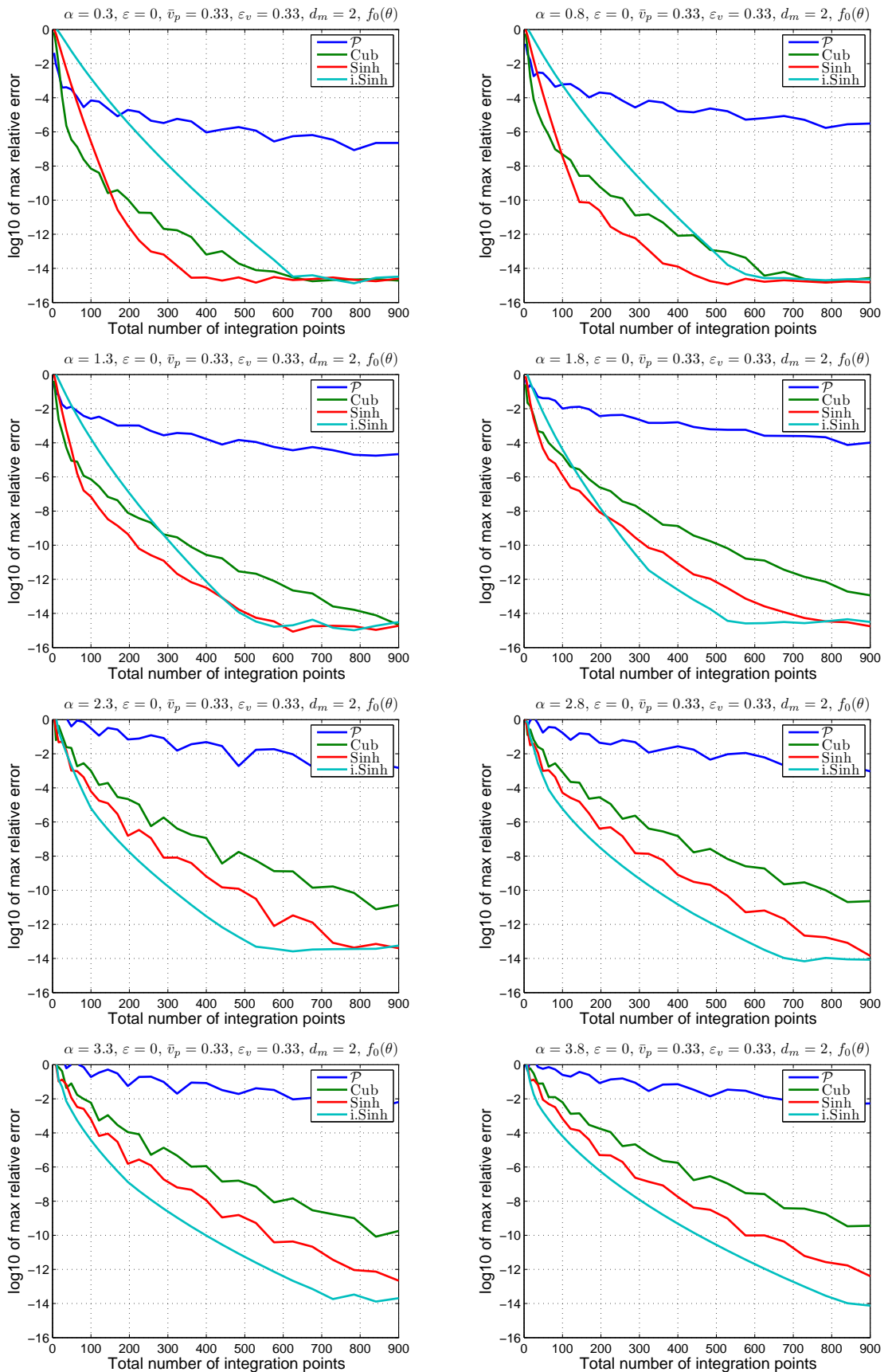


Figure 4.7.: Near-singular integral for $\alpha > 2$, part 2

Figure 4.8.: Numerical results for an adjacent triangle ($\varepsilon = 0$)

4.7 Numerical results

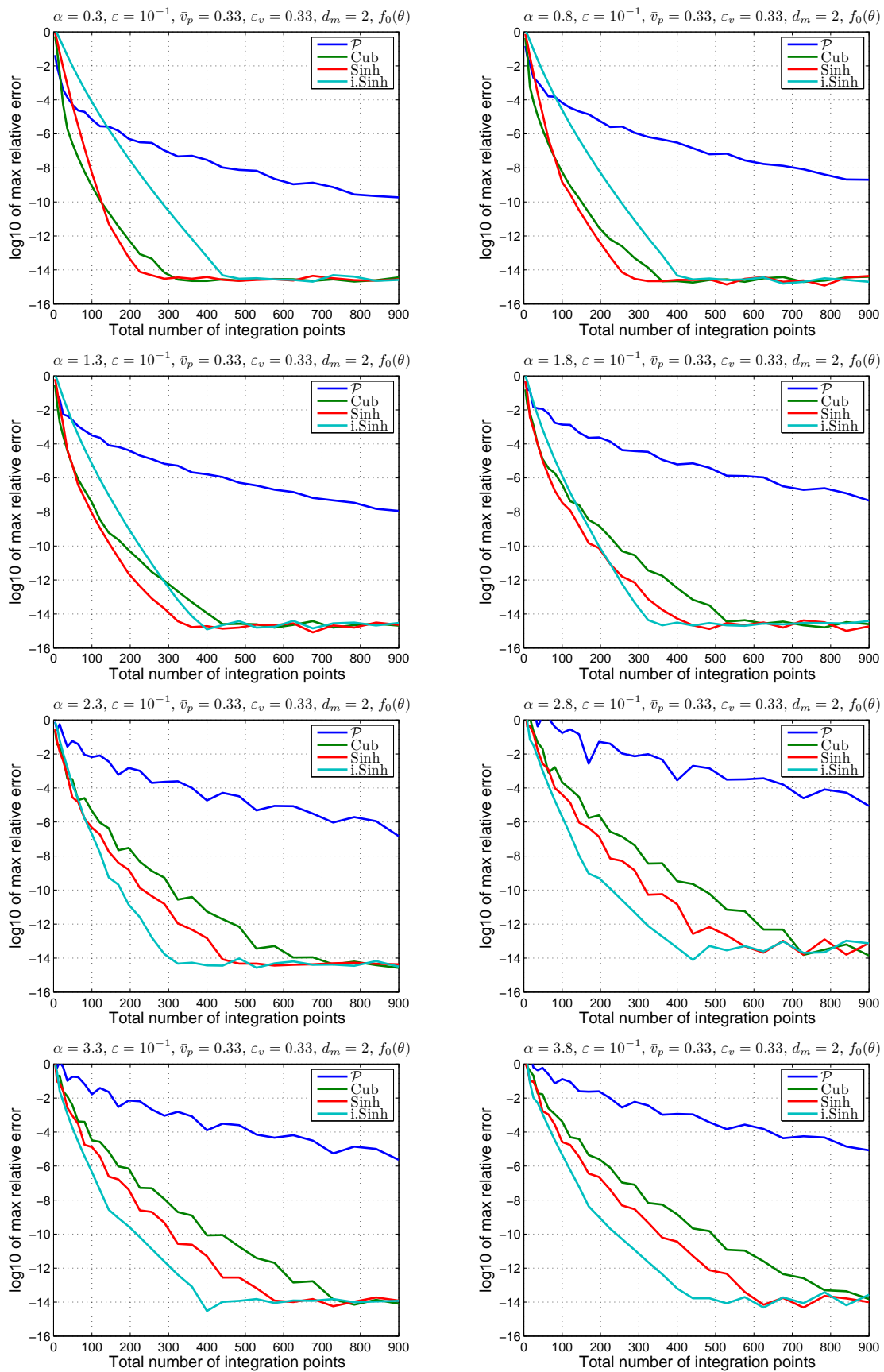


Figure 4.9.: Numerical results for an adjacent triangle ($\varepsilon > 0$)

5. The singular integral in 3D

5.1. Overview

This chapter is dedicated to the computation of the vertex-singular integral:

$$I = \iiint_P \frac{g(\mathbf{x})}{f(\mathbf{x} - \mathbf{x}_0)} d\mathbf{x}, \quad (5.1)$$

where P is a trilinear pyramid (sec. 2.2.3) with apex \mathbf{x}_0 such that $J_P > 0$ in the interior of C_3 , g is a regular integrable function and f is an α -positively homogeneous function, i.e. $f(t\mathbf{x}) = t^\alpha f(\mathbf{x})$, for $t > 0$. We assume that f vanishes nowhere apart from the origin. A typical example in terms of the Euclidean distance would be $f(\mathbf{x}) = |\mathbf{x}|^\alpha$. The real parameter α is the singularity strength, with $\alpha < 3$ for (5.1) to be finite.

As in the previous chapters, we denote the parent coordinates as $\bar{\mathbf{u}} = (\bar{u}, \bar{v}, \bar{w})$ and keep the notation $\mathbf{u} = (u, v, w)$ for the transformed coordinates. Applying the pyramidal transformation (2.16), (2.18) to the integral in (5.1) results in

$$I = \iiint_{C_3} g(\mathbf{x}(\bar{\mathbf{u}})) \bar{u}^{2-\alpha} \phi(\bar{v}, \bar{w}) d\bar{\mathbf{u}}, \quad (5.2)$$

where $C_3 = [0, 1]^3$, the scalar function $\phi(\bar{v}, \bar{w})$ is defined by

$$\phi(\bar{v}, \bar{w}) = \frac{\sum_{\mathbf{i} \in I_2} N_{\mathbf{i}}(\bar{v}, \bar{w}) V_{\mathbf{i}}}{f(\mathbf{r}(\bar{v}, \bar{w}))}, \quad (5.3)$$

and $\mathbf{r}(\bar{v}, \bar{w})$ is given in (2.20) and rewritten here for convenience:

$$\mathbf{r}(\bar{v}, \bar{w}) = \sum_{\mathbf{i} \in I_2} N_{\mathbf{i}}(\bar{v}, \bar{w}) (\mathbf{x}_{1i_1 i_2} - \mathbf{x}_0). \quad (5.4)$$

We notice that $g(\mathbf{x}(\bar{\mathbf{u}}))$ is regular since g is regular and \mathbf{x} is a polynomial map. The regular part of the integrand, g , is typically composed of a polynomial of arbitrary degree related to isoparametric shape functions and their derivatives. Moreover, in certain problems related to crack growth or fracture mechanics, branch functions may appear as a factor of g (see sec. 5.5 for details).

Thus, the application of the pyramidal transformation conveys a double benefit: the integral I in (5.2) is expressed over a standard domain, whereas its singular kernel becomes factorized into a radial part, $\bar{u}^{2-\alpha}$, and an angular part, $\phi(\bar{v}, \bar{w})$. Unfortunately, this transformation may not completely remove all singularities. For

instance, the radial term $\bar{u}^{2-\alpha}$ is regular for integer α , but for non-integer α its successive derivatives may be singular at $\bar{u} = 0$. In fact, if $\alpha > 2$ the integrand itself is still singular at $\bar{u} = 0$, as pointed out in [49].

On the other hand, the angular term $\phi(\bar{v}, \bar{w})$, is non-singular in $C_2 = [0, 1]^2$ since, according to sec. 2.2, \mathbf{r} does not vanish and neither does $f(\mathbf{r})$. However, it will be shown that $\phi(\bar{v}, \bar{w})$ may have near-singularities over C_2 , i.e., points where the function and/or its partial derivatives take very large, yet finite values.

The next subsections describe how to deal with the remaining singularities in each separate part of the kernel. More specifically, a radial transformation will be introduced to treat the singularity in the term $\bar{u}^{2-\alpha}$, whereas angular transformations will take care of the near-singularities in ϕ .

5.2. The radial kernel

Several strategies have been devised to treat the radial singularity. Some authors try to soften the singularity by applying quadrature rules adapted to specific kernels, by means of moment fitting methods. For example, Gauss-Jacobi and composite Gauss-Legendre rules are used in [7, 8] and Gauss-Jacobi rules in [11]. On the other hand, there exist transformation methods that aim at attenuating the \bar{u} -singularity and produce the simplest possible kernel in terms of integration, namely a polynomial. They consist of a map of the unit interval $[0, 1]$ onto itself, such that the exponent of the new variable in the kernel is increased to an integer value, to make the function softer without compromising the computational cost of the procedure (see e.g. [49]).

Extending the ideas in sec. 3.5, we consider an a posteriori map $\bar{u} = \bar{u}(u)$ that verifies the following equation

$$\bar{u}(u)^{2-\alpha} \frac{d\bar{u}}{du} = c_1 \frac{d\sigma(u)}{du}, \quad (5.5)$$

where c_1 is a constant to be determined and σ is a polynomial that maps $[0, 1]$ onto itself, whose purpose is to make \bar{u} as smooth as possible. Thus, the radial factor of the kernel becomes a polynomial in u , that is written in terms of the derivative of another polynomial, σ , in order to simplify the subsequent developments.

By direct integration of (5.5) we obtain the solution \bar{u} in closed form

$$\begin{aligned} \bar{u}(u) &= \sigma(u)^{\frac{1}{3-\alpha}}, \\ c_1 &= \frac{1}{3-\alpha}. \end{aligned}$$

In the simplest case where $\sigma(u) = u$, the solution of (5.5) takes the form

$$\bar{u}(u) = u^{\frac{1}{3-\alpha}},$$

which is smooth enough for values of α close to 3. However, if $\alpha < \frac{5}{2}$, the second or even the first derivative of \bar{u} may be singular at $u = 0$, affecting severely the accuracy

of the quadrature rule. Following the reasoning in sec. 3.5 we take $\sigma(u) = u^{n_1+1}$, where n_1 is a small, suitable integer, from where

$$\bar{u}(u) = u^{\frac{n_1+1}{3-\alpha}}. \quad (5.6)$$

If α is an integer or a half-integer, the value of n_1 can be easily chosen so that the exponent in (5.6) is an integer. For instance, if $\alpha = \frac{1}{2}, 1, \frac{3}{2}, 2, \frac{5}{2}$, it suffices taking $n_1 = 4, 1, 2, 0, 0$.

For more arbitrary values of α , the choice of n_1 might not be so immediate. It is clear that the larger n_1 , the stronger the softening effect on $\bar{u}(u)$. More specifically, if $\frac{n_1+1}{3-\alpha} \geq k$, then the first k derivatives of $\bar{u}(u)$ are non-singular at $u = 0$. However, the degree of the polynomials involved increases with n_1 , and this affects the exactness of the rule. Numerical simulations allow to determine the optimal trade-off value of n_1 for which the quadrature error reaches a minimum. For example, if monomials up to degree two are used as the regular part of the integrand, i.e., $g(x, y, z) = x^i y^j z^k$, $i + j + k \leq 2$ over the standard pyramid P_1 (sec. 2.2.3), the optimal values of n_1 can be picked from Tab. 5.1.

Table 5.1.: Optimal exponent n_1 for $\bar{u}(u) = u^{\frac{n_1+1}{3-\alpha}}$

α	< 1.1	< 1.4	< 1.8	< 2.1	< 2.4	< 2.6	< 2.8	< 3
n_1	7	6	5	4	3	2	1	0

We remark that the idea of increasing the exponent to soften \bar{u} has been used in [49], for α being an integer or the ratio of two small integers. The proposed transformation (5.6) can be readily used for any value of $\alpha \in (0, 3)$. Particularly, fast convergence rates are achieved for strong singularities with $\alpha > 2$.

5.3. The angular kernel

Unlike the radial singularity, less attention has been devoted in the literature to the near-singularities in the angular kernel of (5.1). In fact, most existing methods implement a plain Gaussian rule on the non-radial variables [11, 47, 49, 55], although Dunavant rules (see [12]) have been used in [55], and some other techniques, such as sparse grids and Sobol' sequences have been considered in [7, 8].

This section describes how the near-singularities in $\phi(\bar{v}, \bar{w})$ happen to be of a quite subtle nature, yet they have a strong influence on the performance of the quadrature rules. In order to illustrate this point, Fig. 5.1 shows the behaviour, for $\alpha = 1.6$ and $f(\mathbf{r}) = |\mathbf{r}|^\alpha$, of $\phi(\bar{v}, \bar{w})$ and its first derivatives $\frac{\partial \phi}{\partial \bar{v}}$, $\frac{\partial \phi}{\partial \bar{w}}$ for a regular element, namely the standard pyramid P_1 (see sec. 2.2.3), and a distorted element whose vertex \mathbf{x}_{100} has been displaced to the point $(0.5, -0.4, -0.2)$ (the same vertical scaling has been used for each pair of graphics). It is clear that much stronger variations occur in the case of the distorted element.

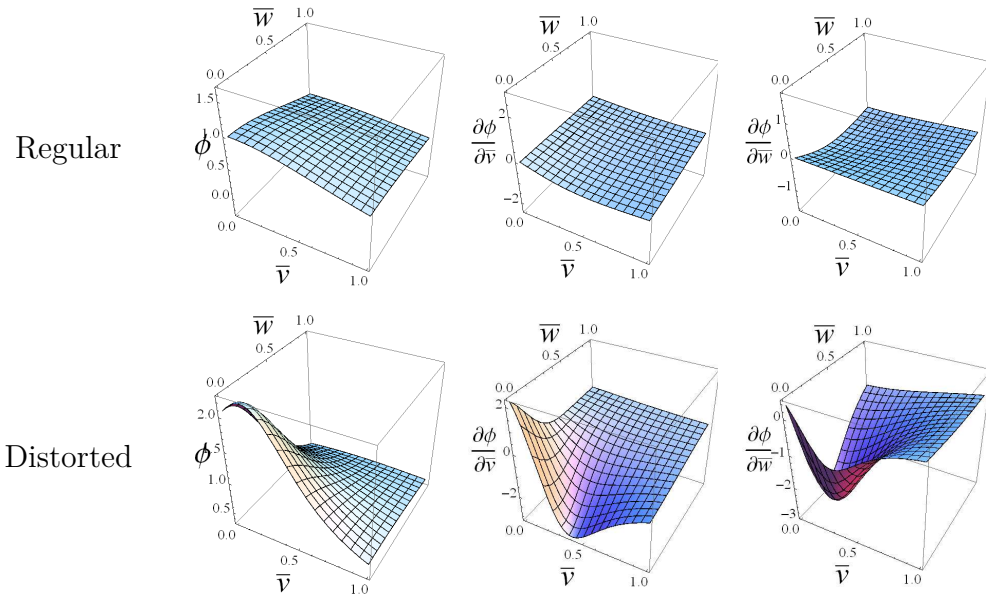


Figure 5.1.: Behaviour of $\phi(\bar{v}, \bar{w})$ for a regular and a distorted element

The standard strategy to soften the near-singularities in the angular kernel would be to treat $\phi(\bar{v}, \bar{w})$ as a weight function, and develop a quadrature rule, by means of moment fitting equations, specific to that particular weight. The obvious disadvantage of this idea is that a new quadrature rule would have to be developed whenever the vertex coordinates, or even the singularity strength α , were changed.

A different approach might be to extend the method introduced in sec. 3.5 to the kernel in two variables, by finding a transformation

$$(\bar{v}, \bar{w}) = (\bar{v}(v, w), \bar{w}(v, w)), \quad (5.7)$$

that maps C_2 onto itself and leaves a polynomial kernel. However, the fact that $\phi(\bar{v}, \bar{w})$ does not have, in general, separated variables, means that this procedure is likely to incur a high computational cost.

5.3.1. The behaviour of ϕ on the boundary of C_2

A simpler approach is possible by focusing on single-variable transformations that soften the angular kernel on the boundary of C_2 , rather than its interior. Numerical experiments show that there exist maps that improve simultaneously the behaviour of ϕ on the boundary of C_2 and its interior for some particular kernels. We next give some evidence on this statement.

Taking (5.4) into account, the restriction of $\phi(\bar{v}, \bar{w})$ to any of the 4 sides of C_2 can be written as

$$\phi_B(\bar{v}) = \frac{(1 - \bar{v})V_1 + \bar{v}V_2}{f((1 - \bar{v})(\mathbf{x}_1 - \mathbf{x}_0) + \bar{v}(\mathbf{x}_2 - \mathbf{x}_0))}, \quad (5.8)$$

where short indices 1, 2 have been used. Here, the volumes V_1, V_2 coincide with one of the volumes $V_{i_1 i_2}$, $\mathbf{x}_1, \mathbf{x}_2$ stand for $\mathbf{x}_{1 i_1 i_2}$ and the variable \bar{w} has been renamed as \bar{v} where necessary. The correspondence between the short indices 1, 2 and the tensor indices $i_1 i_2$ can be easily obtained from (5.3).

We look for a single-variable map $\bar{v} = \bar{v}(v)$ such that the near-singularities in the composite function $\phi_B(\bar{v}(v))$ become attenuated. One transformation will be applied to one of the boundaries $(\bar{v}, 0)$ or $(\bar{v}, 1)$, wherever ϕ_B behaves less smoothly (Fig. 5.1). Similarly, another transformation will be applied to one of the boundaries $(0, \bar{w})$ or $(1, \bar{w})$. We impose that all maps leave $[0, 1]$ invariant, in order to avoid hidden singularities on the boundaries of non-standard domains, as pointed out in e.g. [3, 60].

5.3.2. The algebraic kernel

Since the actual form of the transformation \bar{v} depends on the particular kernel considered, we now focus on the algebraic case, that occurs when $f(\mathbf{r}) = |\mathbf{r}|^\alpha$ in (5.3), i.e.:

$$\phi(\bar{v}, \bar{w}) = \frac{\sum_{\mathbf{i} \in I_2} N_{\mathbf{i}}(\bar{v}, \bar{w}) V_{\mathbf{i}}}{|\mathbf{r}(\bar{v}, \bar{w})|^\alpha}. \quad (5.9)$$

Then, the restriction of (5.9) to the boundary of C_2 takes the form:

$$\phi_B(\bar{v}) = \frac{(1 - \bar{v})V_1 + \bar{v}V_2}{|(1 - \bar{v})(\mathbf{x}_1 - \mathbf{x}_0) + \bar{v}(\mathbf{x}_2 - \mathbf{x}_0)|^\alpha}. \quad (5.10)$$

We recall that an expression for the denominator of (5.10) had already been obtained in equation (2.12), that is rewritten here for convenience:

$$|(1 - \bar{v})(\mathbf{x}_1 - \mathbf{x}_0) + \bar{v}(\mathbf{x}_2 - \mathbf{x}_0)| = |\mathbf{x}_1 - \mathbf{x}_2| \left((v - v_p)^2 + \varepsilon_v^2 \right)^{1/2},$$

with \bar{v}_p and ε_v as defined in sec. 2.2.2. It is then immediate that

$$\phi_B(\bar{v}) = \frac{(1 - \bar{v})V_1 + \bar{v}V_2}{|\mathbf{x}_1 - \mathbf{x}_2|^\alpha} \phi_N(\bar{v}),$$

with ϕ_N defined in (3.10).

This reasoning leads to the remarkable conclusion that the boundary-restricted angular kernel in the 3D singular problem, equals a linear term multiplied by the same near-singular kernel in 1D already considered in chapter 3 and chapter 4.

Numerical experiments show that some of the angular transformations already utilized in the previous chapters to soften ϕ_N , most notably the cubic and the sinh transformations, are able to improve simultaneously the behaviour of the bivariate kernel $\phi(\bar{v}, \bar{w})$ on the boundary of C_2 and its interior.

We remark that the bivariate kernel ϕ in (5.9) depends on 12 parameters (the three spatial coordinates of the four vertices opposite to the pyramid apex), whereas the 2D near-singular kernel in (4.1)-(4.2) depends at most on 7 parameters (the two

planar coordinates of the triangle vertices plus the near-singular perturbation ε). In consequence, $\phi(\bar{v}, \bar{w})$ is likely to be a more complicated function, in the general case, than the near-singular kernel in 2D, and the existence of a purely bivariate transformation (5.7) remains an open question.

5.3.3. Implementation of the methods proposed

From a practical point of view, the softening transformations are applied separately to the variables \bar{v} and \bar{w} . In each case, the transformation is applied on the boundary where ϕ_N behaves less smoothly, i.e., the one for which ε_v has the smallest value, according to the following steps:

1. On boundaries $(\bar{v}, 0)$, $(\bar{v}, 1)$ compute $\varepsilon_v = \frac{h_T}{|\mathbf{x}_1 - \mathbf{x}_2|}$ and take the smallest value.
2. Calculate r_0 from (3.17) or μ from (3.19).
3. Compute t_0 and t_1 by means of (3.15).
4. Construct \bar{v} and its Jacobian from (3.11).
5. Repeat steps 1-4 on boundaries $(0, \bar{w})$, $(1, \bar{w})$ to obtain \bar{w} and its Jacobian.

Even though \bar{v} and \bar{w} are applied on the boundary of C_2 , numerical experiments will show noticeable improvements in convergence speed when compared to methods that implement no angular softening.

We remark that the use of separate univariate maps in both variables \bar{v} and \bar{w} has already been considered by a number of authors for the ordinary near-singular 2D kernel [24, 46, 73]. Further developments of [24] can be found, e.g., in [25, 26, 27].

5.4. The Jacobian of the composite transformation

The Jacobian of the regularizing transformation \mathcal{R} described in the previous sections is

$$J_{\mathcal{R}}(\mathbf{u}) = \frac{n_1 + 1}{3 - \alpha} \bar{u}(u)^{\alpha-2} u^{n_1} \frac{d\bar{v}}{dv} \frac{d\bar{w}}{dw}.$$

Thus, the composition of the pyramidal and regularizing maps has a Jacobian

$$J_{\mathcal{P} \circ \mathcal{R}}(\mathbf{u}) = \frac{n_1 + 1}{3 - \alpha} \bar{u}(u)^\alpha \sum_{\mathbf{i} \in I_2} (N_{\mathbf{i}}(\bar{v}(v), \bar{w}(w)) V_{\mathbf{i}}) u^{n_1} \frac{d\bar{v}}{dv} \frac{d\bar{w}}{dw}.$$

5.5. Numerical results

The algorithms detailed in the previous sections are now tested in a variety of situations, comparing its performance with some existing methods [11, 47, 49, 55].

Integrations are always performed in the physical domain by means of modified nodes and weights, that recalling (1.3)-(1.4) are obtained from

$$\begin{aligned}\mathbf{x}_j &= \mathbf{x}(\bar{\mathbf{u}}(\mathbf{u}_j)), \\ w_j^* &= J_{\mathcal{P} \circ \mathcal{R}}(\mathbf{u}_j)w_j,\end{aligned}$$

for $j = 1, \dots, n_w$, where \mathbf{u}_j and w_j are the standard Gaussian nodes and weights, respectively, for the quadrature rule of order n_w .

The singular part of the physical integrand is $\frac{1}{|\mathbf{x}-\mathbf{x}_0|^\alpha}$. Regarding the regular integrand, the following functions are taken:

$$g(x, y, z) = (x - x_0)^i (y - y_0)^j (z - z_0)^k f_\ell(\theta),$$

with $i + j + k \leq d_m$, d_m being the total degree of monomials, $\theta = \tan^{-1} \frac{y-y_0}{x-x_0}$ and $f_\ell(\theta)$ is the angular part of the crack-tip, or branch functions, whose explicit form was given in sec. 3.6.

5.5.1. Simulations over pyramids

The methods implemented for comparison purposes are:

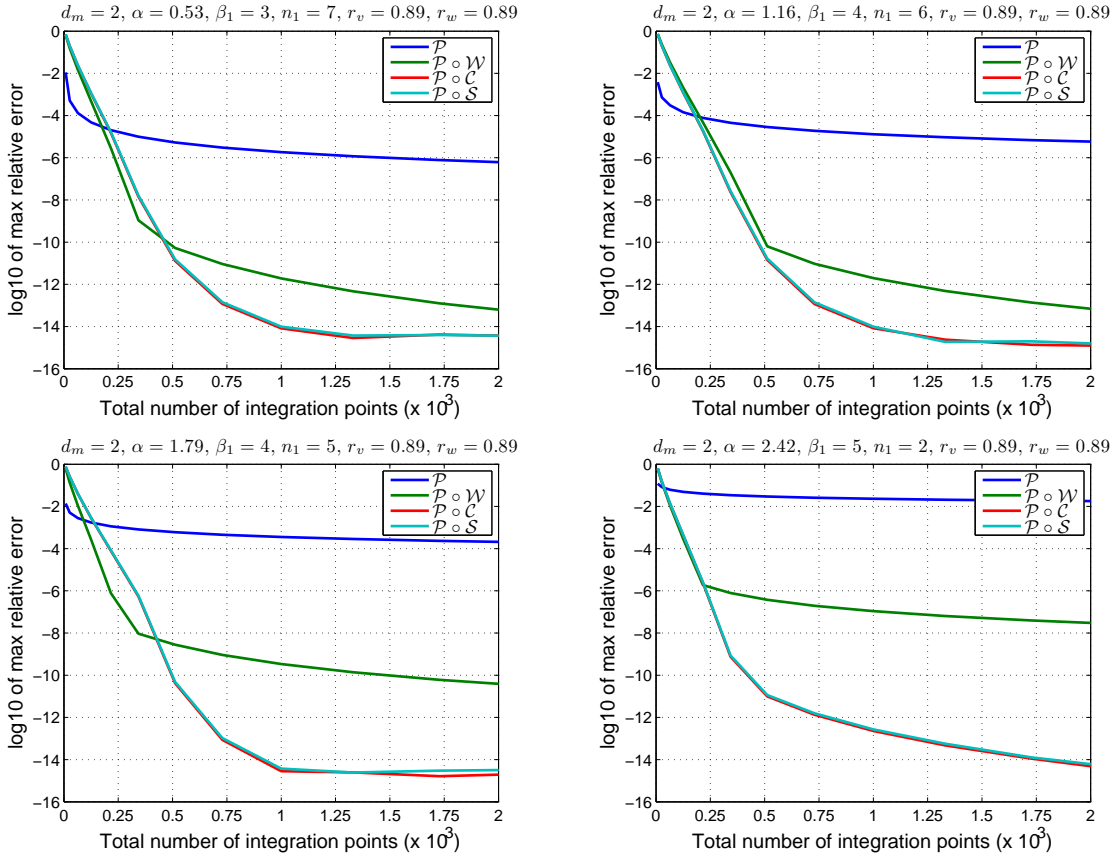
- \mathcal{P} : Pyramidal transformation in 3D, already described in subsection sec. 2.2.3.
- $\mathcal{P} \circ \mathcal{C}$: Composition of \mathcal{P} with the radial softening in sec. 5.2 and the cubic transformation in both angular variables (sec. 3.4.3).
- $\mathcal{P} \circ \mathcal{S}$: Same scheme but instead of cubic, the sinh transformation (sec. 3.4.4) is implemented in the angular variables.
- $\mathcal{P} \circ \mathcal{W}$: Composition of \mathcal{P} with the power transformation in the radial variable. This method, which does not incorporate angular softening, is an extension of [49] to arbitrary pyramids given by

$$\begin{aligned}\mathbf{x}(u, v, w) - \mathbf{x}_0 &= u^{\beta_1} \mathbf{r}(v, w), \\ J_{\mathcal{P} \circ \mathcal{W}}(\mathbf{u}) &= \beta_1 u^{3\beta_1 - 1} \sum_{\mathbf{i} \in \mathcal{I}_2} N_{\mathbf{i}}(\mathbf{v}) V_{\mathbf{i}}.\end{aligned}$$

The efficiency of the $\mathcal{P} \circ \mathcal{W}$ method greatly relies on an adequate choice of the parameter β_1 , that plays a similar role to the parameter n_1 in (5.6). The authors in [49] point out that when the singularity strength, α , is an integer or the ratio of two small integers (like $\frac{1}{2}$, $\frac{1}{3}$, $\frac{2}{3}$ and so on), then the value of β_1 should be equal to the denominator of α . However, when α has a more arbitrary value, no systematic way of finding β_1 is provided. As with n_1 , the optimal value of β_1 can be picked from Tab. 5.2, that was obtained empirically.

Table 5.2.: Optimal exponent β_1 for $\mathcal{P} \circ \mathcal{W}$

α	< 1	< 2	< 2.3	< 2.6	< 3
β_1	3	4	5	6	7

**Figure 5.2.:** Performance of the methods over the standard pyramid P_1

Numerical experiments The exact value of the integrals is evaluated by means of a high-degree rule, with a total monomial degree of $d_m = 2$. On top of each graphic, the parameters $d_m, \alpha, \beta_1, n_1, r_v$ (r_0 for \bar{v}), and r_w (r_0 for \bar{w}) are displayed.

All methods are initially tested on the standard pyramid P_1 (see sec. 2.2.3), for $\alpha = 0.53 + 0.63k, k = 0, 1, 2, 3$. The cases with integer or half-integer α are similar to the examples displayed, with \mathcal{P} and $\mathcal{P} \circ \mathcal{W}$ being coincident for integer α . Notice that angular softening in the cubic transformation already applies (i.e., $r_v, r_w < 1$) to this apparently non-distorted case (Fig. 5.2).

A moderately distorted pyramid is considered as well. If we take $\mathbf{x}_0 = (0, 0, 0), \mathbf{x}_{100} = (1, 0.5, 0.5), \mathbf{x}_{101} = (1, -0.5, 1), \mathbf{x}_{110} = (1.5, 3, 0.5), \mathbf{x}_{111} = (0.5, 4.5, 4)$, the angular softening becomes quite significant, as depicted in Fig. 5.3.

For a more distorted pyramid, typically with obtuse tip angles θ_0 , all methods

perform more poorly, and the effect of angular softening is less evident. For example, taking $\mathbf{x}_0 = (0, 0, 0)$, $\mathbf{x}_{100} = (2, -0.5, -0.5)$, $\mathbf{x}_{101} = (1, -1, 1)$, $\mathbf{x}_{110} = (1.5, 1, -1)$, $\mathbf{x}_{111} = (0.5, 3, 3)$, yields the results shown in Fig. 5.4.

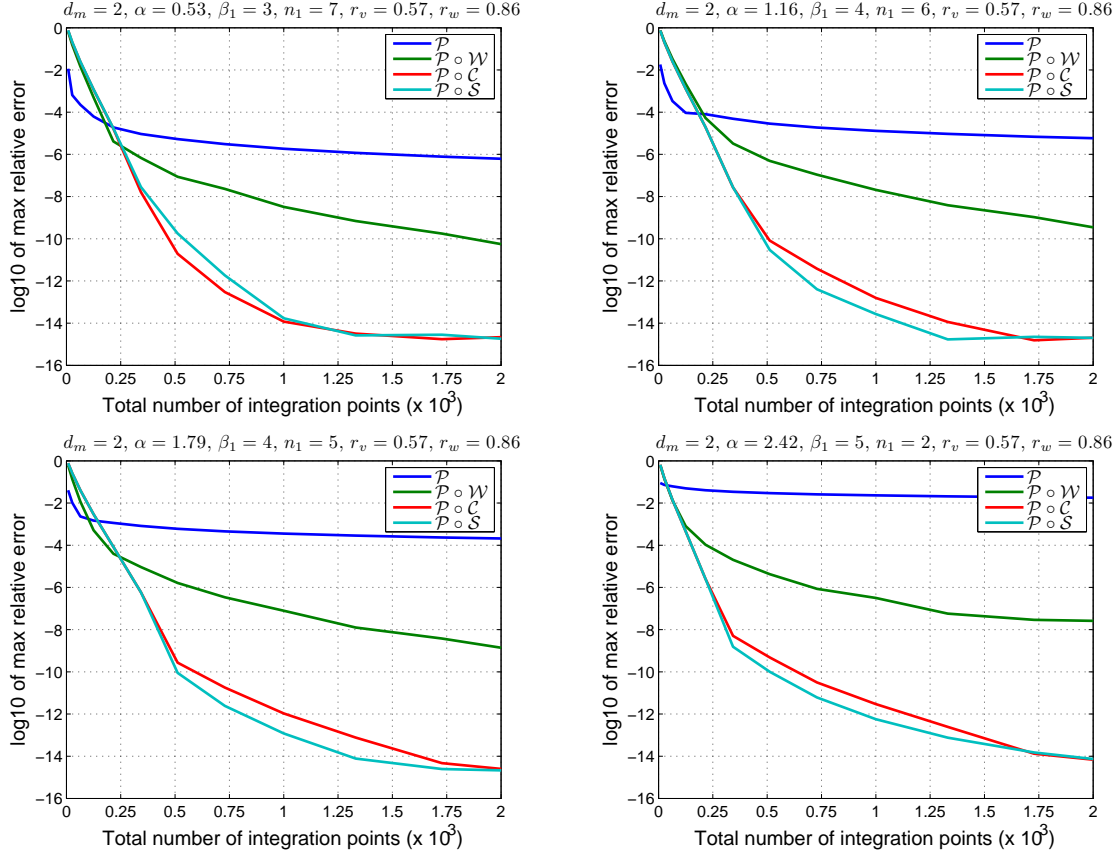


Figure 5.3.: Moderately distorted pyramid

5.5.2. Simulations over tetrahedra

We assume without loss of generality that the vertex \mathbf{x}_{101} collapses onto \mathbf{x}_{100} to form a tetrahedron, in other words, the boundary $(0, \bar{w})$ now reduces to a point.

All methods implemented for pyramids can be readily reformulated for arbitrary tetrahedra. Moreover, two additional transformations are considered:

Trigonometric transformation Denoted by \mathcal{T} , it is a modification of the method proposed in [55]. More specifically it consists of two stages:

1. An affine transformation whose inverse maps an arbitrary tetrahedron T (in coordinates x, y, z) onto the standard tetrahedron T_0 (in coordinates r, s, t), with vertices $(0, 0, 0)$, $(1, 0, 0)$, $(0, 1, 0)$, $(0, 0, 1)$.

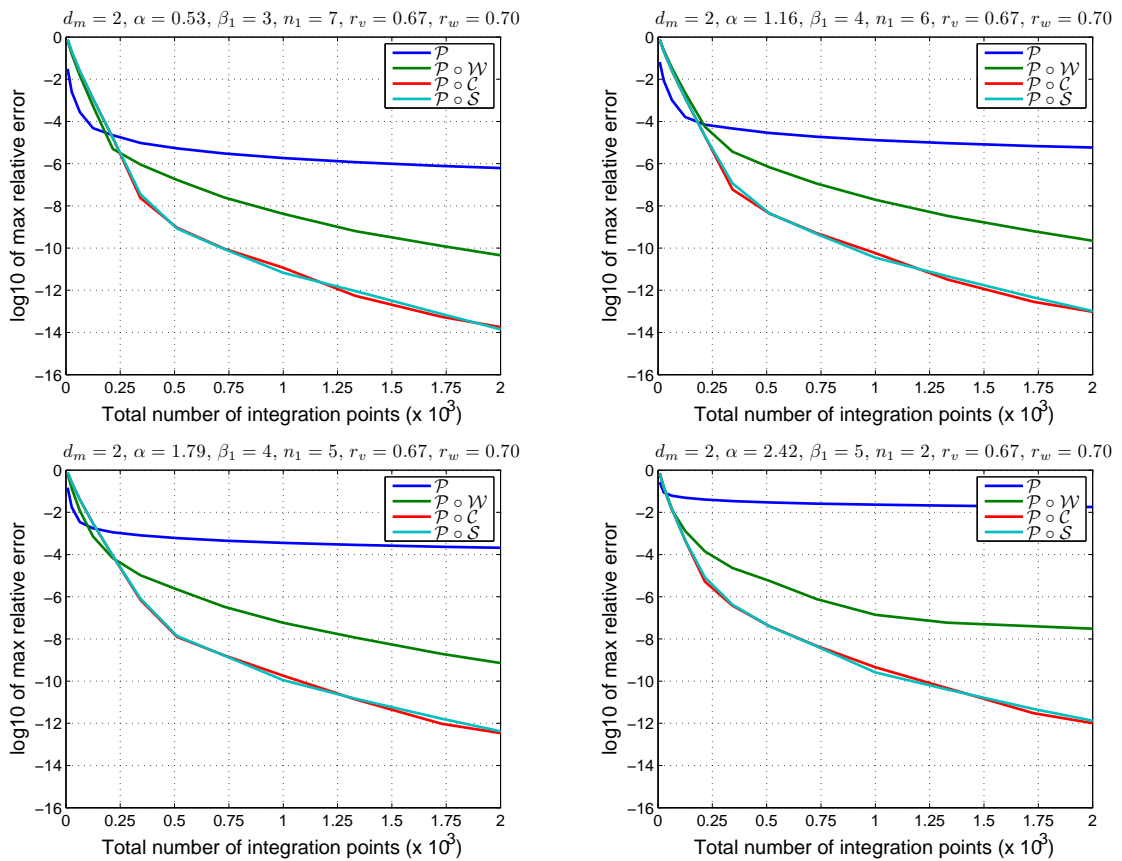


Figure 5.4.: Strongly distorted pyramid

2. A trigonometric transformation whose inverse maps T_0 onto the unit cube C_3 (in coordinates u, v, w), with parametric equations

$$\begin{aligned}
 r(\mathbf{u}) &= u \cos^2\left(\frac{\pi}{2}v\right), \\
 s(\mathbf{u}) &= u \cos^2\left(\frac{\pi}{2}(1-v+vw)\right), \\
 t(\mathbf{u}) &= u - r(\mathbf{u}) - s(\mathbf{u}), \\
 J(\mathbf{u}) &= \frac{\pi^2}{4}u^2v \sin(\pi v) \sin(\pi(1-v+vw)).
 \end{aligned}$$

Hyperbolic transformation Denoted by \mathcal{H} , it is an implementation in two steps of the method described in [47]:

1. An affine transformation whose inverse maps an arbitrary tetrahedron T (in coordinates x, y, z) onto T_0 (in coordinates ξ, η, ζ).

2. A hyperbolic transformation whose inverse maps T_0 onto C_3 , given by

$$\begin{aligned}\xi(\mathbf{u}) &= u^2 \frac{1 - \sinh(\beta_2(2v - 1))}{2} (1 - w), \\ \eta(\mathbf{u}) &= u^2 \frac{1 + \sinh(\beta_2(2v - 1))}{2} (1 - w), \\ \zeta(\mathbf{u}) &= u^2 w, \\ J(\mathbf{u}) &= 2\beta_2 u^5 (1 - w) \cosh(\beta_2(2v - 1)),\end{aligned}$$

with $\beta_2 = \sinh^{-1} 1 = \log(1 + \sqrt{2})$.

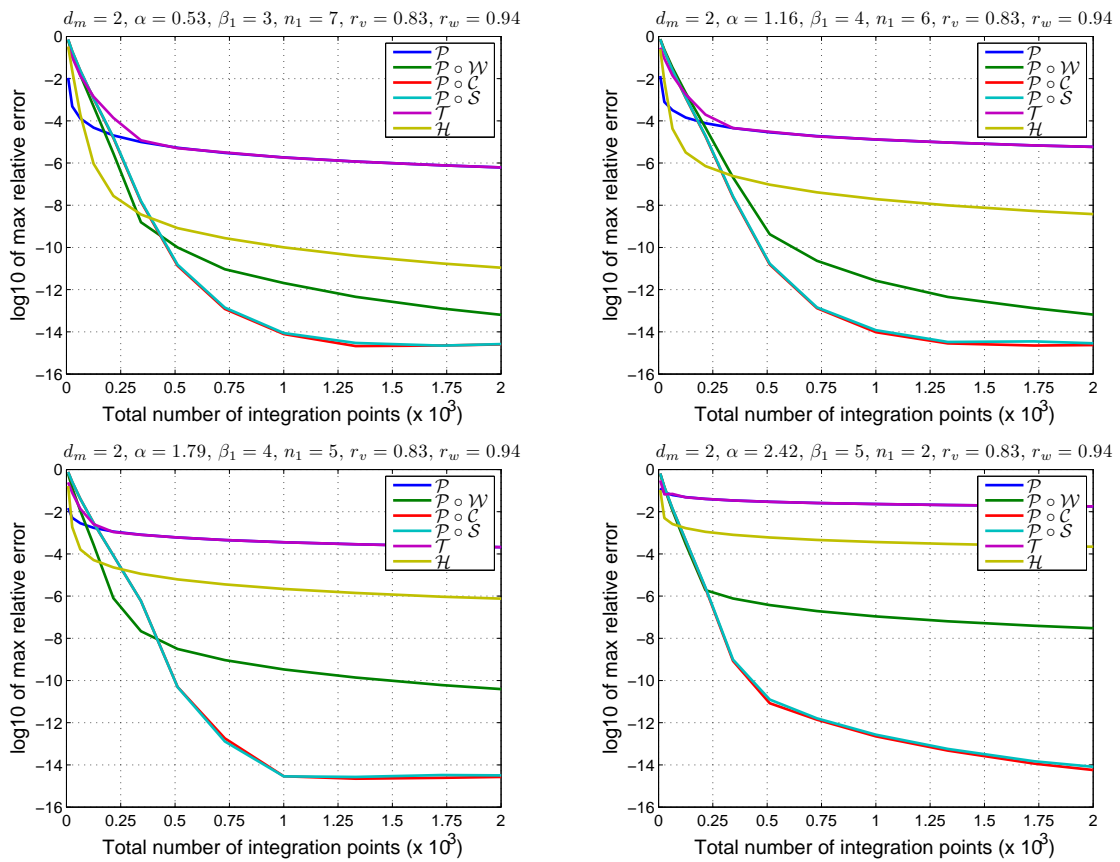


Figure 5.5.: Standard tetrahedron T_1

Numerical experiments The results are very similar to the pyramid case: all methods degrade when applied to distorted elements, specially for large values of α .

The first element tested is the standard tetrahedron T_1 (see sec. 2.2.3), with results displayed in Fig. 5.5. Notice that angular softening in the cubic transformation is already needed (i.e., $r_v, r_w < 1$) for this non-distorted case.

The second element tested is a distorted tetrahedron with vertices $\mathbf{x}_0 = (0, 0, 0)$, $\mathbf{x}_{100} = (1, 0, 0)$, $\mathbf{x}_{110} = (1, 4, 0)$, $\mathbf{x}_{111} = (0.5, 4, 3)$. As expected, all methods show a slower convergence (Fig. 5.6).

It is worth noting that in general, when using pyramids as well as tetrahedra, the performance of all methods deteriorates when crack-tip functions are part of the regular integrand. This effect is more evident as the tip angles θ_0 become larger.

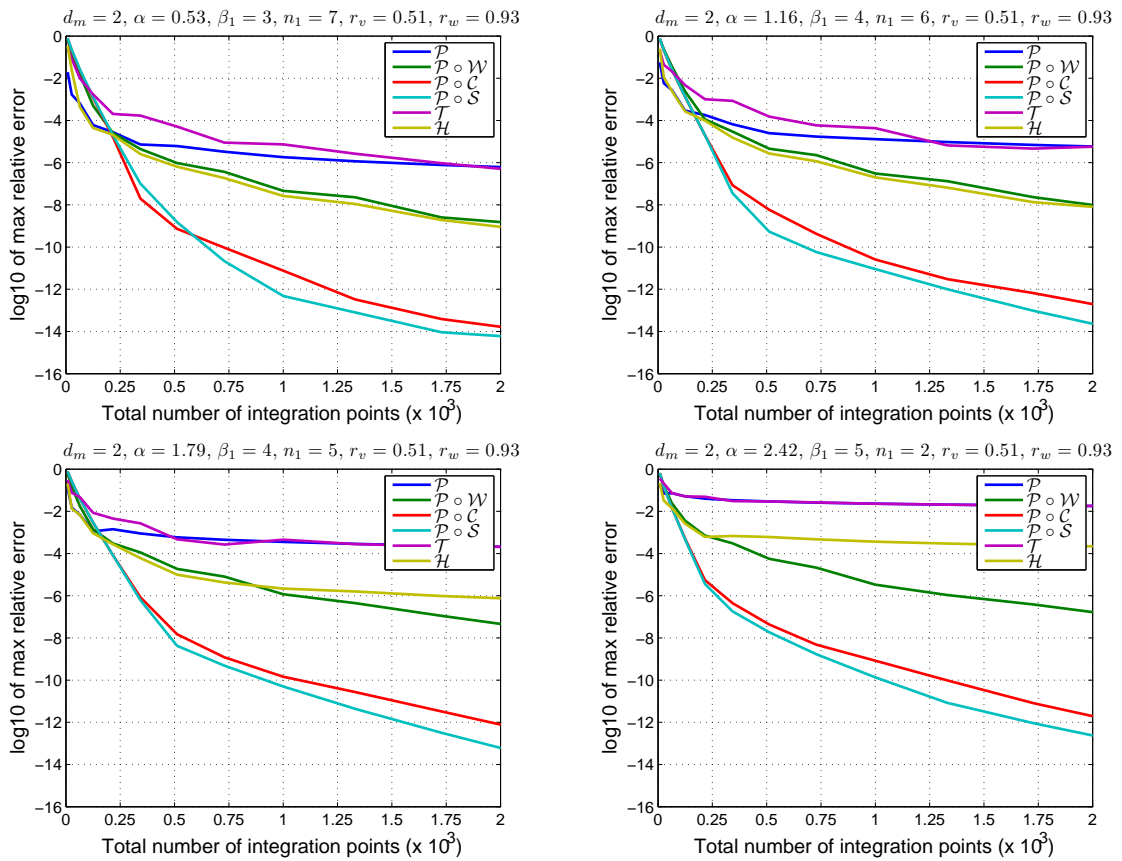


Figure 5.6.: Strongly distorted tetrahedron

6. The optimal form of the cubic transformation

6.1. Overview

Throughout the previous chapters, several non-linear transformations of the form

$$\bar{v}(v) = \bar{v}_p + h(t(v)), \quad (6.1)$$

have been considered with the purpose of softening the near-singular kernel

$$\phi_N(\bar{v}) = \frac{1}{((\bar{v} - \bar{v}_p)^2 + \varepsilon_v^2)^{\alpha/2}}, \quad (6.2)$$

whose complex poles are originally located at

$$\bar{v} = \bar{v}_p \pm i\varepsilon_v.$$

The cubic transformation is a particular case of (6.1) with

$$h(t) = rt + (1 - r)t^3, \quad (6.3)$$

where r is a free parameter whose optimal value, i.e., the one that minimizes the error in the quadrature rules, is established in what follows. A remarkable conclusion of this chapter will be that this optimal value depends on the geometric form factor ε_v , but not on the position of the kernel peak point \bar{v}_p (sec. 2.2.2). We also recall that $t(v)$ is an affine transformation given by

$$t(v) = t_0 + (t_1 - t_0)v, \quad (6.4)$$

$$t_j = h^{-1}(j - \bar{v}_p), \quad (6.5)$$

whose purpose is to renormalize the integration interval to $v \in [0, 1]$.

As already pointed out in sec. 3.4.1, the truncation error in the quadrature rules decreases as the semi-axis sum in (3.12) increases. Thus, the optimal value of the cubic transformation will be such that a maximum (largest) ellipse of analyticity \mathcal{E}_p is originated. This chapter develops a proof that the largest \mathcal{E}_p occurs for a critical, or optimal value r_0 , already established without proof in (3.18)-(3.19), and whose expression is now justified. Some details on the structure of the proof are outlined below.

The cubic transformation can be regarded as the composition of three steps, each one having an effect over the integration interval:

1. A translation $\bar{v} = \bar{v}_p + h$ from $\bar{v} \in [0, 1]$ to $h \in [-\bar{v}_p, 1 - \bar{v}_p]$.
2. A cubic transformation (6.3) from $t \in [t_0, t_1]$ onto $h \in [-\bar{v}_p, 1 - \bar{v}_p]$, with $t_j = h^{-1}(j - \bar{v}_p)$.
3. An affine renormalization $t(v)$ from $v \in [0, 1]$ to $t \in [t_0, t_1]$.

After the first two steps, a transformed kernel of the form

$$\phi_N(\bar{v}_p + h(t)) = \frac{1}{((rt + (1-r)t^3)^2 + \varepsilon_v^2)^{\alpha/2}}, \quad (6.6)$$

is obtained, with poles on the complex plane t . After the renormalization in step 3, these poles are moved to

$$v = \frac{t - t_0}{t_1 - t_0}, \quad (6.7)$$

on the complex plane v . The complex poles of (6.6) will be denoted t -poles from now on, whereas their renormalization to (6.7) will be denoted v -poles.

The preceding discussion motivates the distribution of the proof in three different parts, namely

- Part 1 establishes that the poles of (6.6) are moved furthest away from the real axis when $r = r_0$. In other words, the closest t -pole has maximum imaginary part $\Im(t)$, in absolute value, for $r = r_0$.
- Part 2 shows that the imaginary part $\Im(v)$ of the v -poles in (6.7) also reaches a maximum for $r = r_0$.
- Part 3 finishes the proof by determining that the largest ellipse of analyticity \mathcal{E}_p occurs for $r = r_0$ in the complex plane v , although an additional hypothesis needs to be introduced for the case $\bar{v}_p < 0$.

These three parts are developed in the corresponding sections below.

6.2. Part 1. Optimality of $\Im(t)$

The complex poles of (6.6) are the 6 roots of the equation

$$(1-r)t^3 + rt \pm i\varepsilon_v = 0.$$

As t is a solution of this equation only if $-t$ is a solution too, it suffices considering the 3 complex roots of

$$(1-r)t^3 + rt - i\varepsilon_v = 0, \quad (6.8)$$

with $\varepsilon_v > 0$. Taking $t = i\tau$ to avoid complex coefficients, (6.8) can be written as

$$P_r(\tau) = 0,$$

with

$$P_r(\tau) = (1 - r)\tau^3 - r\tau + \varepsilon_v. \quad (6.9)$$

Hence, the objective of this section is the determination of the value of r for which the roots of $P_r(\tau)$ are moved furthest away from the imaginary axis of the complex plane τ . In other words, we aim at maximizing the real part of the closest root of $P_r(\tau)$ to the imaginary axis. It will be proved that this happens when (6.9) has a double real root.

We start by establishing two preliminary results.

Lemma 5. *For $\frac{\partial P_r}{\partial \tau} \neq 0$, the derivative of τ with respect to r is*

$$\frac{d\tau}{dr} = \frac{\tau(r)(\tau(r)^2 + 1)}{\frac{\partial P_r}{\partial \tau}}. \quad (6.10)$$

Proof. The Implicit Function theorem guarantees that $P_r(\tau) = 0$ defines a function $\tau(r)$ whose derivative is given by

$$\frac{d\tau}{dr} = -\frac{\frac{\partial P_r}{\partial r}}{\frac{\partial P_r}{\partial \tau}},$$

with (6.10) obtained after substituting $\frac{\partial P_r}{\partial r} = -\tau^3 - \tau$ into the numerator above. \square

Lemma 6. *$P_r(\tau)$ has a double real root for the value $r = r_0$ that satisfies*

$$\frac{4}{27\varepsilon_v^2}r_0^3 = 1 - r_0. \quad (6.11)$$

Proof. Since the coefficients of (6.9) have one change of sign, it is a consequence of the Descartes' rule of signs that $P_r(\tau)$ has exactly one negative root. Besides, $P_r(\tau)$ has two or zero positive roots depending on the sign of $P_r(\tau)$ at the local minimum point

$$\tau_m(r) = \sqrt{\frac{r}{3(1-r)}}.$$

Therefore, $P_r(\tau)$ has a double root for a value $r = r_0$ such that $P_{r_0}(\tau_m) = 0$, a condition that can be written, after some manipulations, in the form (6.11). \square

Corollary 7. $r_0 \in (0, 1)$

Proof. It follows from (6.11) having consistent signs on both sides. \square

The previous results lead to considering a partition of the interval $r \in [0, 1]$ into two subintervals, namely $r \in [0, r_0]$ and $r \in (r_0, 1]$. We analyze the optimality of the t -poles in each subinterval separately.

6.2.1. Left subinterval $0 \leq r \leq r_0$

Theorem 8. *The maximum distance of the closest root of (6.9) to the imaginary axis τ occurs at the right endpoint of the subinterval, namely $r = r_0$.*

Proof. In this case, $P_r(\tau)$ has one real, negative root, τ_1 , and two complex conjugate roots τ_{23} . The two complex roots merge into a double real (positive) root in the limit case $r = r_0$, as displayed in Fig. 6.1. Since it can be easily checked that

$$\left. \frac{\partial P_r}{\partial \tau} \right|_{\tau_1} > 0,$$

it follows from (6.10) that $\frac{d\tau_1}{dr} < 0$, i.e., $\tau_1(r)$ is a decreasing function in $r \in [0, r_0]$.

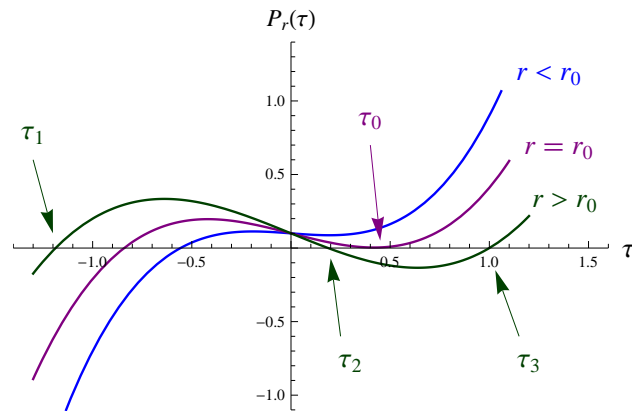


Figure 6.1.: Real roots of $P_r(\tau)$

On the other hand, one of the well-known Vieta's formulas states that the sum of the three roots of a monic polynomial of third degree equals its quadratic coefficient with sign changed. Since in our case this coefficient is zero, we have that the real part of the complex roots τ_{23} verifies

$$\Re(\tau_{23}) = -\frac{\tau_1}{2},$$

i.e., τ_{23} are always closer than τ_1 to the imaginary axis. Moreover, their real part is a positive and strictly increasing function of r . Hence, its maximum τ_0 (Fig. 6.1) is reached at r_0 , with

$$\tau_0(\varepsilon_v) = \frac{3\varepsilon_v}{2r_0(\varepsilon_v)}. \quad (6.12)$$

□

6.2.2. Right subinterval $r_0 < r \leq 1$

Theorem 9. *The distance of the closest root of (6.9) to the imaginary axis τ is smaller than τ_0 , as defined in (6.12).*

Proof. In this case, $P_r(\tau)$ has three real roots, with exactly one negative root, i.e.

$$\tau_1 < 0 < \tau_2 < \tau_3,$$

as illustrated in Fig. 6.1. The abovementioned formula of Vieta establishes that

$$\tau_1 + \tau_2 + \tau_3 = 0,$$

from where it is clear that $|\tau_1| > |\tau_2|$. Thus, the closest root to the imaginary axis is τ_2 , for which it can be easily checked that

$$\left. \frac{\partial P_r}{\partial \tau} \right|_{\tau_2} < 0,$$

which, together with (6.10), means that $\frac{d\tau_2}{dr} < 0$. Therefore, $\tau_2(r)$ is a decreasing function in $r \in (r_0, 1]$, satisfying

$$\tau_2(r) < \lim_{r \rightarrow r_0} \tau_2(r) = \tau_0.$$

□

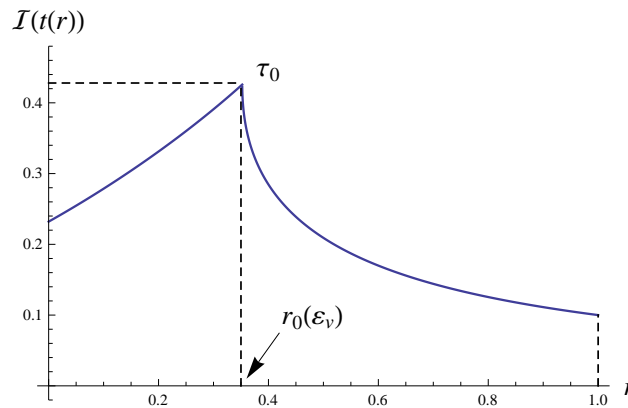


Figure 6.2.: Optimality of $\mathfrak{S}(t)$

6.2.3. The explicit value of r_0

The main result of this section can now be stated.

Theorem 10. *The closest t -pole of (6.6) is moved furthest away from the real axis of the plane t by the cubic transformation (6.3) with $r = r_0$ satisfying (6.11).*

Proof. Recalling $t = i\tau$, the statement is a direct consequence of the theorems in the last two subsections. This result is illustrated in Fig. 6.2, that shows the imaginary part (in absolute value) of the closest t -pole as a function of the variable r . □

With regard to the explicit value of r_0 , we start by noticing that (6.11) has exactly one real root, as justified in sec. A.2. Its expression was already anticipated in (3.18)-(3.19) and is rewritten here for convenience:

$$\begin{aligned} r_0(\varepsilon_v) &= \frac{3}{2}\varepsilon_v^{2/3} \left[\left(\sqrt{1 + \varepsilon_v^2} + 1 \right)^{1/3} - \left(\sqrt{1 + \varepsilon_v^2} - 1 \right)^{1/3} \right], \\ &= 3\varepsilon_v \sinh \left[\frac{1}{3} \sinh^{-1} \left(\frac{1}{\varepsilon_v} \right) \right]. \end{aligned}$$

These values are obtained by explicit inversion of the cubic equation (6.11), refer to sec. A.2 for details.

6.3. Part 2. Optimality of $\mathfrak{S}(v)$

A proof that the t -poles of (6.6) are moved furthest away from the real axis for $r = r_0$ has been developed in the previous section. However, this result is formulated in the complex plane t , where the integration interval width has been modified by a non-linear (cubic) transformation. More specifically, the original integration interval $\bar{v} \in [0, 1]$ has been transformed onto $t \in [t_0, t_1]$, with $t_j = h^{-1}(j - \bar{v}_p)$.

Since the interval width $t_1 - t_0$ has a non-linear dependence in the variable r , the optimality condition might not hold when renormalizing back to $v \in [0, 1]$ through the affine transformation $t(v)$. Therefore, it is necessary to prove that the closest v -pole in (6.7) keeps reaching its maximum distance to the real axis v for the same condition $r = r_0$, which is the objective of the current section.

Some preliminary properties of $t(v)$ are established in the next subsection.

6.3.1. The affine transformation $t(v)$

It is clear from (6.2) that the near-singular kernel is symmetric under a change of parameter $\bar{v}_p \rightarrow 1 - \bar{v}_p$, since a simple change of variable $\bar{v} \rightarrow 1 - \bar{v}$ leaves the kernel invariant and keeps the integration interval $\bar{v} \in [0, 1]$. As t_j in (6.5) satisfy

$$(1 - r)t_j^3 + rt_j = j - \bar{v}_p, \quad j = 0, 1, \quad (6.13)$$

it suffices considering the affine transformation $t(v)$ for values of \bar{v}_p that lie at, say, the left of the symmetry center $\bar{v}_p = \frac{1}{2}$.

Furthermore, the behaviour of t_j depends on whether \bar{v}_p belongs or not to the integration interval $\bar{v} \in [0, 1]$. Thus, for the rest of this chapter, two different cases will be considered regarding the parameter \bar{v}_p :

1. $0 < \bar{v}_p \leq \frac{1}{2}$
2. $\bar{v}_p < 0$

6.3 Part 2. Optimality of $\mathfrak{S}(v)$

We remark that the cases $\frac{1}{2} \leq \bar{v}_p < 1$ and $\bar{v}_p > 1$ are symmetric to the cases considered above. Moreover, the trivial case $\bar{v}_p = 0$, and its symmetric $\bar{v}_p = 1$, are such that $t_1 - t_0 = 1$ and, according to (6.7), $\mathfrak{S}(v) = \mathfrak{S}(r)$. Hence, nothing needs to be proved thereafter.

We next establish the monotonicity of the interval width $t_1 - t_0$ when considered as a function of the variable r .

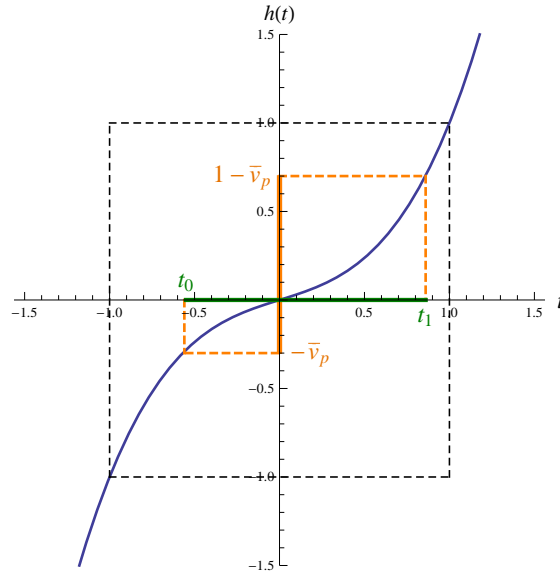


Figure 6.3.: Behaviour of $t_1 - t_0$ for $0 < \bar{v}_p \leq \frac{1}{2}$

Theorem 11. *In case $0 < \bar{v}_p \leq \frac{1}{2}$, $(t_1 - t_0)(r)$ is a decreasing function in $r \in [0, 1]$. In case $\bar{v}_p < 0$, $(t_1 - t_0)(r)$ is an increasing function in the same interval.*

Proof. Taking implicit derivatives with respect to r in (6.13) yields

$$\frac{dt_j}{dr} = t_j(r) \frac{t_j(r)^2 - 1}{3(1-r)t_j(r)^2 + r},$$

and thus

$$\frac{d(t_1 - t_0)}{dr} = t_1(r) \frac{t_1(r)^2 - 1}{3(1-r)t_1(r)^2 + r} - t_0(r) \frac{t_0(r)^2 - 1}{3(1-r)t_0(r)^2 + r}. \quad (6.14)$$

In case $0 < \bar{v}_p \leq \frac{1}{2}$ it can be readily verified from (6.13) that

$$-1 < t_0 < 0 < t_1 < 1,$$

as illustrated in Fig. 6.3, hence

$$t_j(r)^2 - 1 < 0, \quad j = 0, 1,$$

from where

$$\frac{d(t_1 - t_0)}{dr} < 0.$$

In case $\bar{v}_p < 0$ it is necessary to consider two subcases. If $-1 < \bar{v}_p < 0$, then it can be verified that

$$0 < t_0 < 1 < t_1,$$

see Fig. 6.4, left. This means that

$$\begin{aligned} t_1(r)^2 - 1 &> 0, \\ t_0(r)^2 - 1 &< 0, \end{aligned}$$

from where

$$\frac{d(t_1 - t_0)}{dr} > 0.$$

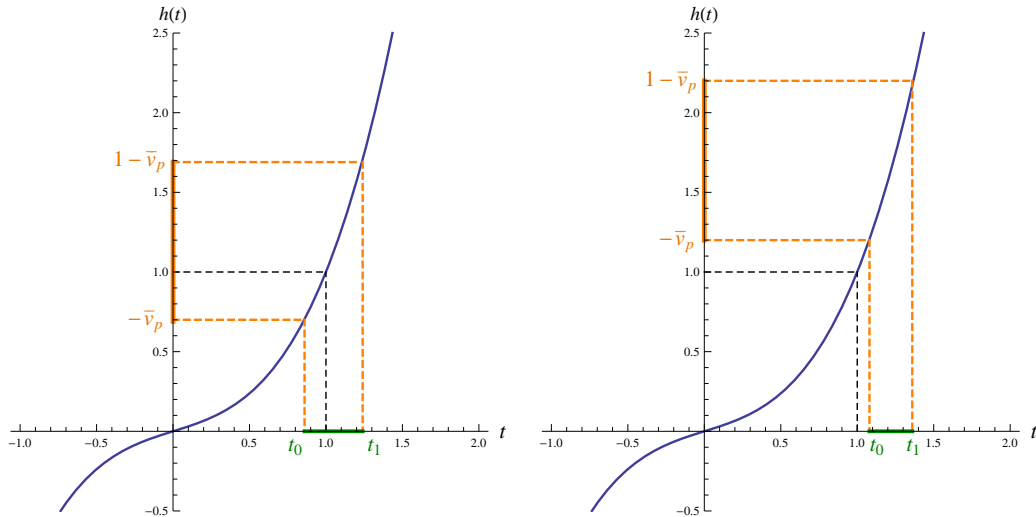


Figure 6.4.: Behaviour of $t_1 - t_0$ for $-1 < \bar{v}_p < 0$ (left) and $\bar{v}_p \leq -1$ (right)

If $\bar{v}_p \leq -1$, then it holds

$$1 \leq t_0 < t_1,$$

see Fig. 6.4, right, from where it is clear that $-t_0 > -t_1$. Thus, the derivative in (6.14) admits the following lower bound

$$\begin{aligned} \frac{d(t_1 - t_0)}{dr} &> t_1(r) \frac{t_1(r)^2 - 1}{3(1-r)t_1(r)^2 + r} - t_0(r) \frac{t_0(r)^2 - 1}{3(1-r)t_0(r)^2 + r} \\ &= t_1(r) \frac{(3-2r)(t_1(r)^2 - t_0(r)^2)}{(3(1-r)t_1(r)^2 + r)(3(1-r)t_0(r)^2 + r)} > 0, \end{aligned}$$

finishing the proof. \square

6.3.2. The explicit form of $\mathfrak{S}(v(r))$

Before actually showing that the closest v -pole is at maximum distance from the real axis for $r = r_0$, it is necessary to find the explicit expression of $\mathfrak{S}(v)$ as a function of r . Since $t_j(r)$ are real functions, it follows from (6.7) that

$$\mathfrak{S}(v(r)) = \frac{\mathfrak{S}(t(r))}{(t_1 - t_0)(r)},$$

with $t(r) = \pm i\tau(r)$. It is clear from (6.9) that $\tau(r)$ are the solutions of

$$\tau^3 - \frac{r}{1-r}\tau + \frac{\varepsilon_v}{1-r} = 0, \quad (6.15)$$

whose inverse can be expressed in terms of trigonometric and hyperbolic functions, as indicated below (refer to sec. A.1 for details).

In the left subinterval $0 < r \leq r_0$, (6.15) has one real solution τ_1 and two complex conjugate solutions τ_{23} given by

$$\tau_1(r) = -\frac{2}{\sqrt{3}}\sqrt{\frac{r}{1-r}} \cosh \left[\frac{1}{3} \cosh^{-1} \left(\frac{3\sqrt{3}}{2r} \sqrt{\frac{1-r}{r}} \varepsilon_v \right) \right], \quad (6.16)$$

$$\tau_{23}(r) = -\frac{\tau_1(r)}{2} \pm i\sqrt{\frac{r}{1-r}} \sinh \left[\frac{1}{3} \cosh^{-1} \left(\frac{3\sqrt{3}}{2r} \sqrt{\frac{1-r}{r}} \varepsilon_v \right) \right], \quad (6.17)$$

where τ_{23} are, as we know (sec. 6.2.1), the closest roots to the imaginary axis τ .

In the right subinterval $r_0 < r \leq 1$, (6.15) has three real and distinct solutions whose explicit expression is

$$\tau_k(r) = \frac{2}{\sqrt{3}}\sqrt{\frac{r}{1-r}} \sin \left[\frac{1}{3} \sin^{-1} \left(\frac{3\sqrt{3}}{2r} \sqrt{\frac{1-r}{r}} \varepsilon_v \right) + \frac{2\pi}{3}(k-2) \right], \quad (6.18)$$

with $k = 1, 2, 3$ and τ_2 being, as we know (sec. 6.2.2), the closest solution to the imaginary axis τ .

With respect to $t_j(r)$, their explicit expressions are obtained in a similar manner. Rewriting (6.13) as

$$t_j^3 + \frac{r}{1-r}t_j = \frac{j - \bar{v}_p}{1-r}, \quad j = 0, 1,$$

its only real solution (sec. A.2) takes the form

$$t_j(r) = \frac{2}{\sqrt{3}}\sqrt{\frac{r}{1-r}} \sinh \left[\frac{1}{3} \sinh^{-1} \left(\frac{3\sqrt{3}}{2r} \sqrt{\frac{1-r}{r}} (j - \bar{v}_p) \right) \right]. \quad (6.19)$$

In order to conclude this subsection, we notice that the v -poles are symmetrically distributed with respect to the real axis v , hence it suffices considering the poles

with positive imaginary part. Thus, the closest v -pole to the real axis satisfies

$$\Im(v(r)) = \begin{cases} \frac{\Re(\tau_{23}(r))}{(t_1 - t_0)(r)} & \text{if } 0 \leq r \leq r_0 \\ \frac{\tau_2(r)}{(t_1 - t_0)(r)} & \text{if } r_0 < r \leq 1, \end{cases} \quad (6.20)$$

with all relevant functions defined in (6.16)-(6.19).

We are now ready to prove the optimality of $\Im(v(r))$ for all possible cases. More specifically, four situations are analyzed, corresponding to the discussion made for the values of \bar{v}_p and r . Each case is developed in a separate subsection.

6.3.3. The case $0 < \bar{v}_p \leq \frac{1}{2}$ and $0 \leq r \leq r_0$

It was proved in sec. 6.2.1 that $\Re(\tau_{23}(r))$ is an increasing function. Besides, it was proved in Theorem 11 that $(t_1 - t_0)(r)$ is a decreasing function. In consequence, their quotient in (6.20) is an increasing function that reaches its maximum at $r = r_0$.

6.3.4. The case $0 < \bar{v}_p \leq \frac{1}{2}$ and $r_0 < r \leq 1$

It was proved (sec. 6.2.2) that $\tau_2(r)$ is a decreasing function, hence

$$\Im(v(r)) = \frac{\tau_2(r)}{(t_1 - t_0)(r)}, \quad (6.21)$$

is the quotient of two decreasing functions, whose behaviour needs to be carefully examined. In order to simplify the further treatment of (6.21), we introduce the change of variable

$$\frac{3\sqrt{3}}{2r} \sqrt{\frac{1-r}{r}} = \frac{1}{s}, \quad (6.22)$$

which is an increasing function that transforms $s \in [\varepsilon_v, \infty)$ onto $r \in [r_0, 1)$. Thus, taking (6.16)-(6.19) into account, the imaginary part of the v -poles becomes

$$\Im(v(r(s))) = \frac{g(s)}{w_1(s) - w_0(s)}, \quad (6.23)$$

with

$$g(s) = \sin \left[\frac{1}{3} \sin^{-1} \left(\frac{\varepsilon_v}{s} \right) \right], \quad (6.24)$$

$$w_j(s) = \sinh \left[\frac{1}{3} \sinh^{-1} \left(\frac{j - \bar{v}_p}{s} \right) \right]. \quad (6.25)$$

A straightforward application of the chain rule yields

$$\frac{d\Im(v(r(s)))}{ds} = \frac{d\Im(v(r))}{dr} \frac{dr}{ds},$$

and since $\frac{dr}{ds} > 0$, it suffices showing that $\mathfrak{S}(v(r(s)))$ is a decreasing function in $s \in [\varepsilon_v, \infty)$, as the optimality of $\mathfrak{S}(v(r))$ follows immediately. We start by finding an upper bound for the derivative of $g(s)$ in (6.24).

Lemma 12. *$g(s)$ is a decreasing function for $s > 0$ that satisfies*

$$\frac{dg}{ds} < -\frac{g(s)}{s}.$$

Proof. It is clear from (6.24) that $0 < g(s) \leq \frac{1}{2}$. Moreover, it satisfies the cubic equation

$$4sg(s)^3 - 3sg(s) + \varepsilon_v = 0,$$

in agreement with (A.2). Taking implicit derivatives with respect to s yields

$$\frac{dg}{ds} = -\frac{g(s)}{s} \frac{3 - 4g(s)^2}{3 - 12g(s)^2} < 0.$$

We also notice that in the rightmost fraction above, both the numerator and the denominator are positive functions, from where

$$\frac{3 - 4g(s)^2}{3 - 12g(s)^2} > 1,$$

finishing the proof. □

We next find bounds for the derivatives of w_j by an analogous procedure.

Lemma 13. *The interval width $w_1(s) - w_0(s)$ is a decreasing function for $s > 0$ and $0 < \bar{v}_p \leq \frac{1}{2}$ that satisfies*

$$-\frac{d(w_1 - w_0)}{ds} < \frac{w_1(s) - w_0(s)}{s}.$$

Proof. According to (A.10), the functions w_j satisfy

$$4sw_j(s)^3 + 3sw_j(s) = j - \bar{v}_p.$$

Taking implicit derivatives with respect to s produces

$$\frac{dw_j}{ds} = -\frac{w_j(s)}{s} \frac{3 + 4w_j(s)^2}{3 + 12w_j(s)^2}.$$

The rightmost fraction above is obviously positive and less than one. Noticing from (6.25) that $w_0(s) < 0 < w_1(s)$, we have that

$$\begin{aligned} -\frac{dw_1}{ds} &< \frac{w_1(s)}{s}, \\ \frac{dw_0}{ds} &< -\frac{w_0(s)}{s}, \end{aligned}$$

from where the claim immediately follows. □

The main result of this subsection can now be stated. Notice that the two previous Lemmas hold for $s > 0$ though the next Theorem only applies for $s > \varepsilon_v$.

Theorem 14. $\Im(v(r(s)))$ is a decreasing function for $s > \varepsilon_v$ and $0 < \bar{v}_p \leq \frac{1}{2}$.

Proof. Taking explicit derivatives in (6.23)

$$\begin{aligned} \frac{d\Im(v(r(s)))}{ds} &= \frac{\frac{dg}{ds}(w_1(s) - w_0(s)) - \frac{d(w_1 - w_0)}{ds}g(s)}{(w_1(s) - w_0(s))^2} \\ &< \frac{-\frac{g(s)}{s}(w_1(s) - w_0(s)) + \frac{w_1(s) - w_0(s)}{s}g(s)}{(w_1(s) - w_0(s))^2} = 0. \end{aligned}$$

□

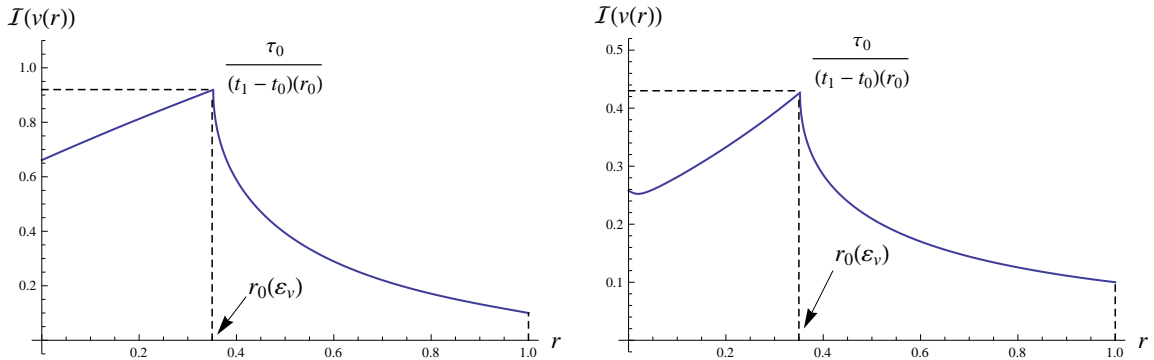


Figure 6.5.: Optimality of $\Im(v(r))$ for $0 < \bar{v}_p \leq \frac{1}{2}$ (left) and $\bar{v}_p < 0$ (right)

The immediate consequence of the two preceding subsections is that $\Im(v(r))$ in (6.20) reaches its maximum at $r = r_0$, as illustrated in Fig. 6.5 (left).

6.3.5. The case $\bar{v}_p < 0$ and $0 \leq r \leq r_0$

Numerical experiments indicate that $\Im(v(r))$ need not be a monotonic function in this case, see Fig. 6.5 (right), and thus the determination of its maximum value is a rather delicate task. A change of variable that has been found to be appropriate for this purpose is

$$\frac{3\sqrt{3}}{2r} \sqrt{\frac{1-r}{r}} \varepsilon_v = \frac{1}{s\sqrt{s}}, \quad (6.26)$$

which is an increasing function that maps $s \in [0, 1]$ onto $r \in [0, r_0]$. Substituting explicitly in (6.20) yields

$$\Im(v(r(s))) = \frac{\frac{1}{2} \cosh \left[\frac{1}{3} \cosh^{-1} \left(\frac{1}{s\sqrt{s}} \right) \right]}{\sinh \left[\frac{1}{3} \sinh^{-1} \left(\frac{1 - \bar{v}_p}{\varepsilon_v} \frac{1}{s\sqrt{s}} \right) \right] - \sinh \left[\frac{1}{3} \sinh^{-1} \left(\frac{-\bar{v}_p}{\varepsilon_v} \frac{1}{s\sqrt{s}} \right) \right]}.$$

According to (A.5) and (A.10), all terms in the numerator and denominator above can be expressed in algebraic form as follows:

$$\cosh \left[\frac{1}{3} \cosh^{-1} \left(\frac{1}{s\sqrt{s}} \right) \right] = \frac{g_1(s)}{2\sqrt{s}}, \quad (6.27)$$

$$\sinh \left[\frac{1}{3} \sinh^{-1} \left(\frac{j - \bar{v}_p}{\varepsilon_v} \frac{1}{s\sqrt{s}} \right) \right] = \frac{w_j(s)}{2\sqrt{s}}, \quad (6.28)$$

with

$$g_1(s) = \left(1 + \sqrt{1 - s^3} \right)^{1/3} + \left(1 - \sqrt{1 - s^3} \right)^{1/3}, \quad (6.29)$$

$$w_j(s) = \left(\sqrt{\left(\frac{j - \bar{v}_p}{\varepsilon_v} \right)^2 + s^3} + \frac{j - \bar{v}_p}{\varepsilon_v} \right)^{1/3} - \left(\sqrt{\left(\frac{j - \bar{v}_p}{\varepsilon_v} \right)^2 + s^3} - \frac{j - \bar{v}_p}{\varepsilon_v} \right)^{1/3} \quad (6.30)$$

and this lets us express the imaginary part of the v -poles as

$$\mathfrak{S}(v(r(s))) = \frac{1}{2} \frac{g_1(s)}{w_1(s) - w_0(s)}. \quad (6.31)$$

The reason for using the change of variable (6.26) is that $g_1(s)$ and $w_j(s)$ have certain monotonicity and convexity properties that do not hold when using other changes of variable. These properties will allow us to prove that (6.31) reaches its maximum at $s = 1$. More specifically, we will find an upper bound of (6.31), with the same value at $s = 1$, that is an increasing function itself.

We start by finding an upper bound for $g_1(s)$, imposing that both g_1 and its bound reach the same value at the right endpoint of the interval, namely $s = 1$.

Lemma 15. $g_1(s)$ is an increasing function in $s \in [0, 1]$.

Proof. $g_1(s)$, defined in (6.29), satisfies the following functional relationship, which can be easily deduced from (A.6)

$$g_1(s)^3 - 3sg_1(s) = 2. \quad (6.32)$$

Taking implicit derivatives with respect to s produces

$$\frac{dg_1}{ds} = \frac{g_1(s)}{g_1(s)^2 - s}. \quad (6.33)$$

From (6.32) it is clear that

$$g_1(s)^2 - s = \frac{2}{g_1(s)} + 2s > 0,$$

which finishes the proof. □

Next, we establish the convexity of g_1 .

Lemma 16. $g_1(s)$ is a concave function in $s \in [0, 1]$.

Proof. It suffices taking the derivative in (6.33) and simplify terms to yield

$$\frac{d^2 g_1}{ds^2} = \frac{-2s g_1(s)}{(g_1(s)^2 - s)^3} < 0.$$

□

As a consequence of the two previous lemmas, g_1 is bounded above by its tangent at $s = 1$. Since

$$g_1(1) = 2, \quad \left. \frac{dg_1}{ds} \right|_{s=1} = \frac{2}{3},$$

it follows that

$$g_1(s) \leq \frac{2}{3}(s + 2), \quad (6.34)$$

with equality holding at $s = 1$.

Our next objective is to prove that the factor $\frac{1}{w_1(s) - w_0(s)}$ in (6.31) is a convex function in $s \in [0, 1]$. We remark that this does not imply that $w_1(s) - w_0(s)$ is a concave function in that interval (in fact, it is not). Furthermore, this convexity property may not hold for other changes of variable different from the one proposed in (6.26). A couple of preliminary results are proved first.

Lemma 17. If $\bar{v}_p < 0$, $w_j(s)$ are decreasing and convex functions in $s \in [0, 1]$.

Proof. The functions w_j defined in (6.30) satisfy the following relationship, as it can be easily deduced from (A.11):

$$w_j(s)^3 + 3s w_j(s) = \frac{2}{\varepsilon_v} (j - \bar{v}_p), \quad j = 0, 1. \quad (6.35)$$

Taking implicit derivatives with respect to s in (6.35) yields

$$\frac{dw_j}{ds} = -\frac{w_j(s)}{w_j(s)^2 + s} < 0.$$

Taking explicit derivatives and simplifying terms, we finally arrive at

$$\frac{d^2 w_j}{ds^2} = \frac{2s w_j(s)}{(w_j(s)^2 + s)^3} > 0.$$

□

Lemma 18. If $\bar{v}_p < 0$, $w_1(s)^2$, $w_1(s)w_0(s)$ and $w_0(s)^2$ are decreasing and convex functions in $s \in [0, 1]$.

Proof. By explicit derivation it holds

$$\begin{aligned}\frac{d(w_1(s)^2)}{ds} &= 2w_1(s)\frac{dw_1}{ds} < 0, \\ \frac{d^2(w_1(s)^2)}{ds^2} &= 2\left(\frac{dw_1}{ds}\right)^2 + 2w_1(s)\frac{d^2w_1}{ds^2} > 0.\end{aligned}$$

The corresponding properties for $w_1(s)w_0(s)$ and $w_0(s)^2$ are proved in a completely analogous way. \square

Theorem 19. *If $\bar{v}_p < 0$, $\frac{1}{w_1(s)-w_0(s)}$ is a convex function in $s \in [0, 1]$.*

Proof. Taking the difference between both equations (6.35) produces

$$w_1(s)^3 - w_0(s)^3 + 3s(w_1(s) - w_0(s)) = \frac{2}{\varepsilon_v}.$$

Applying the identity $w_1^3 - w_0^3 = (w_1 - w_0)(w_1^2 + w_1w_0 + w_0^2)$ it follows that

$$\frac{1}{w_1(s) - w_0(s)} = \frac{\varepsilon_v}{2} [w_1(s)^2 + w_1(s)w_0(s) + w_0(s)^2 + 3s],$$

where all the functions within the brackets above are convex. \square

An immediate consequence of this theorem is that $\frac{1}{w_1(s)-w_0(s)}$ is bounded above by its chord, namely

$$\frac{1}{w_1(s) - w_0(s)} \leq \frac{1-s}{w_1(0) - w_0(0)} + \frac{s}{w_1(1) - w_0(1)}, \quad (6.36)$$

with equality at both endpoints $s = 0$ and $s = 1$.

Summarizing the last steps, we have found upper bounds (6.34) and (6.36) for both factors in (6.31). This allows us to write $\mathfrak{S}(v(r(s))) \leq B_1(s)$, with equality at $s = 1$, where B_1 is the upper bound given by

$$B_1(s) = \frac{1}{3}(s+2) \left[\frac{1-s}{w_1(0) - w_0(0)} + \frac{s}{w_1(1) - w_0(1)} \right]. \quad (6.37)$$

Therefore, in order to conclude this subsection, it suffices showing that $B_1(s)$ is an increasing function in $s \in [0, 1]$. We start by explicitly computing

$$\frac{d^2B_1}{ds^2} = \frac{2}{3} \left[\frac{1}{w_1(1) - w_0(1)} - \frac{1}{w_1(0) - w_0(0)} \right], \quad (6.38)$$

where the term in brackets can be positive, negative or zero, depending on the values of ε_v and \bar{v}_p . Numerical examples for both situations can be easily found from the definitions in (6.30).

In case (6.38) is non-negative, B_1 is a convex function and its minimum slope occurs at $s = 0$, that can be evaluated to

$$\frac{1}{3(w_1(0) - w_0(0))} + \frac{2}{3} \left[\frac{1}{w_1(1) - w_0(1)} - \frac{1}{w_1(0) - w_0(0)} \right] > 0,$$

meaning that B_1 is an increasing function.

In case (6.38) is negative, B_1 is a concave function and its minimum slope occurs at $s = 1$, that can be evaluated to

$$\frac{1}{3(w_1(0) - w_0(0))} + \left[\frac{1}{w_1(1) - w_0(1)} - \frac{1}{w_1(0) - w_0(0)} \right],$$

hence, our next objective is to show that the expression above is positive. This condition is equivalent to

$$\frac{w_1(1) - w_0(1)}{w_1(0) - w_0(0)} < \frac{4}{3}, \quad (6.39)$$

where, according to (6.28) and (6.30)

$$w_j(1) = 2 \sinh \left[\frac{1}{3} \sinh^{-1} \left(\frac{j - \bar{v}_p}{\varepsilon_v} \right) \right], \quad (6.40)$$

$$w_j(0) = 2^{1/3} \left(\frac{j - \bar{v}_p}{\varepsilon_v} \right)^{1/3}. \quad (6.41)$$

We next prove a condition that is, in fact, stronger than (6.39).

Theorem 20. *If $\varepsilon_v > 0$ and $\bar{v}_p < 0$, then*

$$\frac{\sinh \left[\frac{1}{3} \sinh^{-1} \left(\frac{1 - \bar{v}_p}{\varepsilon_v} \right) \right] - \sinh \left[\frac{1}{3} \sinh^{-1} \left(\frac{-\bar{v}_p}{\varepsilon_v} \right) \right]}{\left(\frac{1 - \bar{v}_p}{\varepsilon_v} \right)^{1/3} - \left(\frac{-\bar{v}_p}{\varepsilon_v} \right)^{1/3}} \leq \frac{1}{2^{1/3}}.$$

Proof. We let

$$-\frac{\bar{v}_p}{\varepsilon_v} = X, \quad X > 0,$$

from where

$$\frac{1 - \bar{v}_p}{\varepsilon_v} = X + \frac{1}{\varepsilon_v}.$$

We write

$$\frac{\sinh \left[\frac{1}{3} \sinh^{-1} \left(X + \frac{1}{\varepsilon_v} \right) \right] - \sinh \left[\frac{1}{3} \sinh^{-1} X \right]}{\left(X + \frac{1}{\varepsilon_v} \right)^{1/3} - X^{1/3}} \leq \frac{1}{k}, \quad (6.42)$$

and try to find the maximum value of the parameter k for which the inequality above holds. Rearranging terms in (6.42) yields

$$k \sinh \left[\frac{1}{3} \sinh^{-1} \left(X + \frac{1}{\varepsilon_v} \right) \right] - \left(X + \frac{1}{\varepsilon_v} \right)^{1/3} \leq k \sinh \left[\frac{1}{3} \sinh^{-1} X \right] - X^{1/3}.$$

As both sides of this inequality are the same function, but with arguments shifted, it suffices finding the largest value of k for which the function

$$k \sinh \left[\frac{1}{3} \sinh^{-1} X \right] - X^{1/3},$$

is decreasing for $X > 0$.

In order to simplify further calculations, we take a new change of variable

$$\frac{1}{3} \sinh^{-1} X = Y \rightarrow X = \sinh(3Y), \quad Y > 0,$$

which is a monotonically increasing function. Thus, our objective is to find the largest value of k such that

$$k \sinh Y - \sinh^{1/3}(3Y),$$

is a decreasing function for $Y > 0$. Taking derivatives with respect to Y , we impose

$$k \cosh Y - \frac{\cosh(3Y)}{\sinh^{2/3}(3Y)} < 0,$$

which is equivalent to

$$k^3 \cosh^3 Y < \frac{\cosh^3(3Y)}{\sinh^2(3Y)}.$$

Substituting $\cosh(3Y) = \cosh Y (4 \sinh^2 Y + 1)$, $\sinh(3Y) = \sinh Y (4 \sinh^2 Y + 3)$, the condition becomes

$$k^3 < \frac{(4 \sinh^2 Y + 1)^3}{\sinh^2 Y (4 \sinh^2 Y + 3)^2}.$$

Putting $\sinh^2 Y = Z$ and manipulating the expression above, a polynomial condition is obtained, namely

$$(4Z + 1)^3 - k^3 Z(4Z + 3)^2 > 0. \tag{6.43}$$

It is clear that this equation has no positive solution for $k = 0$. Thus, we impose that the left-hand side of (6.43) has a double (positive) root. Taking derivatives with respect to Z , equating to zero and simplifying terms it follows

$$4(4Z + 1) - k^3(4Z + 3) = 0,$$

whose only positive solution is

$$Z = \frac{4 - 3k^3}{4(k^3 - 4)}.$$

Substituting into (6.43) and solving for k we obtain

$$k^3 = 2,$$

which finishes the proof, since if $k > 2^{1/3}$ the left-hand side of (6.43) would take negative values for some positive value of Z . \square

Going back to (6.39), and taking (6.40)-(6.41) into account, it is an immediate consequence of the previous theorem that

$$\frac{w_1(1) - w_0(1)}{w_1(0) - w_0(0)} \leq \frac{2}{2^{1/3}} \frac{1}{2^{1/3}} = 2^{1/3} < \frac{4}{3}.$$

We conclude that $B_1(s)$ is an increasing function also in case (6.38) is positive, hence $\Im(v(r(s)))$ reaches its maximum at $s = 1$, and so does $\Im(v(r))$ at $r = r_0$.

6.3.6. The case $\bar{v}_p < 0$ and $r_0 < r \leq 1$

It was proven in Theorem 9 that $\tau_2(r)$ is a decreasing function. Moreover, $(t_1 - t_0)(r)$ is an increasing function, according to Theorem 11. In consequence, their quotient in (6.20) is a decreasing function that reaches its maximum at $r = r_0$.

The results of the two preceding subsections are illustrated in Fig. 6.5, right.

6.3.7. Lower bounds for $\Im(t(r_0))$ and $\Im(v(r_0))$

Once the optimality of the closest t and v -poles has been established, it might be interesting to provide a measure of the distance gain to their respective real axes.

Theorem 21. *The imaginary parts $\Im(t(r_0))$ and $\Im(v(r_0))$ are bounded below by $\left(\frac{\varepsilon_v}{2}\right)^{1/3}$ and $\frac{\varepsilon_v^{1/3}}{2}$ respectively.*

Proof. $\Im(t(r_0))$ coincides with τ_0 in (6.12). Recalling (6.11) and Corollary 7, it can be easily derived that

$$r_0(\varepsilon_v) \leq 3 \left(\frac{\varepsilon_v}{2}\right)^{2/3}, \quad (6.44)$$

from where

$$\Im(t(r_0(\varepsilon_v))) \geq \left(\frac{\varepsilon_v}{2}\right)^{1/3},$$

finishing the first part of the theorem.

On the other hand, it follows from (6.12) and (6.20) that

$$\Im(v(r_0)) = \frac{3\varepsilon_v}{2r_0(t_1(r_0) - t_0(r_0))}, \quad (6.45)$$

and an upper bound for the second factor in the denominator is found next. We consider t_j as functions of the parameter \bar{v}_p and recall that they satisfy (6.13), that can be rewritten as

$$(1 - r)t_j(\bar{v}_p)^3 + rt_j(\bar{v}_p) = j - \bar{v}_p, \quad j = 0, 1. \quad (6.46)$$

We try to find the maximum of the function $t_1(\bar{v}_p) - t_0(\bar{v}_p)$ for arbitrary r . Taking implicit derivatives with respect to \bar{v}_p

$$\frac{d(t_1 - t_0)}{d\bar{v}_p} = \frac{3(1 - r)(t_1(\bar{v}_p)^2 - t_0(\bar{v}_p)^2)}{(3(1 - r)t_1(\bar{v}_p)^2 + r)(3(1 - r)t_0(\bar{v}_p)^2 + r)}.$$

Equating to zero and taking into account that $t_1 > t_0$, we arrive at the condition $t_1(\bar{v}_p) = -t_0(\bar{v}_p)$. Substituting in (6.46) and summing equations for $j = 0, 1$ we obtain $\bar{v}_p = \frac{1}{2}$. This way, the equation for t_1 takes the form

$$(1 - r)t_1^3 + rt_1 - \frac{1}{2} = 0.$$

Taking implicit derivatives with respect to r it is easy to determine that $t_1(r)$ is a decreasing function in $r \in [0, 1]$. Thus, its maximum is reached at $r = 0$ for which $t_1 = \frac{1}{2^{1/3}}$, and we have that for $\bar{v}_p = \frac{1}{2}$, $t_1 \leq \frac{1}{2^{1/3}}$. Since $t_1 = -t_0$ we conclude that $t_1 - t_0 = 2t_1 \leq 2^{2/3}$. Substituting this, together with (6.44) into (6.45), we finally arrive at

$$\Im(v(r_0)) \geq \frac{\varepsilon_v^{1/3}}{2},$$

which finishes the proof. □

6.4. Part 3. The optimal ellipse of analiticity \mathcal{E}_p

It has already been mentioned (sec. 6.1), that, in order to determine the optimal form of the cubic transformation, it does not suffice with proving the optimality of the imaginary part of the v -poles, as their real part might be closer to midpoint of the integration interval, resulting in a smaller ellipse of analiticity \mathcal{E}_p .

This section proves that the optimal (largest) ellipse, in the sense defined in sec. 3.4.1, occurs in fact for $r = r_0$, although an additional hypothesis, that produces a slightly weaker result, is introduced for the case $\bar{v}_p < 0$. Most of the results established in Parts 1 and 2 of the proof will have to be used throughout this final section of the proof.

It was already mentioned in sec. 3.4.1 that the equation of an ellipse with foci at points $(0, 0)$ and $(1, 0)$ is

$$\frac{(X - \frac{1}{2})^2}{b^2 + \frac{1}{4}} + \frac{Y^2}{b^2} = 1,$$

with b being its semi-minor (vertical) axis. Since none of these ellipses intersect, the continuous uniparametric family of all confocal ellipses fill the plane, noticing that the integration interval $[0, 1]$ corresponds to the degenerate case $b = 0$.

Given a complex pole of the near-singular kernel at the critical value $r = r_0$, the value of the semi-minor axis of the confocal ellipse determined by $v(r_0)$ satisfies the equation

$$\frac{\left(\Re(v(r_0)) - \frac{1}{2}\right)^2}{b^2 + \frac{1}{4}} + \frac{\Im(v(r_0))^2}{b^2} = 1, \tag{6.47}$$

where b is the only positive solution of the biquadratic equation above. We remark that b depends on the geometric parameters ε_v and \bar{v}_p , that determine the position of the transformed poles $v(r_0)$. However the explicit dependence $b = b(\varepsilon_v, \bar{v}_p)$ will be omitted for the rest of this section, unless otherwise indicated.

Hence, in order to show that the critical ellipse is the optimal one, it suffices showing that if $r \in [0, 1]$, then

$$\frac{\left(\Re(v(r)) - \frac{1}{2}\right)^2}{b^2 + \frac{1}{4}} + \frac{\Im(v(r))^2}{b^2} \leq 1, \quad (6.48)$$

with equality holding for $r = r_0$.

Taking (6.7) and (6.16)-(6.19) into account, it is clear that in case $0 \leq r \leq r_0$ the 6 v -poles can be written in explicit form as

$$\begin{aligned} v(r) &= \frac{-t_0(r)}{(t_1 - t_0)(r)} \pm \frac{i}{(t_1 - t_0)(r)} 2\Re(\tau_{23}(r)), \\ v(r) &= \frac{\pm \Im(\tau_{23}(r)) - t_0(r)}{(t_1 - t_0)(r)} \pm \frac{i}{(t_1 - t_0)(r)} \Re(\tau_{23}(r)). \end{aligned}$$

It is straightforward to find numerical examples of these poles lying outside the ellipse of analyticity, except for the case

$$v(r) = \frac{\Im(\tau_{23}(r)) - t_0(r)}{(t_1 - t_0)(r)} \pm \frac{i}{(t_1 - t_0)(r)} \Re(\tau_{23}(r)), \quad (6.49)$$

which is the pole displayed in orange (only the positive imaginary part is shown) in Fig. 6.6.

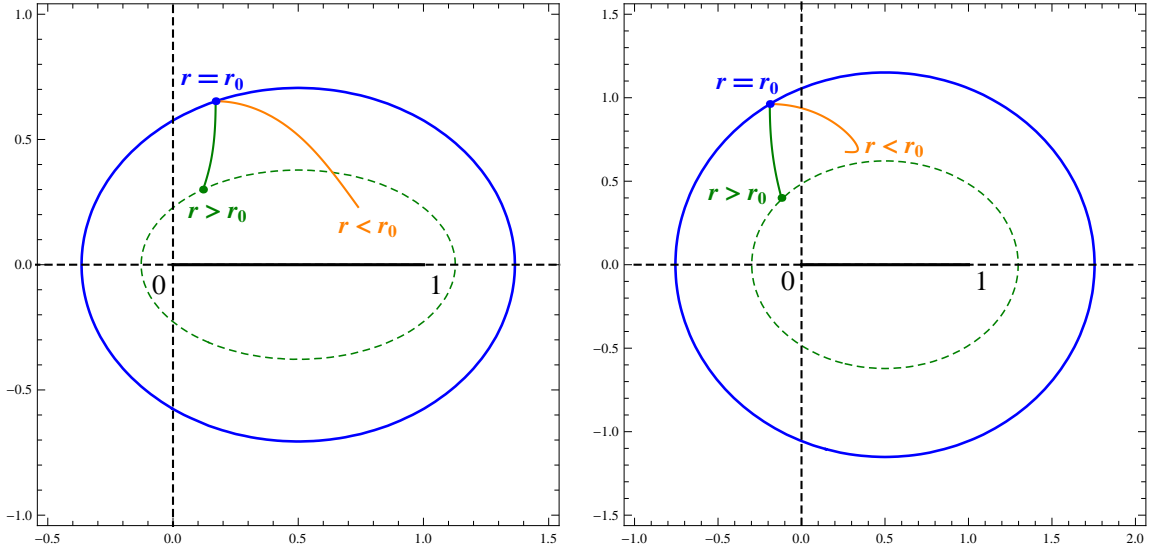


Figure 6.6.: Critical ellipse and v -poles for $0 < \bar{v}_p \leq \frac{1}{2}$ (left) and $\bar{v}_p < 0$ (right)

On the other hand, if $r_0 < r \leq 1$ the 6 v -poles are given by

$$v(r) = \frac{-t_0(r)}{(t_1 - t_0)(r)} \pm \frac{i}{(t_1 - t_0)(r)} \tau_k(r), \quad k = 1, 2, 3. \quad (6.50)$$

Again, numerical examples exist with the poles corresponding to $k = 1$ and $k = 3$ lying outside the ellipse of analiticity. Thus, the only poles that seem to remain inside the ellipse are the ones corresponding to $k = 2$, as displayed in green (only the positive imaginary part is shown) in Fig. 6.6.

Summarizing the ideas above, Fig. 6.6 shows the critical ellipse, together with the locus of the closest complex poles $v(r)$ in (6.49) and (6.50) with $k = 2$. The green dot at $r = 1$ corresponds to the original position of the kernel poles, together with the ellipse of analiticity before applying the cubic transformation. Only the poles with positive imaginary part are shown, since the poles with negative imaginary part are obviously symmetric. Two different situations are shown, corresponding to values $0 < \bar{v}_p \leq \frac{1}{2}$ and $\bar{v}_p < 0$.

The aim of this section is, therefore, to show that the poles displayed in Fig. 6.6 do not “escape” from the ellipse of analiticity. More specifically, a proof of (6.48) is developed for the case $0 < \bar{v}_p \leq \frac{1}{2}$ and a slightly weaker result for the case $\bar{v}_p < 0$. The explicit form of the real part of the v -poles is provided first.

6.4.1. The explicit form of $\Re(v(r))$

According to the previous subsection, the v -poles under consideration for the rest of this section have a real part given by

$$\Re(v(r)) = \begin{cases} \frac{\Im(\tau_{23}(r)) - t_0(r)}{(t_1 - t_0)(r)} & \text{if } 0 \leq r \leq r_0 \\ \frac{-t_0(r)}{(t_1 - t_0)(r)} & \text{if } r_0 < r \leq 1, \end{cases} \quad (6.51)$$

with all relevant functions defined in (6.16)-(6.19). The same four cases as in sec. 6.3 are examined in the respective subsections below.

6.4.2. The case $0 < \bar{v}_p \leq \frac{1}{2}$ and $0 \leq r \leq r_0$

We apply the same change of variable already considered in sec. 6.3.4, namely

$$\frac{3\sqrt{3}}{2r} \sqrt{\frac{1-r}{r}} = \frac{1}{s}, \quad (6.52)$$

although in this case the interval $s \in [0, \varepsilon_v)$ is transformed onto $r \in [0, r_0)$. Taking into account the expressions for the real and imaginary parts of the closest v -pole in (6.20) and (6.51), it follows

$$v(r(s)) = \frac{g_2(s) - w_0(s)}{w_1(s) - w_0(s)} + i \frac{g_1(s)}{w_1(s) - w_0(s)}, \quad (6.53)$$

with

$$g_1(s) = \frac{1}{2} \cosh \left[\frac{1}{3} \cosh^{-1} \left(\frac{\varepsilon_v}{s} \right) \right], \quad (6.54)$$

$$g_2(s) = \frac{\sqrt{3}}{2} \sinh \left[\frac{1}{3} \cosh^{-1} \left(\frac{\varepsilon_v}{s} \right) \right], \quad (6.55)$$

$$w_j(s) = \sinh \left[\frac{1}{3} \sinh^{-1} \left(\frac{j - \bar{v}_p}{s} \right) \right], \quad (6.56)$$

noticing that w_j are formally the same functions as in (6.25), though defined over a different interval. Thus, $w_0 < 0 < w_1$ also holds in this case. Moreover, it is readily shown that the following relationship exists between g_1 and g_2 :

$$g_2(s)^2 = 3g_1(s)^2 - \frac{3}{4}. \quad (6.57)$$

The condition (6.48) can then be written in equivalent form as

$$4b^2 \left(\Re(v(r(s))) - \frac{1}{2} \right)^2 + (4b^2 + 1) \Im(v(r(s)))^2 \leq b^2(4b^2 + 1), \quad (6.58)$$

with equality at $s = \varepsilon_v$. This means that it is necessary to show that the left-hand side of this inequality reaches its maximum at $s = \varepsilon_v$. The first parenthesis in (6.58) is computed to

$$\frac{1}{4} \frac{(w_1(s) + w_0(s))^2}{(w_1(s) - w_0(s))^2} - \frac{w_1(s) + w_0(s)}{(w_1(s) - w_0(s))^2} g_2(s) + \frac{g_2(s)^2}{(w_1(s) - w_0(s))^2}.$$

Noting that $g_2(s) \geq 0$, $g_2(\varepsilon_v) = 0$ and taking (6.57) into account, it is clear that

$$\left(\Re(v(r(s))) - \frac{1}{2} \right)^2 \leq \frac{1}{4} \frac{(w_1(s) + w_0(s))^2}{(w_1(s) - w_0(s))^2} + \frac{3g_1(s)^2 - \frac{3}{4}}{(w_1(s) - w_0(s))^2},$$

from where it follows

$$4b^2 \left(\Re(v(r(s))) - \frac{1}{2} \right)^2 + (4b^2 + 1) \Im(v(r(s)))^2 \leq b^2 \frac{(w_1(s) + w_0(s))^2}{(w_1(s) - w_0(s))^2} + \frac{(16b^2 + 1)g_1(s)^2 - 3b^2}{(w_1(s) - w_0(s))^2}, \quad (6.59)$$

with equality guaranteed at $s = \varepsilon_v$ by the definition of b in (6.47). Therefore, it suffices proving that (6.59) reaches its maximum at $s = \varepsilon_v$. We start by showing that the first fraction in (6.59) is an increasing function.

Lemma 22. *If $0 < \bar{v}_p \leq \frac{1}{2}$, the function $w_1(s) + w_0(s)$ is positive for $s \in [0, \varepsilon_v)$.*

Proof. We know from (A.10) that the function $Z(Y) = \sinh \left[\frac{1}{3} \sinh^{-1} Y \right]$ satisfies the functional relationship

$$Y = 3Z + 4Z^3.$$

Taking implicit derivatives with respect to Y produces

$$\frac{dZ}{dY} = \frac{1}{3(4Z^2 + 1)} > 0,$$

meaning that Z is an increasing function.

Since $0 < \bar{v}_p \leq \frac{1}{2}$, it follows that $1 - \bar{v}_p \geq \bar{v}_p$ from where it is clear that

$$\frac{1 - \bar{v}_p}{s} > \frac{\bar{v}_p}{s},$$

for $s > 0$. In consequence

$$\sinh \left[\frac{1}{3} \sinh^{-1} \left(\frac{1 - \bar{v}_p}{s} \right) \right] - \sinh \left[\frac{1}{3} \sinh^{-1} \left(\frac{\bar{v}_p}{s} \right) \right] > 0,$$

finishing the proof. □

On the other hand, it is obvious that

$$\frac{w_1(s) + w_0(s)}{w_1(s) - w_0(s)} > 0,$$

and we prove that this fraction is also an increasing function.

Lemma 23. *If $0 < \bar{v}_p \leq \frac{1}{2}$, the function $\frac{w_1(s) + w_0(s)}{w_1(s) - w_0(s)}$ is increasing for $s \in [0, \varepsilon_v]$.*

Proof. It can be readily shown that

$$\frac{d}{ds} \left(\frac{w_1 + w_0}{w_1 - w_0} \right) = \frac{2}{(w_1(s) - w_0(s))^2} \left[w_1(s) \frac{dw_0}{ds} - w_0(s) \frac{dw_1}{ds} \right]. \quad (6.60)$$

Since, according to (A.10), w_j satisfy

$$4sw_j(s)^3 + 3sw_j(s) = j - \bar{v}_p, \quad (6.61)$$

it follows, by implicit derivation with respect to s , that

$$\frac{dw_j}{ds} = -\frac{w_j(s)}{3s} \left(1 + \frac{2}{4w_j(s)^2 + 1} \right). \quad (6.62)$$

Substituting into the bracket in (6.60) and rearranging terms it follows

$$\frac{d}{ds} \left(\frac{w_1 + w_0}{w_1 - w_0} \right) = \frac{-16w_1(s)w_0(s)}{3s(w_1(s) - w_0(s))} \frac{w_1(s) + w_0(s)}{(4w_1(s)^2 + 1)(4w_0(s)^2 + 1)}, \quad (6.63)$$

which is positive, as $w_0 < 0$ for $0 < \bar{v}_p \leq \frac{1}{2}$. □

As a consequence of the two previous lemmas, we conclude that the first fraction in (6.59) is an increasing function.

We now take under consideration the second fraction in (6.59), and show that its maximum is also reached at $s = \varepsilon_v$. We remark that the numerator of this fraction is positive since, according to (6.57):

$$(16b^2 + 1)g_1(s)^2 - 3b^2 = 4b^2g_2(s)^2 + (4b^2 + 1)g_1(s)^2.$$

As the next step, we find an upper bound for $g_1(s)^2$, with g_1 defined in (6.54).

Lemma 24. *If $X \geq 1$ then*

$$\cosh^2 \left[\frac{1}{3} \cosh^{-1}(X^{3/2}) \right] \leq \frac{X}{2^{4/3}} + 1 - \frac{1}{2^{4/3}}. \quad (6.64)$$

Proof. The equality holds trivially for $X = 1$. The explicit derivative of the left-hand side above is

$$\frac{1}{2} \sqrt{\frac{X}{X^3 - 1}} \sinh \left[\frac{2}{3} \cosh^{-1}(X^{3/2}) \right]. \quad (6.65)$$

We let

$$\frac{1}{3} \cosh^{-1}(X^{3/2}) = Y \rightarrow X = \cosh^{2/3}(3Y), \quad Y \geq 0,$$

and thus, (6.65) takes the form

$$\frac{1}{2} \frac{\cosh^{1/3}(3Y)}{\sinh(3Y)} \sinh(2Y).$$

Raising to the third power, and manipulating the expression above by means of the appropriate hyperbolic identities (indicated within braces), it follows

$$\begin{aligned} & \frac{1}{8} \frac{\cosh(3Y)}{\sinh^3(3Y)} \sinh^3(2Y) \quad \{\sinh(2Y) = 2 \sinh Y \cosh Y\} \\ = & \frac{\cosh(3Y)}{\sinh^3(3Y)} \sinh^3 Y \cosh^3 Y \quad \{\sinh(3Y) = 3 \sinh Y + 4 \sinh^3 Y\} \\ = & \frac{\cosh(3Y)}{(3 + 4 \sinh^2 Y)^3} \cosh^3 Y \quad \{\cosh(3Y) = 4 \cosh^3 Y - 3 \cosh Y\} \\ = & \frac{1}{16} \frac{4 \cosh^2 Y - 3}{4 \sinh^2 Y + 3} \frac{\cosh^4 Y}{(\sinh^2 Y + \frac{3}{4})^2} \quad \{\cosh^2 Y = \sinh^2 Y + 1\} \\ = & \frac{1}{16} \frac{4 \sinh^6 Y + 9 \sinh^4 Y + 6 \sinh^2 Y + 1}{4 \sinh^6 Y + 9 \sinh^4 Y + \frac{27}{4} \sinh^2 Y + \frac{27}{16}} \\ < & \frac{1}{16}. \end{aligned}$$

In consequence, the derivative of the left-hand side of (6.64) is less than $\frac{1}{2^{4/3}}$. Since the derivative of the right-hand side of (6.64) equals $\frac{1}{2^{4/3}}$, the lemma follows as a consequence of Rolle's theorem. \square

Corollary 25. Taking $X = \left(\frac{\varepsilon_v}{s}\right)^{2/3}$ it follows that

$$g_1(s)^2 \leq g_3(s),$$

with equality holding for $s = \varepsilon_v$, where g_3 is defined as

$$g_3(s) = \frac{1}{4} \left(\frac{1}{2^{4/3}} \left(\frac{\varepsilon_v}{s} \right)^{2/3} + 1 - \frac{1}{2^{4/3}} \right). \quad (6.66)$$

Going back to (6.59), we consider the upper bound for its second fraction, namely

$$\frac{(16b^2 + 1)g_3(s) - 3b^2}{(w_1(s) - w_0(s))^2}, \quad (6.67)$$

whose numerator is obviously positive, and show that it is an increasing function for $s \in [0, \varepsilon_v)$.

The derivative of (6.67) is

$$\frac{(16b^2 + 1) \frac{dg_3}{ds} (w_1(s) - w_0(s)) + 2 [(16b^2 + 1)g_3(s) - 3b^2] \frac{d[-(w_1 - w_0)]}{ds}}{(w_1(s) - w_0(s))^3}. \quad (6.68)$$

Recalling from Lemma 13 that $w_1 - w_0$ is a decreasing function for $s > 0$, we next find a lower bound for $\frac{d[-(w_1 - w_0)]}{ds}$. It is a consequence of Lemma 22 that $w_0(s)^2 < w_1(s)^2$. Hence, taking (6.62) into account, it follows

$$\begin{aligned} \frac{dw_0}{ds} &> -\frac{w_0(s)}{3s} \left(1 + \frac{2}{4w_1(s)^2 + 1} \right), \\ \frac{d[-(w_1 - w_0)]}{ds} &> \frac{w_1(s) - w_0(s)}{3s} \left(1 + \frac{2}{4w_1(s)^2 + 1} \right). \end{aligned}$$

Therefore, (6.68) is bounded below by

$$\frac{3s(16b^2 + 1) \frac{dg_3}{ds} + 2 [(16b^2 + 1)g_3(s) - 3b^2] + \frac{4[(16b^2 + 1)g_3(s) - 3b^2]}{4w_1(s)^2 + 1}}{3s(w_1(s) - w_0(s))^2}, \quad (6.69)$$

and, in order to show that (6.67) is increasing, it suffices proving that the numerator of (6.69) is positive. We start by finding an explicit expression for the sum of the first two terms in the numerator of (6.69). From (6.66) it is immediate that

$$\frac{dg_3}{ds} = -\frac{1}{6} \frac{1}{2^{4/3}} \left(\frac{\varepsilon_v}{s} \right)^{2/3} \frac{1}{s},$$

from where it follows, after some algebraic manipulations, that

$$\begin{aligned} &3s(16b^2 + 1) \frac{dg_3}{ds} + 2 [(16b^2 + 1)g_3(s) - 3b^2] \\ &= \frac{1}{2} \left(1 - \frac{1}{2^{4/3}} \right) - 2 \left(2^{2/3} - 1 \right) b^2 \\ &\approx 0.3016 - 1.1748b^2. \end{aligned}$$

We remark that this expression is independent of s . Moreover, it is clearly non-negative for

$$b \leq b_1 = \frac{1}{2\sqrt{2}}\sqrt{2^{1/3} + 2^{-1/3}} \approx 0.5067, \quad (6.70)$$

and since the third term in the numerator of (6.69) is always positive, the optimality condition (6.48) is proved whenever (6.70) holds.

In order to prove (6.48) when (6.70) does not hold, it is necessary to find a lower bound for the third term in the numerator of (6.69), that can be written as

$$\frac{4b^2(16g_3(s) - 3) + 4g_3(s)}{4w_1(s)^2 + 1}. \quad (6.71)$$

We start by proving the following

Lemma 26. *If $X \geq 0$ then*

$$\sinh \left[\frac{1}{3} \sinh^{-1}(X^3) \right] \leq \frac{X}{2^{2/3}}.$$

Proof. It is immediate that the equality holds for $X = 0$. We let

$$\frac{1}{3} \sinh^{-1}(X^3) = Y \rightarrow X = \sinh^{1/3}(3Y), \quad Y \geq 0,$$

and try to prove

$$\sinh Y \leq \frac{\sinh^{1/3}(3Y)}{2^{2/3}},$$

which is equivalent, after raising to the third power, to

$$4 \frac{\sinh^3 Y}{\sinh(3Y)} \leq 1.$$

The left-hand side of this expression can now be manipulated with the help of the appropriate hyperbolic identities, indicated within braces:

$$\begin{aligned} & 4 \frac{\sinh^3 Y}{\sinh(3Y)} \quad \{\sinh^3 Y = \frac{1}{4}(\sinh(3Y) - 3 \sinh Y)\} \\ = & \frac{\sinh(3Y) - 3 \sinh Y}{\sinh(3Y)} \quad \{\sinh(3Y) = 3 \sinh Y + 4 \sinh^3 Y\} \\ = & 1 - \frac{3}{3 + 4 \sinh^2 Y} \\ \leq & 1, \end{aligned}$$

which concludes the proof. □

Corollary 27. Taking $X = \frac{(1 - \bar{v}_p)^{1/3}}{s^{1/3}}$ it follows

$$w_1(s) < \frac{1}{2^{2/3}} \frac{(1 - \bar{v}_p)^{1/3}}{s^{1/3}}, \quad s \in (0, \varepsilon_v).$$

The lower bound for (6.71) can now be written explicitly as follows

$$b^2 \frac{4 \left[2^{2/3} \varepsilon_v^{2/3} - (2^{2/3} - 1) s^{2/3} \right]}{2^{2/3} (1 - \bar{v}_p)^{2/3} + s^{2/3}} + \frac{\varepsilon_v^{2/3} + (2^{4/3} - 1) s^{2/3}}{4(1 - \bar{v}_p)^{2/3} + 2^{4/3} s^{2/3}}. \quad (6.72)$$

In this expression, the first fraction is clearly a decreasing function of s , and thus

$$\begin{aligned} & b^2 \frac{4 \left[2^{2/3} \varepsilon_v^{2/3} - (2^{2/3} - 1) s^{2/3} \right]}{2^{2/3} (1 - \bar{v}_p)^{2/3} + s^{2/3}} \\ & \geq b^2 \frac{4 \varepsilon_v^{2/3}}{2^{2/3} (1 - \bar{v}_p)^{2/3} + \varepsilon_v^{2/3}} \\ & \geq b^2 \frac{4 \varepsilon_v^{2/3}}{2^{2/3} + \varepsilon_v^{2/3}}. \end{aligned}$$

With respect to the second fraction in (6.72), it is the quotient of two affine functions in $s^{2/3}$, from where it can be easily shown that

- it is an increasing function if $\frac{\varepsilon_v^{2/3}}{(1 - \bar{v}_p)^{2/3}} < 4 - 2^{2/3}$.
- it is a constant function if $\frac{\varepsilon_v^{2/3}}{(1 - \bar{v}_p)^{2/3}} = 4 - 2^{2/3}$.
- it is a decreasing function if $\frac{\varepsilon_v^{2/3}}{(1 - \bar{v}_p)^{2/3}} > 4 - 2^{2/3}$.

The first condition can be written alternatively as

$$\varepsilon_v < (4 - 2^{2/3})^{3/2} (1 - \bar{v}_p).$$

Since $0 < \bar{v}_p \leq \frac{1}{2}$, a sufficient condition for this is

$$\varepsilon_v < \frac{1}{2} (4 - 2^{2/3})^{3/2} \approx 1.8737. \quad (6.73)$$

Thus, in case (6.73) holds, the second fraction in (6.72) can be bounded below as follows

$$\frac{\varepsilon_v^{2/3} + (2^{4/3} - 1) s^{2/3}}{4(1 - \bar{v}_p)^{2/3} + 2^{4/3} s^{2/3}} \geq \frac{\varepsilon_v^{2/3}}{4(1 - \bar{v}_p)^{2/3}} \geq \frac{\varepsilon_v^{2/3}}{4},$$

which is a result that will be used at the end of this subsection.

Summarizing the last steps, the numerator in (6.69) admits the following lower bound

$$\frac{1}{2} \left(1 - \frac{1}{2^{4/3}} \right) - 2 \left(2^{2/3} - 1 \right) b^2 + \frac{\varepsilon_v^{2/3}}{4} + \frac{4 \varepsilon_v^{2/3}}{2^{2/3} + \varepsilon_v^{2/3}} b^2. \quad (6.74)$$

A bound for the semi-minor axis, b Before showing that (6.74) is positive for any $b > 0$, we need to find an upper bound for the semi-minor axis as a function of the geometric parameters. Thus, for the rest of this subsection, the explicit dependence of the semi-minor axis will be written, i.e. $b(\varepsilon_v, \bar{v}_p)$. The dependence of the functions w_j is explicitly written too, i.e. $w_j(s, \bar{v}_p)$.

Fixing ε_v , two functions are now introduced to be conveniently used later on:

$$h_1(\bar{v}_p) = (w_1(\varepsilon_v, \bar{v}_p) - w_0(\varepsilon_v, \bar{v}_p))^2, \quad (6.75)$$

$$h_2(\bar{v}_p) = w_1(\varepsilon_v, \bar{v}_p)w_0(\varepsilon_v, \bar{v}_p) + \frac{1}{4}. \quad (6.76)$$

A proof that both are monotonic functions of \bar{v}_p is provided below.

Lemma 28. $h_1(\bar{v}_p)$ is an increasing function for $0 < \bar{v}_p \leq \frac{1}{2}$.

Proof. It is clear from (6.61) that, at $s = \varepsilon_v$, the functions w_j satisfy

$$4\varepsilon_v w_j(\varepsilon_v, \bar{v}_p)^3 + 3\varepsilon_v w_j(\varepsilon_v, \bar{v}_p) = j - \bar{v}_p.$$

Taking implicit derivatives with respect to \bar{v}_p yields:

$$\frac{dw_j(\varepsilon_v, \bar{v}_p)}{d\bar{v}_p} = -\frac{1}{3\varepsilon_v} \frac{1}{4w_j(\varepsilon_v, \bar{v}_p)^2 + 1},$$

from where it is immediate that

$$\frac{d(w_1(\varepsilon_v, \bar{v}_p) - w_0(\varepsilon_v, \bar{v}_p))}{d\bar{v}_p} = \frac{4}{3\varepsilon_v} \frac{w_1(\varepsilon_v, \bar{v}_p)^2 - w_0(\varepsilon_v, \bar{v}_p)^2}{(4w_1(\varepsilon_v, \bar{v}_p)^2 + 1)(4w_0(\varepsilon_v, \bar{v}_p)^2 + 1)}.$$

We know from Lemma 22 that $w_1(\varepsilon_v, \bar{v}_p) + w_0(\varepsilon_v, \bar{v}_p) > 0$, hence the numerator of the right-hand side fraction is positive. In consequence,

$$\frac{dh_1(\bar{v}_p)}{d\bar{v}_p} = 2(w_1(\varepsilon_v, \bar{v}_p) - w_0(\varepsilon_v, \bar{v}_p)) \frac{d(w_1(\varepsilon_v, \bar{v}_p) - w_0(\varepsilon_v, \bar{v}_p))}{d\bar{v}_p} > 0,$$

finishing the proof. \square

Lemma 29. $h_2(\bar{v}_p)$ is a decreasing function for $0 < \bar{v}_p \leq \frac{1}{2}$.

Proof. It suffices computing the explicit value of the derivative

$$\frac{dh_2}{d\bar{v}_p} = -\frac{1}{3\varepsilon_v} \frac{4(w_1(\varepsilon_v, \bar{v}_p)^3 + w_0(\varepsilon_v, \bar{v}_p)^3) + w_1(\varepsilon_v, \bar{v}_p) + w_0(\varepsilon_v, \bar{v}_p)}{(4w_1(\varepsilon_v, \bar{v}_p)^2 + 1)(4w_0(\varepsilon_v, \bar{v}_p)^2 + 1)}.$$

As $w_1(\varepsilon_v, \bar{v}_p) + w_0(\varepsilon_v, \bar{v}_p) > 0$ implies $w_1(\varepsilon_v, \bar{v}_p)^3 + w_0(\varepsilon_v, \bar{v}_p)^3 > 0$, it is clear that the numerator of the fraction above is positive, concluding the proof. \square

It is interesting to remark that these two lemmas are valid for all values of $\bar{v}_p \leq \frac{1}{2}$, i.e., they are not restricted to the current case under consideration, $0 < \bar{v}_p \leq \frac{1}{2}$.

We next focus on equation (6.47) that defines the semi-minor axis $b(\varepsilon_v, \bar{v}_p)$. First, (6.53) is evaluated at $s = \varepsilon_v$, taking into account that (6.55) implies $g_2(\varepsilon_v) = 0$ and (6.54) implies $g_1(\varepsilon_v) = \frac{1}{2}$. Substituting its real and imaginary parts into (6.47) and recalling the definitions in (6.75) and (6.76), a biquadratic equation for $b(\varepsilon_v, \bar{v}_p)$ is obtained:

$$h_1(\bar{v}_p)b(\varepsilon_v, \bar{v}_p)^4 - h_2(\bar{v}_p)b(\varepsilon_v, \bar{v}_p)^2 - \frac{1}{16} = 0, \quad (6.77)$$

that allows us to prove the following

Theorem 30. *If ε_v is fixed and $0 < \bar{v}_p \leq \frac{1}{2}$, the semi-minor axis $b(\varepsilon_v, \bar{v}_p)$ is a decreasing function of \bar{v}_p .*

Proof. Since $b(\varepsilon_v, \bar{v}_p) > 0$ it suffices proving that $b(\varepsilon_v, \bar{v}_p)^2$ is decreasing. Taking implicit derivatives with respect to \bar{v}_p in (6.77) yields

$$\frac{d(b(\varepsilon_v, \bar{v}_p)^2)}{d\bar{v}_p} = b(\varepsilon_v, \bar{v}_p)^2 \frac{\frac{dh_2}{d\bar{v}_p} - \frac{dh_1}{d\bar{v}_p} b(\varepsilon_v, \bar{v}_p)^2}{2h_1(\bar{v}_p)b(\varepsilon_v, \bar{v}_p)^2 - h_2(\bar{v}_p)}.$$

The numerator of this expression is clearly negative as a consequence of the two previous lemmas. With respect to the denominator, it follows from (6.77) that

$$h_1(\bar{v}_p)b(\varepsilon_v, \bar{v}_p)^2 - h_2(\bar{v}_p) = \frac{1}{16b(\varepsilon_v, \bar{v}_p)^2} > 0,$$

from where it is immediate that $2h_1(\bar{v}_p)b(\varepsilon_v, \bar{v}_p)^2 - h_2(\bar{v}_p) > 0$. \square

Corollary 31. *In case $0 < \bar{v}_p \leq \frac{1}{2}$ it holds $b(\varepsilon_v, \bar{v}_p) \leq b(\varepsilon_v, 0)$, with equality at $\bar{v}_p = 0$.*

It is now straightforward to obtain the explicit value of $b(\varepsilon_v, 0)$. Taking (6.56) into account, it is clear that $w_0(\varepsilon_v, 0) = 0$ and $w_1(\varepsilon_v, 0) = \sinh \left[\frac{1}{3} \sinh^{-1} \left(\frac{1}{\varepsilon_v} \right) \right]$. Hence, (6.77) reduces to

$$w_1(\varepsilon_v, 0)^2 b(\varepsilon_v, 0)^4 - \frac{1}{4} b(\varepsilon_v, 0)^2 - \frac{1}{16} = 0,$$

whose positive solution can be written as

$$b(\varepsilon_v, 0)^2 = \frac{1}{8w_1(\varepsilon_v, 0)^2} + \frac{1}{4} \sqrt{\frac{1}{4w_1(\varepsilon_v, 0)^4} + \frac{1}{w_1(\varepsilon_v, 0)^2}}. \quad (6.78)$$

We next obtain a more convenient (in fact, linear) upper bound for $b(\varepsilon_v, 0)$. An upper bound for $\frac{1}{w_1(\varepsilon_v, 0)}$ is found first.

Lemma 32. *If $X > 0$ then*

$$\frac{1}{\sinh \left[\frac{1}{3} \sinh^{-1} \left(\frac{1}{X} \right) \right]} \leq 3X + \frac{1}{\sqrt{3}}.$$

Proof. We try to find the smallest value of k such that the inequality

$$\frac{1}{\sinh \left[\frac{1}{3} \sinh^{-1} \left(\frac{1}{X} \right) \right]} \leq 3X + k,$$

holds. We let

$$\frac{1}{3} \sinh^{-1} \left(\frac{1}{X} \right) = Y \rightarrow \frac{1}{X} = \sinh(3Y), \quad Y > 0,$$

and obtain an equivalent form for the condition above, namely:

$$\frac{3 \sinh Y}{\sinh(3Y)} + k \sinh Y \geq 1.$$

Using the identity $\sinh(3Y) = 3 \sinh Y + 4 \sinh^3 Y$, and after some manipulations, the condition becomes

$$k(3 + 4 \sinh^2 Y) \geq 4 \sinh Y.$$

This is a quadratic inequality in $\sinh Y$ such that equality holds if

$$\sinh Y = \frac{1}{2k} \pm \frac{1}{2} \sqrt{\frac{1}{k^2} - 3}.$$

Thus, the smallest value of k that prevents the equality from having two different real solutions is $k = \frac{1}{\sqrt{3}}$ and the proof is finished. \square

Corollary 33. *Taking $X = \varepsilon_v$ it follows*

$$\frac{1}{w_1(\varepsilon_v, 0)} \leq 3\varepsilon_v + \frac{1}{\sqrt{3}}.$$

Going back to (6.78), the term under the square root can be bounded above as follows

$$\frac{1}{4w_1(\varepsilon_v, 0)^4} + \frac{1}{w_1(\varepsilon_v, 0)^2} \leq \frac{81\varepsilon_v^4}{4} + 9\sqrt{3}\varepsilon_v^3 + \frac{27}{2}\varepsilon_v^2 + \frac{7}{\sqrt{3}}\varepsilon_v + \frac{13}{36}.$$

It is straightforward to verify that the right-hand side polynomial is bounded above itself by $\left(\frac{3\varepsilon_v}{\sqrt{2}} + a_1\right)^4$, with $a_1 = \frac{\sqrt[3]{7}}{\sqrt{6}} \approx 0.7810$. Hence, it follows from (6.78) that

$$b(\varepsilon_v, 0)^2 < \frac{1}{8} \left(3\varepsilon_v + \frac{1}{\sqrt{3}} \right)^2 + \frac{1}{4} \left(\frac{3\varepsilon_v}{\sqrt{2}} + a_1 \right)^2.$$

Again, it is straightforward to check that the right-hand side polynomial is, once more, bounded above by $\left(\frac{3\varepsilon_v}{2} + a_2\right)^2$, with

$$a_2 = \frac{1}{2} \sqrt{a_1^2 + \frac{1}{6}} = \frac{1}{2} \sqrt{\frac{7^{2/3} + 1}{6}} \approx 0.4406. \quad (6.79)$$

Summarizing the steps above, a chain of upper bounds has been found for the semi-minor axis in case $0 < \bar{v}_p \leq \frac{1}{2}$, namely

$$b(\varepsilon_v, \bar{v}_p) \leq b(\varepsilon_v, 0) < \frac{3\varepsilon_v}{2} + a_2. \quad (6.80)$$

It is interesting to mention that a similar reasoning leads to a lower bound for the semi-minor axis, more specifically

$$b(\varepsilon_v, \bar{v}_p) \geq b\left(\varepsilon_v, \frac{1}{2}\right) > \frac{3\varepsilon_v}{2},$$

although this fact will not be used in the rest of the proof.

We are now ready to prove that (6.74) is positive for any $b(\varepsilon_v, \bar{v}_p) > 0$. An iterative procedure will be followed, as explained below.

For the first iteration, we know that (6.74) is positive for $b(\varepsilon_v, \bar{v}_p) \leq b_1$, with the value of b_1 defined in (6.70), and rewritten here for convenience

$$b_1 = \frac{1}{2\sqrt{2}} \sqrt{2^{1/3} + 2^{-1/3}} \approx 0.5067.$$

Taking (6.79) and (6.80) into account, a sufficient condition to ensure $b(\varepsilon_v, \bar{v}_p) \leq b_1$ comes from imposing

$$\frac{3\varepsilon_v}{2} + a_2 \leq b_1.$$

Solving the equality produces $\varepsilon_v = \frac{2}{3}(b_1 - a_2) \approx 0.04403$ and thus we can take $\varepsilon_{v1} = 0.04$ as the value for the first iteration (see Tab.6.1). Since the optimality is now guaranteed for $\varepsilon_v \leq \varepsilon_{v1}$, we can assume $\varepsilon_v > \varepsilon_{v1}$ to find a lower bound of the last two fractions in (6.74). Since both $\frac{\varepsilon_v^{2/3}}{4}$ and $\frac{4\varepsilon_v^{2/3}}{2^{2/3} + \varepsilon_v^{2/3}}$ are increasing functions of ε_v , it follows that

$$\begin{aligned} & \frac{\varepsilon_v^{2/3}}{4} + \frac{4\varepsilon_v^{2/3}}{2^{2/3} + \varepsilon_v^{2/3}} b(\varepsilon_v, \bar{v}_p)^2 \\ & > \frac{\varepsilon_{v1}^{2/3}}{4} + \frac{4\varepsilon_{v1}^{2/3}}{2^{2/3} + \varepsilon_{v1}^{2/3}} b(\varepsilon_v, \bar{v}_p)^2 \\ & \approx 0.03116 + 0.2912b(\varepsilon_v, \bar{v}_p)^2, \end{aligned}$$

and in consequence (6.74) is bounded below by

$$\begin{aligned} & \frac{1}{2} \left(1 - \frac{1}{2^{4/3}}\right) - 2 \left(2^{2/3} - 1\right) b(\varepsilon_v, \bar{v}_p)^2 \\ & + 0.03116 + 0.2912b(\varepsilon_v, \bar{v}_p)^2 \\ & \approx 0.3327 - 0.8836b(\varepsilon_v, \bar{v}_p)^2, \end{aligned}$$

which is positive for $b(\varepsilon_v, \bar{v}_p) \lesssim 0.6136$. This ensures that (6.74) is positive for $b(\varepsilon_v, \bar{v}_p) \leq b_2$, where we can take $b_2 = 0.60$.

Table 6.1.: Iterations for $b(\varepsilon_v, \bar{v}_p)$

Iteration	b_i	ε_{vi}
1	0.506	0.04
2	0.60	0.10
3	0.71	0.17
4	0.84	0.26
5	1.06	0.41
6	1.75	0.87

The procedure just described is now iterated, as summarized in Tab. 6.1. After the sixth iteration, the lower bound for (6.74) becomes

$$0.5294 + 0.2841b(\varepsilon_v, \bar{v}_p)^2,$$

which is obviously positive for all values of $b(\varepsilon_v, \bar{v}_p)$, and the proof that (6.74) is positive is finished. We remark that all iterations above satisfy the condition (6.73), ensuring that (6.74) is a lower bound of the numerator of (6.69).

6.4.3. The case $0 < \bar{v}_p \leq \frac{1}{2}$ and $r_0 < r \leq 1$

Applying once more the change of variable in (6.22) produces

$$v(r(s)) = \frac{-w_0(s)}{w_1(s) - w_0(s)} + i \frac{g(s)}{w_1(s) - w_0(s)}, \quad (6.81)$$

with $s \in [\varepsilon_v, \infty)$ and

$$g(s) = \sin \left[\frac{1}{3} \sin^{-1} \left(\frac{\varepsilon_v}{s} \right) \right], \quad (6.82)$$

$$w_j(s) = \sinh \left[\frac{1}{3} \sinh^{-1} \left(\frac{j - \bar{v}_p}{s} \right) \right], \quad (6.83)$$

noticing that w_j are the same functions as in (6.25). Substituting the real and imaginary parts of (6.81) into (6.48), the condition to be proved becomes

$$\frac{1}{4b^2 + 1} \frac{(w_1(s) + w_0(s))^2}{(w_1(s) - w_0(s))^2} + \frac{1}{b^2} \frac{g(s)^2}{(w_1(s) - w_0(s))^2} \leq 1. \quad (6.84)$$

The optimality of the imaginary part of (6.81) was already proved in sec. 6.3.4, i.e., we know that $\frac{g(s)}{w_1(s) - w_0(s)}$ is a positive and decreasing function in $s \in [\varepsilon_v, \infty)$, hence its square is a decreasing function too and reaches its maximum at $s = \varepsilon_v$. However, it was already proved in Lemma 23 that $\frac{w_1(s) + w_0(s)}{w_1(s) - w_0(s)}$ is an increasing

function for $0 < \bar{v}_p \leq \frac{1}{2}$ and in consequence, the left-hand side of (6.84) might not reach its maximum at the same point.

In order to simplify further calculations, we start by finding an upper bound for $g(s)$ in (6.82).

Lemma 34. *If $s \in [\varepsilon_v, \infty)$ then $g(s) \leq \frac{\varepsilon_v}{2s}$.*

Proof. The equality holds at $s = \varepsilon_v$ by trivial substitution in (6.82). In case $s > \varepsilon_v$ we let

$$\frac{1}{3} \sin^{-1} \left(\frac{\varepsilon_v}{s} \right) = X, \quad X \in \left(0, \frac{\pi}{6} \right),$$

and the condition to be proved can be expressed as

$$\sin X < \frac{1}{2} \sin(3X).$$

Applying the identity $\sin(3X) = (2 \cos(2X) + 1) \sin X$, the condition becomes

$$\frac{1}{2} < \cos(2X),$$

that holds trivially. □

A consequence of this lemma is that the confocal ellipse containing the point

$$P_1(s) = \left(\frac{-w_0(s)}{w_1(s) - w_0(s)}, \frac{g(s)}{w_1(s) - w_0(s)} \right),$$

is always interior to the confocal ellipse containing the point

$$P_2(s) = \left(\frac{-w_0(s)}{w_1(s) - w_0(s)}, \frac{\varepsilon_v}{2s(w_1(s) - w_0(s))} \right).$$

Thus, in order to prove (6.84), it suffices showing that the ellipse containing $P_2(s)$ is always interior to the critical ellipse that contains the point $P_1(\varepsilon_v) = P_2(\varepsilon_v)$. More specifically, it will be shown that the semi-axis minor $b(s)$ of the ellipse containing $P_2(s)$ is smaller than the semi-axis minor of the critical ellipse, i.e.

$$b(s) \leq b(\varepsilon_v) = b, \tag{6.85}$$

with equality holding at $s = \varepsilon_v$.

Taking (6.47) into account, it is clear that the semi-axis minor $b(s)$ of the ellipse determined by $P_2(s)$ must satisfy the equation

$$\frac{1}{4b(s)^2 + 1} \frac{(w_1(s) + w_0(s))^2}{(w_1(s) - w_0(s))^2} + \frac{\varepsilon_v^2}{4s^2 b(s)^2 (w_1(s) - w_0(s))^2} = 1. \tag{6.86}$$

The remaining objective of this subsection is to prove that $b(s)$ defined above is a decreasing function in $s \in [\varepsilon_v, \infty)$.

We define two auxiliary functions

$$\begin{aligned} h_1(s) &= s^2(w_1(s) - w_0(s))^2, \\ h_2(s) &= s^2w_1(s)w_0(s) + \frac{\varepsilon_v^2}{4}, \end{aligned}$$

that allow us to rewrite (6.86) as

$$h_1(s)b(s)^4 - h_2(s)b(s)^2 - \frac{\varepsilon_v^2}{16} = 0. \quad (6.87)$$

It is now shown that $h_1(s)$ and $h_2(s)$ are both monotonic functions. The proof of the next two Lemmas makes use of bounds for the derivatives of $w_j(s)$, already proved in Lemma 13, and rewritten here in a slightly different manner:

$$\frac{dw_1}{ds} > -\frac{w_1(s)}{s}, \quad (6.88)$$

$$-\frac{dw_0}{ds} > \frac{w_0(s)}{s}. \quad (6.89)$$

Lemma 35. $h_1(s)$ is an increasing function.

Proof. Since $s(w_1(s) - w_0(s)) > 0$ it suffices proving that $s(w_1(s) - w_0(s))$ is increasing. Computing explicitly its derivative and applying (6.88)-(6.89) yields

$$\begin{aligned} \frac{d(s(w_1(s) - w_0(s)))}{ds} &= w_1(s) - w_0(s) + s \left(\frac{dw_1}{ds} - \frac{dw_0}{ds} \right) \\ &> w_1(s) - w_0(s) + s \left(\frac{-w_1(s)}{s} + \frac{w_0(s)}{s} \right) \\ &= 0. \end{aligned}$$

□

Lemma 36. $h_2(s)$ is a decreasing function.

Proof. The explicit value of the derivative admits the expression

$$\frac{dh_2}{ds} = 2sw_1(s)w_0(s) + s^2 \left[\left(-\frac{dw_1}{ds} \right) (-w_0(s)) + w_1(s) \frac{dw_0}{ds} \right],$$

where all functions in the right-hand side bracket are positive. In this case the bounding properties (6.88)-(6.89) are more conveniently written as

$$\begin{aligned} -\frac{dw_1}{ds} &< \frac{w_1(s)}{s}, \\ \frac{dw_0}{ds} &< -\frac{w_0(s)}{s}, \end{aligned}$$

from where

$$\begin{aligned} \frac{dh_2(s)}{ds} &< 2sw_1(s)w_0(s) + s^2 \left[\frac{w_1(s)}{s}(-w_0(s)) + w_1(s) \left(-\frac{w_0(s)}{s} \right) \right] \\ &= 0. \end{aligned}$$

□

We are now ready to prove the main result in this subsection.

Theorem 37. $b(s)$, as defined in (6.87), is a decreasing function.

Proof. Since $b(s) > 0$ it suffices showing that $b(s)^2$ is decreasing. Taking implicit derivatives with respect to s in (6.87) yields

$$\frac{d(b(s)^2)}{ds} = b(s)^2 \frac{\frac{dh_2}{ds} - \frac{dh_1}{ds} b(s)^2}{2h_1(s)b(s)^2 - h_2(s)}. \quad (6.90)$$

The numerator of the fraction in (6.90) is clearly negative. With respect to its denominator, it follows from (6.87) that

$$h_1(s)b(s)^2 - h_2(s) = \frac{\varepsilon_v^2}{16b(s)^2} > 0,$$

from where it is obvious that $2h_1(s)b(s)^2 - h_2(s) > 0$. □

6.4.4. The case $\bar{v}_p < 0$ and $0 \leq r \leq r_0$

A direct proof of (6.48) seems too difficult in this case. For this reason, we will give a proof of optimality from a different point of view. Instead of proving that the closest v -pole lies inside the critical ellipse \mathcal{E}_p , two different bounds for its real part will be provided, recalling that the optimality of the imaginary part was already established in sec. 6.3.5. More specifically:

- A lower bound for the real part of the closest v -pole will be provided first, namely $\Re(v(r)) \geq \Re(v(r_0))$, with equality at $r = r_0$.
- An upper bound of the form $\Re(v(r)) \leq 1$ will be provided. This condition is in fact stronger than (6.48), but an additional hypothesis, without practical relevance, will need to be introduced, producing a slightly weaker result.

Lower Bound of $\Re(v(r))$ In order to prove that $\Re(v(r))$ reaches its minimum at $r = r_0$, it will be more practical to show the equivalent condition

$$1 - \Re(v(r)) = \frac{t_1(r) - \Im(\tau_{23}(r))}{t_1(r) - t_0(r)} \leq 1 - \Re(v(r_0)), \quad (6.91)$$

that involves a positive bound. Applying the same change of variable from $s \in [0, 1]$ onto $r \in [0, r_0]$ as in (6.26), namely

$$\frac{3\sqrt{3}}{2r} \sqrt{\frac{1-r}{r}} \varepsilon_v = \frac{1}{s\sqrt{s}}, \quad (6.92)$$

it follows that

$$1 - \Re(v(r(s))) = \frac{w_1(s) - g_2(s)}{w_1(s) - w_0(s)}, \quad (6.93)$$

with w_j and g_2 given by

$$w_j(s) = \left(\sqrt{\left(\frac{j-\bar{v}_p}{\varepsilon_v}\right)^2 + s^3 + \frac{j-\bar{v}_p}{\varepsilon_v}} \right)^{1/3} - \left(\sqrt{\left(\frac{j-\bar{v}_p}{\varepsilon_v}\right)^2 + s^3 - \frac{j-\bar{v}_p}{\varepsilon_v}} \right)^{1/3} \quad (6.94)$$

$$= 2\sqrt{s} \sinh \left[\frac{1}{3} \sinh^{-1} \left(\frac{j-\bar{v}_p}{\varepsilon_v} \frac{1}{s\sqrt{s}} \right) \right]. \quad (6.95)$$

$$g_2(s) = \frac{\sqrt{3}}{2} \left[\left(1 + \sqrt{1-s^3}\right)^{1/3} - \left(1 - \sqrt{1-s^3}\right)^{1/3} \right] \\ = \sqrt{3}s \sinh \left[\frac{1}{3} \cosh^{-1} \left(\frac{1}{s\sqrt{s}} \right) \right]. \quad (6.96)$$

We remark that w_j are the same functions already defined in (6.30).

In order to prove (6.91), two lower bounds for g_2 are deduced first.

Lemma 38. $g_2(s)$ is a concave function in $s \in [0, 1]$.

Proof. By explicit derivation of (6.96) we obtain

$$\frac{d^2 g_2}{ds^2} = \frac{\sqrt{3}}{4} \left(\frac{s}{1-s^3} \right)^{3/2} \left\{ \sqrt{1-s^3} \sinh \left[\frac{1}{3} \cosh^{-1} \left(\frac{1}{s\sqrt{s}} \right) \right] - 3 \cosh \left[\frac{1}{3} \cosh^{-1} \left(\frac{1}{s\sqrt{s}} \right) \right] \right\}$$

We put

$$\frac{1}{3} \cosh^{-1} \left(\frac{1}{s\sqrt{s}} \right) = X \rightarrow \frac{1}{s^3} = \cosh^2(3X), \quad (6.97)$$

and the term within braces above becomes

$$\underbrace{\frac{\sinh(3X)}{\cosh(3X)}}_{<1} \sinh X - 3 \cosh X < \underbrace{\sinh X}_{<\cosh X} - 3 \cosh X < 0.$$

□

As a consequence of this lemma, g_2 is bounded below by its chord, namely

$$g_2(s) \geq \frac{\sqrt{3}}{2^{2/3}} (1-s), \quad (6.98)$$

with equality at $s = 0$ and $s = 1$.

Lemma 39. $g_2(s)^2$ is a convex function in $s \in [0, 1]$.

Proof. By explicit derivation we obtain

$$\frac{d^2 g_2^2}{ds^2} = \frac{2\sqrt{1-s^3} \cosh \left[\frac{2}{3} \cosh^{-1} \left(\frac{1}{s\sqrt{s}} \right) \right] - (s^3 + 2) \sinh \left[\frac{2}{3} \cosh^{-1} \left(\frac{1}{s\sqrt{s}} \right) \right]}{\frac{4}{3}s(1-s^3)^{3/2}}.$$

Applying the same change of variable as in (6.97), the numerator of this expression becomes

$$\frac{2 \cosh(3X) \sinh(3X) \cosh(2X) - (1 + 2 \cosh^2(3X)) \sinh 2X}{\cosh^2(3X)},$$

where the identities

$$\cosh(3X) = \cosh X (4 \sinh^2 X + 1), \quad (6.99)$$

$$\sinh(3X) = \sinh X (4 \sinh^2 X + 3), \quad (6.100)$$

$$\cosh(2X) = 2 \sinh^2 X + 1,$$

$$\sinh(2X) = 2 \sinh X \cosh X,$$

can be used to yield

$$\frac{8 \sinh^3 X \cosh X}{\cosh^2(3X)} > 0.$$

□

A consequence of this lemma is that $g_2(s)^2$ is bounded below by its tangent at $s = 1$. It can be readily computed that

$$\left. \frac{dg_2^2}{ds} \right|_{s=1} = -1,$$

hence, it follows that $g_2(s)^2 \geq 1 - s$ and thus

$$g_2(s) \geq \sqrt{1-s}, \quad (6.101)$$

with equality at $s = 1$.

According to Lemma 17, w_j are decreasing and convex functions, and thus are bounded above as follows

$$w_j(s) \leq w_j^*(s),$$

with $w_j^*(s)$ being the chords given by

$$w_j^*(s) = w_j(0)(1-s) + w_j(1)s, \quad j = 0, 1. \quad (6.102)$$

On the other hand, it was established, as a consequence of Theorem 19, that

$$\frac{1}{w_1(s) - w_0(s)} \leq \frac{1-s}{w_1(0) - w_0(0)} + \frac{s}{w_1(1) - w_0(1)},$$

with equality at $s = 0$ and $s = 1$. This allows us to write an upper bound for $1 - \Re(v(r(s)))$. However, we remark that the numerator in (6.93) can take negative values, and thus the upper bound needs to be carefully expressed as

$$1 - \Re(v(r(s))) = \frac{w_1(s) - g_2(s)}{w_1(s) - w_0(s)} \leq \max \{0, B_2(s)\},$$

where $B_2(s)$ is the bounding function given by

$$B_2(s) = [w_1^*(s) - g_2^*(s)] \left[\frac{1-s}{w_1(0) - w_0(0)} + \frac{s}{w_1(1) - w_0(1)} \right], \quad (6.103)$$

w_1^* is the upper bound for w_1 given in (6.102) and g_2^* is one of the two lower bounds for g_2 previously obtained in (6.98) and (6.101).

Since $1 - \Re(v(r(1))) > 0$, it suffices for the rest of this section to show that $B_2(s)$ reaches its maximum at $s = 1$, as $\max \{0, B_2(s)\}$ would reach its maximum at $s = 1$ too. To this purpose, it is necessary to consider the term in brackets in (6.38), rewritten here for convenience

$$\left[\frac{1}{w_1(1) - w_0(1)} - \frac{1}{w_1(0) - w_0(0)} \right]. \quad (6.104)$$

We recall that (6.104) can take positive, negative and zero values, depending on ε_v and \bar{v}_p . The next steps of the proof can be outlined as follows:

1. If (6.104) is non-negative, take $g_2^*(s) = \frac{\sqrt{3}}{2^{2/3}}(1-s)$, prove that $B_2(s)$ is convex and $B_2(0) < B_2(1)$, thus $B_2(s)$ reaches its maximum at $s = 1$.
2. If (6.104) is negative, take $g_2^*(s) = \sqrt{1-s}$ and proceed as in the first case, i.e., prove that $B_2(s)$ is convex and $B_2(0) < B_2(1)$.

In the first case, where (6.104) is non-negative, we obtain by explicit derivation

$$\frac{d^2 B_2}{ds^2} = 2 \left(\frac{\sqrt{3}}{2^{2/3}} - w_1(0) + w_1(1) \right) \left[\frac{1}{w_1(1) - w_0(1)} - \frac{1}{w_1(0) - w_0(0)} \right], \quad (6.105)$$

where the bracket is non-negative by hypothesis. In order to show that the first parenthesis above is always positive, we next find the maximum of $w_1(0) - w_1(1)$.

Lemma 40. $w_1(0) - w_1(1)$ has a maximum value of $\sqrt{2\sqrt{3} - 3}$

Proof. Taking (6.94) and (6.95) into account, it is clear that

$$w_1(0) - w_1(1) = 2^{1/3} \left(\frac{1 - \bar{v}_p}{\varepsilon_v} \right)^{1/3} - 2 \sinh \left[\frac{1}{3} \sinh^{-1} \left(\frac{1 - \bar{v}_p}{\varepsilon_v} \right) \right].$$

With the changes

$$\frac{1 - \bar{v}_p}{\varepsilon_v} = X, \quad X > 0, \quad (6.106)$$

$$\frac{1}{3} \sinh^{-1} X = Y \rightarrow X = \sinh(3Y), \quad Y > 0, \quad (6.107)$$

the problem reduces to finding the maximum, for $Y > 0$, of

$$2^{1/3} \sinh^{1/3}(3Y) - 2 \sinh Y. \quad (6.108)$$

By explicit derivation, the following condition is imposed

$$\frac{2^{1/3} \cosh(3Y)}{\sinh^{2/3}(3Y)} = 2 \cosh Y.$$

Raising to the third power, using the hyperbolic identities (6.99) and (6.100) and simplifying terms, it follows

$$48 \sinh^4 Y + 24 \sinh^2 Y - 1 = 0,$$

which is a biquadratic equation in $\sinh Y$ whose only positive solution is

$$\sinh Y = \frac{1}{2} \sqrt{\frac{2}{\sqrt{3}} - 1}.$$

This way, it is easily shown that

$$X = \sinh(3Y) = \left(\frac{4}{27}\right)^{1/4}.$$

Substituting $\sinh Y$ and $\sinh(3Y)$ into (6.108) yields

$$w_1(0) - w_1(1) \leq \sqrt{2\sqrt{3} - 3} \approx 0.6813.$$

□

As an immediate consequence of this Lemma we have that

$$\frac{\sqrt{3}}{2^{2/3}} - w_1(0) + w_1(1) \gtrsim 0.4099 > 0,$$

meaning that $B_2(s)$ is a convex function. It is now time to show that $B_2(0) < B_2(1)$, namely

$$\frac{w_1(0) - \frac{\sqrt{3}}{2^{2/3}}}{w_1(0) - w_0(0)} < \frac{w_1(1)}{w_1(1) - w_0(1)}. \quad (6.109)$$

We will prove, in fact, a stronger condition.

Lemma 41. *The minimum value of k for which*

$$\frac{w_1(0) - k}{w_1(0) - w_0(0)} \leq \frac{w_1(1)}{w_1(1) - w_0(1)}, \quad (6.110)$$

is $k = \frac{1}{2^{1/3}}$.

Proof. Rearranging terms and substituting the explicit expressions for $w_j(0)$ and $w_j(1)$ in (6.94) and (6.95), we arrive at

$$\frac{k - 2^{1/3} \left(\frac{1-\bar{v}_p}{\varepsilon_v} \right)^{1/3}}{\sinh \left[\frac{1}{3} \sinh^{-1} \left(\frac{1-\bar{v}_p}{\varepsilon_v} \right) \right]} \leq \frac{k - 2^{1/3} \left(\frac{-\bar{v}_p}{\varepsilon_v} \right)^{1/3}}{\sinh \left[\frac{1}{3} \sinh^{-1} \left(\frac{-\bar{v}_p}{\varepsilon_v} \right) \right]}.$$

We notice that both sides of this inequality are the same function, but with shifted argument. Therefore, it suffices imposing that the left-hand side is a decreasing function for any positive argument. With the same changes as in (6.106) and (6.107) we impose that the function

$$\frac{k - 2^{1/3} \sinh^{1/3}(3Y)}{\sinh Y},$$

is decreasing for $Y > 0$, or, equivalently, find the minimum value of k for which that function has a critical point (with vanishing derivative). By explicit derivation, the condition obtained is

$$\frac{2^{4/3}}{\sinh^{2/3}(3Y)} = \frac{k}{\sinh Y}.$$

Raising to the third power, using (6.100) and rearranging terms we arrive at

$$16 \sinh Y = k^3 (4 \sinh^2 Y + 3)^2.$$

Putting $\sinh Y = Z$ and expanding terms we arrive at the polynomial equation

$$16Z^4 + 24Z^2 - \frac{16}{k^3}Z + 9 = 0. \quad (6.111)$$

Imposing that this equation has a double (positive) root it follows

$$4Z^3 + 3Z = \frac{1}{k^3}.$$

Substituting this into (6.111) yields

$$16Z^4 + 8Z^2 - 3 = 0,$$

whose only positive root is $Z = \frac{1}{2}$, from where $k = \frac{1}{2^{1/3}}$ is easily obtained. \square

Going back to (6.109), since

$$\frac{\sqrt{3}}{2^{2/3}} > \frac{1}{2^{1/3}},$$

it follows that $B_2(0) < B_2(1)$ and thus the proof is finished for the case in which (6.104) is non-negative.

In the second case, where (6.104) is negative, we take $g_2^*(s) = \sqrt{1-s}$, and follow a similar reasoning as before. In this case, $B_2(s)$ can be regarded as the sum of two terms, the first one being

$$w_1^*(s) \left[\frac{1-s}{w_1(0) - w_0(0)} + \frac{s}{w_1(1) - w_0(1)} \right], \quad (6.112)$$

with w_1^* defined in (6.102). The second derivative of (6.112) is

$$-2(w_1(0) - w_1(1)) \left[\frac{1}{w_1(1) - w_0(1)} - \frac{1}{w_1(0) - w_0(0)} \right] > 0,$$

where the bracket is negative by hypothesis. Thus, the first term of $B_2(s)$ is a convex function.

With respect to the second term, given by

$$-\sqrt{1-s} \left[\frac{1-s}{w_1(0) - w_0(0)} + \frac{s}{w_1(1) - w_0(1)} \right], \quad (6.113)$$

its second derivative is

$$\frac{1}{4(1-s)^{3/2}} \left\{ 4^{1-s} \left[\frac{1}{w_1(1) - w_0(1)} - \frac{1}{w_1(0) - w_0(0)} \right] + \frac{1-s}{w_1(0) - w_0(0)} + \frac{s}{w_1(1) - w_0(1)} \right\}$$

The term into braces is a first-degree function, and hence it suffices verifying that it takes positive values at both endpoints of the interval $s \in [0, 1]$. At $s = 0$ the brace should verify

$$\frac{4}{w_1(1) - w_0(1)} - \frac{3}{w_1(0) - w_0(0)} > 0,$$

that is equivalent to

$$\frac{w_1(1) - w_0(1)}{w_1(0) - w_0(0)} < \frac{4}{3},$$

which is the same condition as in (6.39), already proved in Theorem 20.

At $s = 1$, the brace should verify

$$\frac{1}{w_1(1) - w_0(1)} > 0,$$

that holds trivially. In consequence, the second term is a convex function, and the sum of both terms, $B_2(s)$, is a convex function too. Hence, it suffices showing that $B_2(0) < B_2(1)$, namely

$$\frac{w_1(0) - 1}{w_1(0) - w_1(1)} < \frac{w_1(1)}{w_1(1) - w_0(1)}.$$

But this condition has already been proved, since it is a particular case of (6.110) with $1 > \frac{1}{2^{1/3}}$. In consequence, (6.91) also holds in this case, and the proof that $\Re(v(r))$ reaches its minimum at $r = r_0$ is finished.

Upper Bound of $\Re(v(r))$ It is now time to provide an upper bound for the real part of the complex poles. More specifically, it will be shown that if

$$\varepsilon_v \leq \frac{4}{3}(1 - \bar{v}_p) \quad (6.114)$$

for $\bar{v}_p < 0$, then $\Re(v(r)) \leq 1$, or, equivalently

$$\Im(\tau_{23}(r)) \leq t_1(r).$$

We remark that this condition is sufficient to ensure that the complex poles $v(r)$ lie in the interior of the critical ellipse, since the optimality of the imaginary part of the closest v -pole has been independently established.

With the same change of variable as in (6.92), the condition to be proved becomes

$$g_2(s) \leq w_1(s),$$

with w_1 and g_2 as in (6.95) and (6.96). This is the purpose of the last theorem in this subsection.

Theorem 42. *If $\bar{v}_p < 0$ and $\varepsilon_v \leq \frac{4}{3}(1 - \bar{v}_p)$ then $g_2(s) \leq w_1(s)$ for $s \in [0, 1]$.*

Proof. If $s = 1$ the theorem holds trivially. If $s < 1$, the inequality to be proved can be explicitly written as

$$\sqrt{3} \sinh \left[\frac{1}{3} \cosh^{-1} \left(\frac{1}{s\sqrt{s}} \right) \right] \leq 2 \sinh \left[\frac{1}{3} \sinh^{-1} \left(\frac{1 - \bar{v}_p}{\varepsilon_v} \frac{1}{s\sqrt{s}} \right) \right]. \quad (6.115)$$

An equivalent, polynomial form of (6.115) is found next.

From the identity (see sec. A.2)

$$\sinh \left[\frac{1}{3} \cosh^{-1} X \right] = \frac{1}{2} \left[(X + \sqrt{X^2 - 1})^{1/3} - (X - \sqrt{X^2 - 1})^{1/3} \right],$$

with $X \geq 1$, it can be readily shown that

$$G = \sinh \left[\frac{1}{3} \cosh^{-1} \left(\frac{1}{s\sqrt{s}} \right) \right],$$

implies

$$\frac{1}{s^3} = (G^2 + 1)(4G^2 + 1)^2, \quad (6.116)$$

with $G \geq 0$. On the other hand, from the identity (sec. A.2)

$$\sinh \left[\frac{1}{3} \sinh^{-1} X \right] = \frac{1}{2} \left[(\sqrt{X^2 + 1} + X)^{1/3} - (\sqrt{X^2 + 1} - X)^{1/3} \right],$$

with $X \geq 0$, it is clear that

$$W = \sinh \left[\frac{1}{3} \sinh^{-1} \left(\frac{1 - \bar{v}_p}{\varepsilon_v} \frac{1}{s\sqrt{s}} \right) \right],$$

implies

$$\frac{1}{s^3} = \left(\frac{\varepsilon_v}{1 - \bar{v}_p} \right)^2 (4W^3 + 3W)^2. \quad (6.117)$$

Equating (6.116) with (6.117) and taking into account that the equality in (6.115) can be written in the form $\sqrt{3}G = 2W$, a biquadratic equation in G is obtained, namely

$$(4G^2 + 1)^2 = \frac{27}{4} \left(\frac{\varepsilon_v}{1 - \bar{v}_p} \right)^2 G^2 (G^2 + 1), \quad (6.118)$$

whose solutions are

$$G^2 = \frac{32 - 27 \left(\frac{\varepsilon_v}{1 - \bar{v}_p} \right)^2 \pm 9 \left(\frac{\varepsilon_v}{1 - \bar{v}_p} \right) \sqrt{9 \left(\frac{\varepsilon_v}{1 - \bar{v}_p} \right)^2 - 16}}{54 \left(\frac{\varepsilon_v}{1 - \bar{v}_p} \right)^2 - 128}.$$

It is then clear that (6.118) cannot have (distinct) real solutions whenever (6.114) holds, which finishes the proof. \square

6.4.5. The case $\bar{v}_p < 0$ and $r_0 < r \leq 1$

Applying the same change of variable as in (6.52) produces the same expressions (6.81)-(6.84) for the complex poles $v(r(s))$. The optimality of the imaginary part of $v(r)$ was already established in sec. 6.3.6, and this result holds in the new variable s since (6.52) is an increasing function. In other words, it is proved that

$$\frac{g(s)}{w_1(s) - w_0(s)},$$

is a positive and decreasing function in $s \in [\varepsilon_v, \infty)$, and in consequence its square, i.e., the second fraction in (6.84), is positive and decreasing too. Therefore, it suffices proving that the first fraction in (6.84) is also a decreasing function.

Theorem 43. *If $\bar{v}_p < 0$, the function*

$$\left(\frac{w_1(s) + w_0(s)}{w_1(s) - w_0(s)} \right)^2, \quad (6.119)$$

is decreasing in $s \in [\varepsilon_v, \infty)$.

Proof. Since in case $\bar{v}_p < 0$ it holds

$$0 < w_0(s) < w_1(s),$$

it is clear that both the numerator and denominator of (6.119) are positive functions and in consequence it is enough to prove that $\frac{w_1(s) + w_0(s)}{w_1(s) - w_0(s)}$ is a decreasing function.

The explicit expression for its derivative was already obtained in (6.63), and is rewritten here for convenience:

$$\frac{d}{ds} \left(\frac{w_1 + w_0}{w_1 - w_0} \right) = \frac{-16w_1(s)w_0(s)}{3s(w_1(s) - w_0(s))} \frac{w_1(s) + w_0(s)}{(4w_1(s)^2 + 1)(4w_0(s)^2 + 1)},$$

whose left-hand side is clearly negative, as claimed above. □

7. Conclusions

7.1. Overview

This work has undertaken a comprehensive treatment of the transformation methods for singular and near-singular integration problems in two and three dimensions, covering their major theoretical and experimental aspects.

From the theoretical point of view, all emphasis has been given to the justification of the proposed transformations, that pursue the double objective of a geometric domain normalization and the algebraic regularization of integrands. A thorough review of the most significant mappings proposed over the last decades has been performed, in order to find the most general form in which these transformations can be expressed, identifying their optimal forms in some cases, and introducing new, more efficient alternatives in other cases.

With respect to geometric considerations, this work has focused exclusively in transformations that map the physical domain onto a standard domain in parent coordinates. In particular, this has excluded the polar transformation from further discussion, in spite of being a very common choice in the two-dimensional case that, nonetheless, adds unnecessary complexity due to the use of trigonometric functions and non-standard domains. A particular case of the isoparametric map, designated as pyramidal transformation, has been found to be the most versatile option, since it allows rather general forms of the physical domain, whilst carrying certain algebraic properties that help attenuate the integrand singularities.

Regarding the algebraic aspects, one of the main outcomes of this work is that the singular and near-singular integration problems are inevitably intertwined, since once the algebraic (near-)singularities have been removed from the kernel, hidden near-singularities may persist in the angular integrand, due to an adverse geometry of the physical domain. Therefore all techniques available for the near-singular problem can be automatically re-utilized in the angular part of the singular problem. Another substantial finding relates to the same transformation being introduced over the time under different forms, a circumstance that can be unveiled by expressing all available transformations over a standard domain.

From the experimental point of view, thorough numerical simulations have been performed for all significant cases of the integrals considered. To this purpose, more than 20 existing methods have been expressed in standard form and implemented in code, in order to benchmark them together with the new methods proposed in this work. The new methods are found to outperform the existing ones for a wide variety of relevant situations.

7.2. Original contributions

The main contributions of this work can be summarized as follows

- Introduction of the pyramidal transformation as the most suitable way to transform a physical domain onto a standard one when the integrand is vertex-singular (chapter 2). This transformation, formulated for the n -dimensional case, generalizes the Duffy-type mappings in use over the last decades, by showing that it is a particular, degenerate case of the well-known isoparametric transformation with a common feature of homogeneity in one of the parent variables.
- Characterization of the most general element, in arbitrary dimension, in which a pyramidal transformation can be formulated (sec. 2.2). Though n -simplices and n -pyramids with hyperplanar base had already been considered in the literature, these domains can be extended to n -pyramids with isoparametric base, but no further generalization is possible, i.e., more general elements such as n -prisms and n -parallelepipeds are excluded from a transformation that is homogeneous in one of its variables.
- In the three-dimensional case, a necessary and sufficient condition for the invertibility of the pyramidal mapping, including an explicit, non-iterative, formula for the computation of its Jacobian (sec. 2.2.4).
- In the two-dimensional case, argumentation that the pyramidal and polar maps are essentially equivalent, eliminating the requirement to implement different regularizing transformations for each case (sec. 2.2.2). The pyramidal scheme becomes the preferred option since it is a purely algebraic transformation, formulated over a standard domain.
- For the singular integration problem in both 2D and 3D, justification that the angular kernel is the same as (chapter 3) or very closely related to (chapter 5) the one-dimensional near-singular kernel. Thus, the same set of well-known near-singular transformations can be successfully applied to the truly singular integration, eliminating the need to introduce ad-hoc, less efficient alternatives in the angular variable.
- Verification that the integration over adjacent triangles admits an analogous treatment as the problem of integrating over source triangles. Extension of the corresponding radial transformations to the adjacent case (sec. 4.6).
- Identification of the most relevant transformations, mainly in the near-singular integration context, that have been proposed under apparently different forms, that are actually the same transformation when expressed in standard form (Appendix B).

- Development of a complete kernel regularization in the two dimensional case, for both singular (sec. 3.5) and near-singular integration (sec. 4.5), by solving, either analytically or numerically, appropriate differential equations imposed over the kernel. In the case of the radial variable, and additional polynomial softening has been found necessary, in both 2D (sec. 3.5.1) and 3D (sec. 5.2), in order to remove the remaining singularities.
- Introduction of a new family of composite transformations for regularization in the near-singular radial variable (sec. 4.4). These transformations represent a compromise between two extreme cases that have been extensively considered in the literature, i.e. purely smooth transformations, and transformations that leave a completely smooth kernel. Numerical experiments have shown that the most appropriate transformations can be chosen according exclusively to the value of the parameter α , since their behaviour is robust enough to withstand changes in the other problem parameters.
- Proof of the optimal form of the cubic transformation, known as one of the most common softening methods in the near-singular integration context since its introduction in 1987 (chapter 6).

7.3. Future developments

The present work admits several lines of extension, including but not limited to

- Finite element implementation in two and three-dimensional problems. In the case of two-dimensional crack-growth problems (XFEM), there are available transformations for source triangles, where the crack-tip lies, and adjacent triangles, where the enrichment functions have a near-singular behaviour.
- Extension to elements of higher order. This work has focused exclusively on first order elements, namely three-node triangles and five-node pyramids, hence an extension of all proposed transformations to higher-order elements is clearly an interesting area to explore. Higher-order elements have edge-nodes and interior nodes, as well as vertex-nodes, helping improve the modelling of curved boundaries.
- Non-pyramidal physical elements. Another area of further research would be the feasibility of the proposed methods when applied to more general elements, typically quadrilaterals in 2D together with prisms and parallelepipeds in 3D, bearing in mind that isoparametric transformations are no longer homogeneous in this case.
- Additional treatment of the bivariate angular kernel in the three-dimensional singular integration. This work proposes univariate softening transformations on the boundary of the angular domain, but the feasibility of a genuine bivariate softening procedure remains an open question.

- Further research on the additional softening necessary in the angular variable after the complete kernel regularization in two dimensions has been performed. Though the radial variable can be successfully softened by means of a power transformation $\sigma(u)$, the characterization of the corresponding polynomials $\tau(v)$ has proved to be more elusive, due to the strong dependences on the geometric parameters \bar{v}_p and ε_v .
- Edge and logarithmic singularities. In spite of the vertex-singular algebraic kernel being one of the most important purposes of the singular integration, vertex-singular logarithmic kernels and edge-singular kernels (both algebraic and logarithmic) are routinely analyzed as well. Since logarithmic kernels are no longer homogeneous functions of their coordinates, new challenges will have to be solved for these specific cases.

A. Inversion of the cubic equation

Classical, well-known procedures exist for the inversion of the cubic equation. Some of them, based on trigonometric and hyperbolic functions, are summarized here (refer e.g. to [28] for details). This Appendix focuses on depressed cubic equations, namely monic trinomials whose quadratic term has coefficient zero. These equations can be expressed as one the two following cases:

1. $Y = X(p^2 - X^2)$
2. $Y = X(p^2 + X^2)$

Both cases are displayed in Fig. A.1.

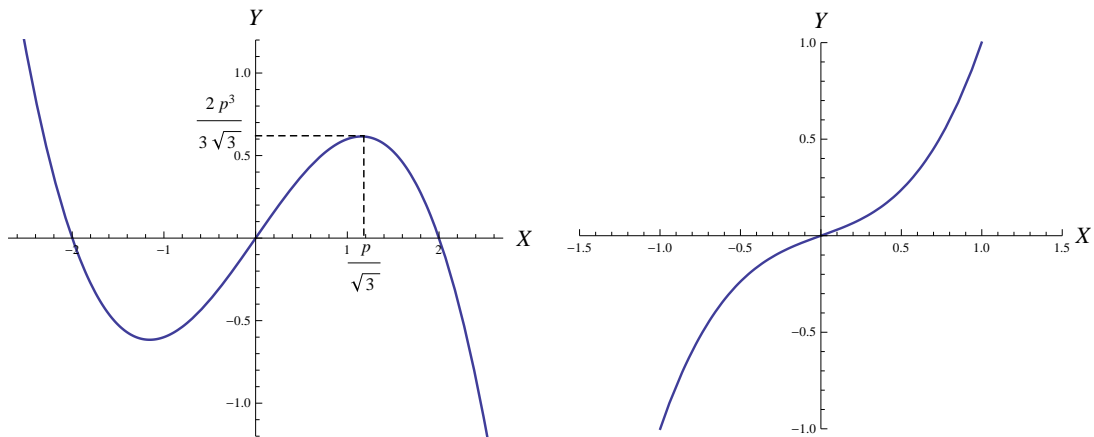


Figure A.1.: Cubic equations $Y = X(p^2 - X^2)$ (left), $Y = X(p^2 + X^2)$ (right)

We next discuss the inversion of each type of equation.

A.1. The equation $Y = X(p^2 - X^2)$

In the irreducible case $|Y| \leq \frac{2p^3}{3\sqrt{3}}$ the equation has three real roots, with a double root if equality holds, see Fig. A.1, left. The Descartes' rule of signs implies the separation of the roots as

- If $Y > 0$, then $X_1 < 0 < X_2 \leq X_3$
- If $Y < 0$, then $X_1 \leq X_2 < 0 < X_3$

These three roots can be explicitly written as

$$X_k = \frac{2p}{\sqrt{3}} \sin \left[\frac{1}{3} \sin^{-1} \left(\frac{3\sqrt{3}}{2p^3} Y \right) + \frac{2\pi}{3}(k-2) \right], \quad k = 1, 2, 3. \quad (\text{A.1})$$

An interesting situation occurs for $p = \frac{\sqrt{3}}{2^{1/3}}$. Letting $X = 2^{2/3}Z$, it is easily shown that the cubic equation and its second (middle) root are reduced to

$$Y = 3Z - 4Z^3 \longleftrightarrow Z = \sin \left[\frac{1}{3} \sin^{-1} Y \right], \quad |Y| \leq 1. \quad (\text{A.2})$$

Formulas of these type are widely used throughout this work, when dealing with more general cases of cubic polynomials.

In case $|Y| > \frac{2p^3}{3\sqrt{3}}$, the cubic equation has one real root (with opposite sign to Y) and two complex conjugate roots, whose real parts have the same sign as Y , see Fig. A.1, left. These roots can be written explicitly as

$$X_1 = -\frac{2p}{\sqrt{3}} \cosh \left[\frac{1}{3} \cosh^{-1} \left(\frac{3\sqrt{3}}{2p^3} Y \right) \right], \quad (\text{A.3})$$

$$X_{23} = \frac{p}{\sqrt{3}} \cosh \left[\frac{1}{3} \cosh^{-1} \left(\frac{3\sqrt{3}}{2p^3} Y \right) \right] \pm ip \sinh \left[\frac{1}{3} \cosh^{-1} \left(\frac{3\sqrt{3}}{2p^3} Y \right) \right]. \quad (\text{A.4})$$

For the condition previously analyzed of $p = \frac{\sqrt{3}}{2^{1/3}}$, and assuming $Y < -1$, we let $X = 2^{2/3}Z$, $Y \rightarrow -Y$ to obtain

$$Y = 4Z^3 - 3Z \longleftrightarrow Z = \cosh \left[\frac{1}{3} \cosh^{-1} Y \right], \quad Y > 1. \quad (\text{A.5})$$

Furthermore, since the hyperbolic functions can be expressed in algebraic form by means of

$$\cosh \left[\frac{1}{3} \cosh^{-1} Y \right] = \frac{1}{2} \left[(Y + \sqrt{Y^2 - 1})^{1/3} + (Y - \sqrt{Y^2 - 1})^{1/3} \right], \quad Y > 1,$$

it follows that (A.5) admits an alternative formulation

$$Y = \frac{1}{2} (Z^3 - 3Z) \longleftrightarrow Z = (Y + \sqrt{Y^2 - 1})^{1/3} + (Y - \sqrt{Y^2 - 1})^{1/3}. \quad (\text{A.6})$$

An analogous expression can be found for the imaginary part of X_{23} in (A.4). First, the hyperbolic functions are expressed in algebraic way

$$\sinh \left[\frac{1}{3} \cosh^{-1} Y \right] = \frac{1}{2} \left[(Y + \sqrt{Y^2 - 1})^{1/3} - (Y - \sqrt{Y^2 - 1})^{1/3} \right].$$

Equating the right-hand side to $\frac{Z}{2}$ and raising to the third power, it follows

$$Z^3 = 2\sqrt{Y^2 - 1} - 3 \left[(Y + \sqrt{Y^2 - 1})^{1/3} - (Y - \sqrt{Y^2 - 1})^{1/3} \right].$$

Since the term into brackets above equals Z , a bicubic relationship can be finally obtained

$$4(Y^2 - 1) = (Z^3 + 3Z)^2 \longleftrightarrow Z = (Y + \sqrt{Y^2 - 1})^{1/3} - (Y - \sqrt{Y^2 - 1})^{1/3}. \quad (\text{A.7})$$

A.2. The equation $Y = X(p^2 + X^2)$

This equation has one real root, with the same sign as Y , and two complex conjugate roots, with opposite signs to Y , see Fig. A.1, right. Their explicit expression is

$$X_1 = \frac{2p}{\sqrt{3}} \sinh \left[\frac{1}{3} \sinh^{-1} \left(\frac{3\sqrt{3}}{2p^3} Y \right) \right], \quad (\text{A.8})$$

$$X_{23} = -\frac{p}{\sqrt{3}} \sinh \left[\frac{1}{3} \sinh^{-1} \left(\frac{3\sqrt{3}}{2p^3} Y \right) \right] \pm ip \cosh \left[\frac{1}{3} \sinh^{-1} \left(\frac{3\sqrt{3}}{2p^3} Y \right) \right]. \quad (\text{A.9})$$

For the situation with $p = \frac{\sqrt{3}}{2^{1/3}}$, we let $X = 2^{2/3}Z$ to obtain

$$Y = 3Z + 4Z^3 \longleftrightarrow Z = \sinh \left[\frac{1}{3} \sinh^{-1} Y \right]. \quad (\text{A.10})$$

In this case the hyperbolic functions can be expressed as

$$\sinh \left[\frac{1}{3} \sinh^{-1} Y \right] = \frac{1}{2} \left[(\sqrt{Y^2 + 1} + Y)^{1/3} - (\sqrt{Y^2 + 1} - Y)^{1/3} \right],$$

from where (A.10) admits the alternative formulation

$$Y = \frac{1}{2} (3Z + Z^3) \longleftrightarrow Z = (\sqrt{Y^2 + 1} + Y)^{1/3} - (\sqrt{Y^2 + 1} - Y)^{1/3}. \quad (\text{A.11})$$

With respect to the imaginary part of X_{23} in (A.9), no further treatment has been necessary in this work. However, its bicubic inversion formula is provided below for completeness:

$$4(Y^2 + 1) = (Z^3 - 3Z)^2 \longleftrightarrow Z = (\sqrt{Y^2 + 1} + Y)^{1/3} + (\sqrt{Y^2 + 1} - Y)^{1/3}.$$

B. Equivalent form of some transformations

B.1. The PART Method

The PART method was introduced in [24, 25, 26]. It proposes a series of mappings on the polar radial variable, see sec. 4.3.1, together with a transformation on the polar angle that can be written, with reference to Fig. 2.4, as

$$t = \frac{h_T}{2} \log \left(\frac{1 + \sin(\theta - \theta_p)}{1 - \sin(\theta - \theta_p)} \right). \quad (\text{B.1})$$

We next show that (B.1) is equivalent to a sinh transformation on the isoparametric variable \bar{v} .

From the well-known identities

$$\begin{aligned} \sinh^{-1} A &= \log \left(A + \sqrt{1 + A^2} \right), \quad A \in \mathbb{R}, \\ \frac{1 + \sin A}{\cos A} &= \sqrt{\frac{1 + \sin A}{1 - \sin A}}, \quad A \in \left[-\frac{\pi}{2}, \frac{\pi}{2} \right], \end{aligned}$$

it is easy to show that

$$\log \sqrt{\frac{1 + \sin A}{1 - \sin A}} = \sinh^{-1}(\tan A), \quad A \in \left[-\frac{\pi}{2}, \frac{\pi}{2} \right].$$

This way, (B.1) reduces to

$$t = h_T \sinh^{-1}(\tan(\theta - \theta_p)) \rightarrow \tan(\theta - \theta_p) = \sinh \left(\frac{t}{h_T} \right).$$

Recalling equation (2.15)

$$\bar{v} = \bar{v}_p + \varepsilon_v \tan(\theta - \theta_p),$$

and applying the appropriate affine transformation $t(v)$ onto $\frac{t}{h_T}$, it follows that (B.1) reduces to

$$\bar{v}(v) = \bar{v}_p + \varepsilon_v \sinh(t(v)),$$

which is the sinh transformation described in sec. 3.4.4.

An almost identical transformation is proposed in [2], namely

$$t = \frac{1}{2} \log \left(\frac{1 + \sin(\theta - \theta_p)}{1 - \sin(\theta - \theta_p)} \right).$$

It is obvious that this mapping is also equivalent to \sinh in the angular variable, as described in sec. 3.4.

Yet another similar transformation appears in [37], that can be written, with reference to Fig. 2.4, as

$$t = \log \left(\tan \left(\frac{\theta}{2} + \frac{\pi}{4} \right) \right). \quad (\text{B.2})$$

This transformation is shown to be equivalent to \sinh in [3], a fact that follows from the well-known identity

$$\tan \frac{A}{2} = \sqrt{\frac{1 + \cos A}{1 - \cos A}}, \quad A \in \left[0, \frac{\pi}{2} \right].$$

Elementary trigonometric manipulations lead from (B.2) to (B.1), which concludes the proof.

B.2. The Exponential distance transformation

An exponential distance transformation was proposed in [45] and later considered in [56]. It can be expressed (sec. 4.3.1) as

$$\bar{u} = \frac{1}{2}(e^t - b^2 e^{-t}), \quad (\text{B.3})$$

with $t_0 = \log b$, $t_1 = \log(1 + \sqrt{1 + b^2})$ and

$$t(u, v) = t_0(v) + (t_1(v) - t_0(v))u. \quad (\text{B.4})$$

We next show that (B.3) is equivalent to a \sinh transformation in the isoparametric radial variable \bar{u} . It suffices manipulating (B.3) as follows:

$$\begin{aligned} \bar{u} &= \frac{b}{2} (b^{-1} e^t - b e^{-t}) \\ &= \frac{b}{2} (e^{t - \log b} - e^{-(t - \log b)}) \\ &= b \sinh(t - \log b). \end{aligned}$$

Renaming $t' = t - \log b$ it is clear that the endpoints for the auxiliary variable t' are

$$\begin{aligned} t'_0 &= 0, \\ t'_1 &= \log \left(\frac{1}{b} + \sqrt{1 + \frac{1}{b^2}} \right) \\ &= \sinh^{-1} \left(\frac{1}{b} \right), \end{aligned}$$

that has the same form as F_1 (\sinh) in Tab. 4.1.

B.3. The Exponential transformation

Another exponential transformation, proposed in [72] and later considered in [68], can be expressed (sec. 4.3.1) as

$$\bar{u} = b(e^t - 1), \tag{B.5}$$

with $t_0 = 0$, $t_1 = \log\left(1 + \frac{1}{b}\right)$ and $t(u, v)$ as in (B.4).

To show that (B.5) is equivalent to a radial transformation $\text{Log-}L_1$ in the PART method (Tab. 4.2) we write

$$\begin{aligned} \bar{u} &= be^t - b \\ &= e^{t+\log b} - b. \end{aligned}$$

Renaming $t' = t + \log b$, it follows that the endpoints of t' are

$$\begin{aligned} t'_0 &= \log b, \\ t'_1 &= \log(b + 1), \end{aligned}$$

which concludes the proof.

C. Newton's method

Specific methods for complete kernel regularization of the singular 2D and near-singular 2D integrals have been developed in sec. 3.5 and sec. 4.5. These methods imply the numerical solution of a first-order Ordinary Differential Equation (ODE) for the angular variable, namely (3.31) and (4.30). These equations can be written in generic form as:

$$\phi(\bar{v}) \frac{d\bar{v}}{dv} = c_2 \frac{d\tau}{dv}, \quad (\text{C.1})$$

where $\phi(\bar{v})$ is the (non-vanishing) angular kernel, $\bar{v} \in [0, 1]$ and $v \in [0, 1]$ are the dependent and independent variables respectively, c_2 is a normalizing constant given by

$$c_2 = \int_0^1 \phi(s) ds,$$

and $\tau(v)$ is a softening polynomial that transforms $[0, 1]$ onto itself, with $\tau(v) = v$ as the simplest example.

The solution of (C.1) need not be obtained by a genuine ODE integration scheme, such as the Euler or the Runge-Kutta methods. Since we only need to know the value of \bar{v} at the discrete set of n_w Gaussian nodes, namely $\{v_i\}_{i=1}^{n_w}$, we can rather solve (C.1) by the Newton's method.

To this purpose, we define

$$F(\bar{v}) = \int_0^{\bar{v}} \phi(s) ds,$$

and integrate both sides of (C.1) between 0 and $\bar{v}(v)$ to yield

$$F(\bar{v}) = c_2 \tau(v), \quad (\text{C.2})$$

from where \bar{v} is implicitly defined by

$$\bar{v}(v) = F^{-1}(c_2 \tau(v)).$$

We notice that the invertibility of (C.2) is guaranteed by the Implicit Function Theorem since

$$\frac{\partial(F(\bar{v}) - c_2 \tau(v))}{\partial \bar{v}} = \phi(\bar{v}) \neq 0.$$

For each known value of v_i , (C.2) takes the form

$$F(\bar{v}_i) - c_2 \tau(v_i) = 0,$$

where the value of $\bar{v}_i = \bar{v}(v_i)$ is unknown. Hence, the Newton iterations take the form

$$\bar{v}_i^k - \bar{v}_i^{k+1} = \frac{F(\bar{v}_i^k) - c_2\tau(v_i)}{\phi(\bar{v}_i^k)}. \quad (\text{C.3})$$

Moreover, $F(\bar{v}_i^k)$ can be expressed in incremental form

$$F(\bar{v}_i^k) = \int_0^{\bar{v}_i^k} \phi(s) ds = \underbrace{\int_0^{\bar{v}_{i-1}} \phi(s) ds}_{F(\bar{v}_{i-1})} + \int_{\bar{v}_{i-1}}^{\bar{v}_i^k} \phi(s) ds, \quad (\text{C.4})$$

where $F(\bar{v}_{i-1})$ is known from the previous iteration, $\bar{v}_i^0 = \bar{v}_{i-1}$ and $\bar{v}_0 = 0$. Substituting (C.4) into (C.3) yields

$$\bar{v}_i^k - \bar{v}_i^{k+1} = \frac{F(\bar{v}_{i-1}) + \int_{\bar{v}_{i-1}}^{\bar{v}_i^k} \phi(s) ds - c_2\tau(v_i)}{\phi(\bar{v}_i^k)}.$$

This procedure provides a very efficient way to solve (C.2). Indeed, numerical experiments show that a few Newton iterations suffice to reach machine precision in the values of \bar{v} .

Once the transformation $\bar{v}(v)$ is known, its derivative is readily computed from (C.1), namely

$$\frac{d\bar{v}}{dv} = \frac{c_2}{\phi(\bar{v})} \frac{d\tau}{dv}.$$

D. Truncation error under affine transformations

This Appendix proves that the truncation error of a one-dimensional Gaussian quadrature rule is not affected by an affine change of variable.

D.1. The error term of the Gaussian quadrature

The truncation error when approximating the integral

$$I = \int_a^b g(x)dx, \quad (\text{D.1})$$

by the Gaussian quadrature rule of order n is given (see e.g. [16], p. 295) by

$$\begin{aligned} E_{ab}(g) &\equiv \int_a^b g(x)dx - \sum_{i=1}^n w_i g(x_i) \\ &= (b-a)^{2n+1} k_n \left. \frac{d^{2n}g(x)}{dx^{2n}} \right|_{x=x_c}, \end{aligned} \quad (\text{D.2})$$

with $x_c \in [a, b]$ and

$$k_n = \frac{(n!)^4}{(2n+1)[(2n)!]^3}.$$

An application of Stirling's rule allows to show that the coefficients k_n decrease exponentially with n , see [16] for details.

D.2. Effect of an affine transformation

We analyze now the effect of an affine change of variable over the truncation error (D.2). More specifically, the affine transformation considered is

$$x(z) = \frac{b-a}{d-c}z + \frac{ad-bc}{d-c}, \quad (\text{D.3})$$

from $z \in [c, d]$ onto $x \in [a, b]$. Applying (D.3) onto (D.1) yields

$$\begin{aligned} I &= \int_c^d g(x(z)) \frac{b-a}{d-c} dz \\ &= \int_c^d f(z) dz, \end{aligned} \quad (\text{D.4})$$

where we have defined

$$f(z) = \frac{b-a}{d-c}g(x(z)).$$

The error in (D.4), taking (D.2) into account, is

$$E_{cd}(f) = (d-c)^{2n+1}k_n \left. \frac{d^{2n}f(z)}{dz^{2n}} \right|_{z=z_c},$$

with $z_c \in [c, d]$. On the other hand, repeated application of the chain rule produces

$$\left. \frac{d^{2n}f(z)}{dz^{2n}} \right|_{z=z_c} = \left(\frac{b-a}{d-c} \right)^{2n+1} \left. \frac{d^{2n}g(x)}{dx^{2n}} \right|_{x=x_c},$$

from where it is immediate that

$$E_{cd}(f) = (b-a)^{2n+1}k_n \left. \frac{d^{2n}f(z)}{dz^{2n}} \right|_{z=z_c} = E_{ab}(f),$$

which finishes the proof.

Bibliography

- [1] E. Alarcón, M. Doblaré, J. Sanz-Serna. An Efficient Nonlinear Transformation for the Numerical Computation of the Singular Integrals Appearing in the 2-D Boundary Element Method. *Bound. Elem. Methods in Eng.*, 472-479 (1990)
- [2] E. Béchet, H. Minnebo, N. Moës, B. Burgardt. Improved implementation and robustness study of the X-FEM for stress analysis around cracks. *Intl. Jrnl. for Num. Meth. in Eng.* **64**, 1033-1056 (2005)
- [3] M. M. Botha. A Family of Augmented Duffy Transformations for Near-Singularity Cancellation Quadrature. *IEEE Trans. on Antennas and Propagation*, **61**(6), 3123-3134 (2013)
- [4] A. Cano, C. Moreno. A new method for numerical integration of singular functions on the plane. *Numer. Algor.*, **68**(3), 547-568 (2015)
- [5] A. Cano, C. Moreno. Transformation Methods for the Numerical Integration of Three-Dimensional Singular Functions. *Jrnl. of Scientific Computing*, **71**(2), 571-593 (2017)
- [6] M. Cerrolaza, E. Alarcón. A Bicubic Transformation for the Efficient Evaluation of General Boundary Element Integrals. *Int. Jrnl. of Num. Meth. in Eng.*, **24**, 937-959 (1989)
- [7] A. Chernov, A. Reinarz. Numerical quadrature for high-dimensional singular integrals over parallelotopes. *Comp. and Math. with Appl.* **66**, 1213-1231 (2013)
- [8] A. Chernov, T. von Petersdorff, C. Schwab. Quadrature algorithms for high dimensional singular integrands on simplices. *Numer. Algor.* **70**(4), 847-874 (2015)
- [9] P. G. Ciarlet. *The Finite Element Method for Elliptic Problems*. SIAM (2002)
- [10] P. J. Davis, P. Rabinowitz. *Methods of Numerical Integration*, 2nd Ed. Academic Press (1984)
- [11] M. G. Duffy. Quadrature over a pyramid or cube of integrands with a singularity at a vertex. *SIAM J. Numer. Anal.* **19**(6), 1260-1262 (1982)
- [12] D. A. Dunavant. High degree efficient symmetrical Gaussian quadrature rules for the triangle. *Intl. Jrnl. for Num. Meth. in Eng.*, **21**, 1129-1148 (1985)
- [13] M. Duruflé, P. Grob, P. Joly. Influence of Gauss and Gauss-Lobatto quadrature rules on the accuracy of a quadrilateral finite element method in the time domain. *Num. Meth. for Partial Diff. Eq.*, **25**(3), 526-551 (2009)

- [14] D. Elliott, P. R. Johnston. Error analysis for a sinh transformation used in evaluating nearly singular boundary element integrals. *Jrnl. of Comp. and Applied Math.*, **203**, 103-124 (2007)
- [15] D. Elliott, P. R. Johnston. The iterated sinh transformation. *Intl. Jrnl. for Num. Meth. in Eng.*, **75**, 43-57 (2008)
- [16] J. F. Epperson. *An Introduction to Numerical Methods and Analysis*, 2nd Ed. Wiley, New Jersey (2013)
- [17] G. Fairweather, F. J. Rizzo, D. J. Shippy. Computation of double integrals in the boundary integral equation method. In: Vichnevetsky, R., Stepleman, R. S. (eds.) *Advances in Computer Methods for Partial Differential Equations - III*, **36**, 331-334. IMACS Publ. Brussels, Belgium (1979)
- [18] J. Fish, T. Belytschko. *A first course in finite elements*. Wiley, New Jersey (2007)
- [19] A. E. Frey, C. A. Hall, T. A. Porsching. Some Results on the Global Inversion of Bilinear and Quadratic Isoparametric Finite Element Transformations. *Math. of Computation*, **32**(143), 725-749 (1978)
- [20] W. Gautschi. Numerical integration over the square in the presence of algebraic/logarithmic singularities with an application to aerodynamics. *Numer. Algor.* **61**(2), 275-290 (2012)
- [21] A. Genz, R. Cools. An adaptive numerical cubature algorithm for simplices. *ACM Transactions on Mathematical Software*, **29**(3), 297-308 (2003)
- [22] Y. Gu, W. Chen, C. Zhang. The sinh transformation for evaluating nearly singular boundary element integrals over high-order geometry elements. *Eng. Anal. with Bound. Elem.*, **37**, 301-308 (2013)
- [23] Y. Gu, Q. Hua, W. Chen, C. Zhang. Numerical evaluation of nearly hyper-singular integrals in the boundary element analysis. *Computers and Structures*, **167**, 15-23 (2016)
- [24] K. Hayami, C. A. Brebbia. A New Coordinate Transformation Method for Singular and Nearly Singular Integrals over General Curved Boundary Elements. In *Boundary Elements IX*, 375-399, Springer (1987)
- [25] K. Hayami. *A Projection Transformation Method for Nearly Singular Surface Boundary Element Integrals*. Lecture Notes in Engineering, 73, Springer-Verlag (1992)
- [26] K. Hayami, H. Matsumoto. A numerical quadrature for nearly singular boundary element integrals. *Eng. Anal. with Bound. Elem.*, **13**, 143-154 (1994)
- [27] K. Hayami. Variable Transformations for Nearly Singular Integrals in the Boundary Element Method. *Publications of the Research Institute for Mathematical Sciences*, **41**(4), 821-842 (2005)

- [28] G. C. Holmes. The use of hyperbolic cosines in solving cubic polynomials. *The Mathematical Gazette*, **86**(507), 473-477 (2002)
- [29] C. Hua. An inverse transformation for quadrilateral isoparametric elements: Analysis and application. *Finite Elements in Analysis and Design*, **7**, 159-166 (1990)
- [30] S. Järvenpää, M. Taskinen, P. Ylä-Oijala. Singularity extraction technique for integral equation methods with higher order basis functions on plane triangles and tetrahedra. *Intl. Jrnl. for Num. Meth. in Eng.*, **58**, 1149-1165 (2003)
- [31] P. R. Johnston. Semi-sigmoidal transformations for evaluating weakly singular boundary element integrals. *Intl. Jrnl. for Num. Meth. in Eng.*, **47**, 1709-1730 (2000)
- [32] P. R. Johnston, D. Elliott. A sinh transformation for evaluating nearly singular boundary element integrals. *Intl. Jrnl. for Num. Meth. in Eng.*, **62**, 564-578 (2005)
- [33] B. M. Johnston, P. R. Johnston, D. Elliott. A sinh transformation for evaluating two-dimensional nearly singular boundary element integrals. *Intl. Jrnl. for Num. Meth. in Eng.*, **69**, 1460-1479 (2007)
- [34] B. M. Johnston, P.R. Johnston, D. Elliott. A new method for the numerical evaluation of nearly singular integrals on triangular elements in the 3D boundary element method. *Jrnl. of Comp. and Applied Math.*, **245**, 148-161 (2013)
- [35] P. R. Johnston, B. M. Johnston, D. Elliott. Using the iterated sinh transformation to evaluate two dimensional nearly singular element integrals. *Eng. Anal, with Bound. Elem.*, **37**, 708-718 (2013)
- [36] M. Kathirkamanayagam, J. H. Curran, S. Shah. Regularizing transformation method for evaluation of singular and near-singular integrals. *Transactions on Modelling and Simulation*, **20**, 247-258 (1998)
- [37] M. A. Khayat, D. R. Wilton, P. W. Fink. An Improved Transformation and Optimized Sampling Scheme for the Numerical Evaluation of Singular and Near-Singular Potentials. *IEEE Antennas and Wireless Propagation Letters*, **7**, 377-380 (2008)
- [38] P. Knabner, G. Summ. The invertibility of the isoparametric mapping for pyramidal and prismatic finite elements. *Numer. Math.*, **88**(4), 661-681 (2001)
- [39] P. Knabner, S. Korotov, G. Summ. Conditions for the invertibility of the isoparametric mapping for hexahedral finite elements. *Finite Elements in Analysis and Design*, **40**, 159-172 (2002)
- [40] P. M. Knupp. On the invertibility of the isoparametric map. *Comp. Methods in Applied Mechanics and Engineering*, **78**, 313-329 (1990)
- [41] E. J. Kubatko, B. A. Yeager, A. L. Maggi. New computationally efficient quadrature formulas for triangular prism elements. *Comp. & Fluids*, **73**, 187-201 (2013)

- [42] J. C. Lachat, J. O. Watson. Effective numerical treatment of Boundary Integral Equations: A formulation for three-dimensional elastostatics. Intl. Jrnl. for Num. Meth. in Eng., **10**, 991-1005 (1976)
- [43] P. Laborde, J. Pommier, Y. Renard, M. Salaün. High-order extended finite element method for cracked domains. Intl. Jrnl. for Num. Meth. in Eng., **64**, 354-381 (2005)
- [44] J. N. Lyness, R. Cools. A Survey of Numerical Cubature over Triangles. Proceedings of Symposia in Applied Math., **48**, 127-150 (1994)
- [45] H. Ma, N. Kamiya. Distance transformation for the numerical evaluation of near singular boundary integrals with various kernels in boundary element method. Eng. Anal. with Bound. Elem., **26**, 329-339 (2002)
- [46] H. Ma, N. Kamiya. A general algorithm for the numerical evaluation of nearly singular boundary integrals of various orders for two- and three-dimensional elasticity. Comput. Mech., **29**, 277-288 (2002)
- [47] H. Minnebo. Three-dimensional integration strategies of singular functions introduced by the XFEM in the LEFM. Intl. Jrnl. for Num. Meth. in Eng., **92**, 1117-1138 (2012)
- [48] N. Moës, A. Gravouil, T. Belytschko. Non-planar 3D crack growth by the extended finite element and level sets - Part I: Mechanical model. Intl. Jrnl. for Num. Meth. in Eng., **53**, 2549-2568 (2002)
- [49] S. E. Mousavi, N. Sukumar. Generalized Duffy transformation for integrating vertex singularities. Comput. Mech., **45**, 127-140 (2010)
- [50] S. E. Mousavi, N. Sukumar. Generalized Gaussian quadrature rules for discontinuities and crack singularities in the extended finite element method. Comput. Methods Appl. Mech. Engrg., **199**, 3237-3249 (2010)
- [51] S. E. Mousavi, J. E. Pask, N. Sukumar. Efficient adaptive integration of functions with sharp gradients and cusps in n -dimensional parallelepipeds. Intl. Jrnl. for Num. Meth. in Eng. **91**(4), 343-357 (2012)
- [52] D. Mustard, J. N. Lyness, J. M. Blatt. Numerical quadrature in n dimensions. Comput. Jrnl., **6**, 75-85 (1963)
- [53] A. Nagarajan, S. Mukherjee. A mapping method for numerical evaluation of two-dimensional integrals with $1/r$ singularity. Comput. Mech., **12**, 19-26 (1993)
- [54] F. W. J. Olver et al. NIST Handbook of Mathematical Functions. Cambridge University Press, Cambridge (2010)
- [55] K. Park, J. P. Pereira, C. A. Duarte, G. H. Paulino. Integration of singular enrichment functions in the generalized/extended finite element method for three-dimensional problems. Intl. Jrnl. for Num. Meth. in Eng., **78**, 1220-1257 (2009)

- [56] X. Qin et al. A general algorithm for the numerical evaluation of nearly singular integrals on 3D boundary element. *Jrnl. of Comp. and Applied Math.*, **235**, 4174-4186 (2011)
- [57] H. T. Rathod, B. Venkatesudu, K. V. Nagaraja. Gauss Legendre quadrature formulas over a tetrahedron. *Intl. Jrnl. of Comp. Eng., Science and Mech.*, **6**(3), 197-205 (2005)
- [58] T. W. Sag, G. Szekeres. Numerical evaluation of high-dimensional integrals. *Math. Comput.*, **18**, 245-253 (1964)
- [59] C. Schwab. Variable order composite quadrature of singular and nearly singular integrals. *Computing*, **53**(2), 173-194 (1994)
- [60] L. Scuderi. On the computation of nearly singular integrals in 3D BEM collocation. *Intl. Jrnl. for Num. Meth. in Eng.*, **74**, 1733-1770 (2008)
- [61] V. Sladek, J. Sladek, M. Tanaka. Numerical integration of logarithmic and nearly logarithmic singularity in BEMs. *Applied Math. Modelling*, **25**, 901-922 (2001)
- [62] A. H. Stroud, D. Secrest. *Gaussian quadrature formulas*. Prentice-Hall Inc., New Jersey (1966)
- [63] N. Sukumar, J.E. Dolbow, N. Moës. Extended finite element method in computational fracture mechanics: a retrospective examination. *Int. Jrnl. Fract.* **196**(1), 189-206 (2015)
- [64] J. C. F. Telles. A self-adaptive co-ordinate transformation for efficient numerical evaluation of general Boundary Element Integrals. *Intl. Jrnl. for Num. Meth. in Eng.*, **24**, 959-973 (1987)
- [65] J. C. F. Telles, R. F. Oliveira. Third degree polynomial transformation for boundary element integrals. Further improvements. *Eng. Anal. with Bound. Elem.*, **13**, 135-141 (1994)
- [66] O. V. Ushakova. Conditions of nondegeneracy of three-dimensional cells. A formula of a volume of cells. *SIAM J. Sci. Comput.* **23**(4), 1274-1290 (2001)
- [67] H. Xiao, Z. Gimbutas. A numerical algorithm for the construction of efficient quadrature rules in two and higher dimensions. *Comp. and Math. with Appl.*, **59**, 663-676 (2010)
- [68] G. Xie, F. Zhou, J. Zhang, X. Zheng, C. Huang. New variable transformations for evaluating nearly singular integrals in 3D boundary element method. *Eng. Anal. with Bound. Elem.*, **37**, 1169-1178 (2013)
- [69] W. Ye. A new transformation technique for evaluating nearly singular integrals. *Comput. Mech.*, **42**, 457-466 (2008)
- [70] K. Y. Yuan, Y. S. Huang, H. T. Yang, T. H. H. Pian. The inverse mapping and distortion measures for 8-node hexahedral isoparametric elements. *Comput. Mech.*, **14**, 189-199 (1994)

-
- [71] S. Zhang. Numerical integration with Taylor truncations for the quadrilateral and hexahedral finite elements. *Jrnl. of Comp. and Applied Math.*, **205**, 325-342 (2007)
- [72] Y. Zhang, C. Sun. A general algorithm for the numerical evaluation of nearly singular boundary integrals in the equivalent non-singular BIES with indirect unknowns. *Jrnl. of the Chinese Institute of Engineers*, **31**, 437-447 (2008)
- [73] Y. Zhang, Y. Gong, X. Gao. Calculation of 2D nearly singular integrals over high-order geometry elements using the sinh transformation. *Eng. Anal. with Bound. Elem.*, **60**, 144-153 (2015)